Role of oncogenic and wild type B-RAF in mouse lung tumor models

---

Untersuchungen zur Rolle der onkogenen und wildtypischen B-RAF Kinase in Lungentumormodellen der Maus

Doctoral thesis for a doctoral degree
at the Graduate School of Life Sciences,
Julius-Maximilians-Universität Würzburg,
Section Infection and Immunity

Submitted by

Emanuele Zanucco

from
San Vito di Cadore (Italy)

Würzburg 2011

Submitted on: ……..…….

Office stamp

Members of the *Promotionskomitee*:

Chairperson: Prof. Thomas Dandekar

Primary Supervisor: Prof. Ulf R. Rapp

Supervisor (Second): Dr. PD Rudolf Götz

Supervisor (Third): Prof. Ricardo Benavente

Supervisor (Fourth): Prof. Roland Benz

Date of Public Defence: ……..…….

Date of receipt of Certificates: ……

Table of contents

Summary

Growth factor induced signaling cascades are key regulatory elements in tissue development, maintenance and regeneration. Deregulation of the cascades has severe consequences, leading to developmental disorders and neoplastic diseases. As a major function in signal transduction, activating mutations in RAF family kinases are the cause of many human cancers.

In the first project described in this thesis we focused on B-RAF V600E that has been identified as the most prevalent B-RAF mutant in human cancer. In order to address the oncogenic function of B-RAF V600E, we have generated transgenic mice expressing the activated oncogene specifically in lung alveolar epithelial type II cells. Constitutive expression of B-RAF V600E caused abnormalities in alveolar epithelium formation that led to airspace enlargements. These lung lesions showed signs of tissue remodeling and were often associated with chronic inflammation and low incidence of lung tumors. Inflammatory cell infiltration did not precede the formation of emphysema-like lesions but was rather accompanied with late tumor development. These data support a model where the continuous regenerative process initiated by oncogenic B-RAF-driven alveolar disruption provides a tumor-promoting environment associated with chronic inflammation.

In the second project we focused on wild type B-RAF and its role in an oncogenic-C-RAF driven mouse lung tumor model. Toward this aim we have generated compound mice in which we could conditionally deplete B-RAF in oncogenic-C-RAF driven lung tumors. Conditional elimination of B-RAF did not block lung tumor formation however led to reduced tumor growth. The diminished

tumor growth was not caused by increased cell death instead was a consequence of reduced cell proliferation. Moreover, B-RAF ablation caused a reduction in the amplitude of the mitogenic signalling cascade. These data indicate that *in vivo* B-RAF is dispensable for the oncogenic potential of active C-RAF; however it cooperates with oncogenic C-RAF in the activation of the mitogenic cascade.

Zusammenfassung

Von Wachstumsfaktoren regulierte Signalkaskaden sind Schlüsselelemente in der Gewebeentwicklung und Geweberegeneration. Eine Deregulation dieser Kaskaden führt zu Entwicklungsstörungen und neoplastischen Krankheiten. Für viele humane Krebsformen sind aktivierende Mutationen der Kinasen der RAF Familie verantwortlich.

Das erste Projekt dieser Doktorarbeit fokussiert auf der Rolle des B-RAF V600E, welches als eine der am häufigsten vorkommenden Mutantionen in humanen Krebszellen identifiziert worden ist. Um die onkogene Funktion des B-RAF V600E zu untersuchen, haben wir transgene Mauslinien hergestellt, welche das aktivierte Onkogen spezifisch in alveolaren Lungenepithelzellen des Typ II exprimieren. Konstitutive Expression des B-RAF V600E führte zu einer abnormen alveolaren Epithelzellbildung und zu Emphysem-ähnlichen Läsionen. Diese Läsionen wiesen Zeichen einer Gewebsumstrukturierung auf, oft in Assoziation mit chronischer Inflammation und geringer Inzidenz von Lungentumoren. Die Infiltration der entzündlichen Zellen erfolgte erst nach der Entstehung von Emphysem-ähnlichen Läsionen und könnte zur späteren Tumorbildung beigetragen haben. Diese Ergebnisse unterstützen ein Modell, in welchem der kontinuierliche regenerative Prozess eine tumorfördernde Umgebung schafft. Dabei induziert die Aktivität des onkogenen B-RAF eine alveolare Störung, welche ursächlich verantwortlich ist für den kontinuierlichen regenerativen Prozess.

Das zweite Projekt fokussiert auf die Rolle von endogenem (wildtypischen) B-RAF in einem durch onkogenes C-RAF induzierten Maus Lungentumormodell.

Für unsere Untersuchungen haben wir eine Mauslinie geschaffen, in welcher B-RAF in den C-RAF Lungentumoren konditionell eliminiert werden kann. Eine konditionelle Eliminierung des B-RAF hat die Entstehung von Lungentumoren nicht blockiert, aber zu reduziertem Tumorwachstum geführt. Dieses reduzierte Tumorwachstum konnte auf eine reduzierte Zellproliferation zurückgeführt werden. Außerdem konnten wir durch die B-RAF Elimination eine Reduktion der Intensität der mitogenen Signalkaskade beobachten. Insgesamt deuten die Ergebnisse darauf hin, dass das onkogene Potential von C-RAF in vivo unabhängig von B-RAF ist und eine Kooperation von B-RAF und C-RAF jedoch für die vollständige Aktivierung der mitogenen Signalkaskade wichtig ist.

1. Introduction

1.1 Lung

1.1.1 Lung development

Mammalian lungs are branched networks containing thousands to millions of airways arrayed in intricate patterns that are crucial for respiration (Metzger, Klein et al. 2008). Lung development is divided into five distinct phases that are generally shared, but vary temporally and regionally among diverse vertebrate species (Maeda, Dave et al. 2007). In the mouse, lung organogenesis starts at embryonic day 9,5 (E9,5) and ends in postnatal age (PN) at about 21 days (PN21) (figure 1.1) (Greenlee, Werb et al. 2007) (Maeda, Dave et al. 2007).

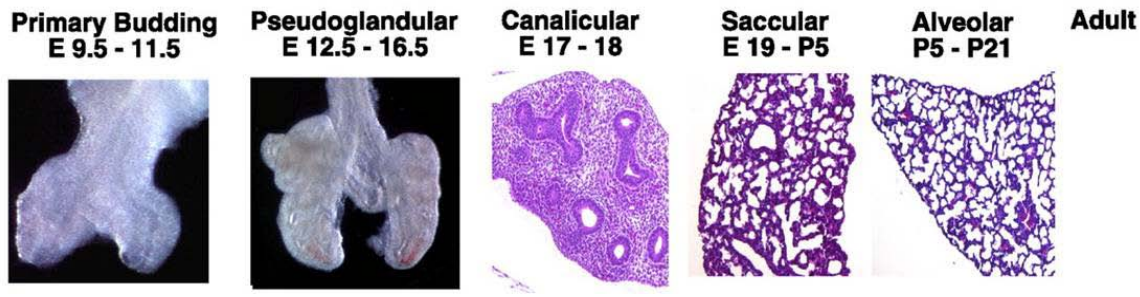

Figure 1.1 Mouse lung development. Five distinct stages of lung development: Primary Budding (E 9.5-11.5), Pseudoglandular (E 12.5-16.5), Canalicular (E 17-18), Saccular (E 19-P5) and Alveolar (P 5-21); E= embryonic, P= Postnatal (Greenlee, Werb et al. 2007).

In the primary budding phase, two lung buds appear on the ventral-lateral aspect of the foregut and evaginate into the splanchnic mesenchyme as the primordial trachea and the two main bronchi are formed. Moreover, the tracheal and bronchial salks extend to form the main bronchi (Maeda, Dave et al. 2007). In the

pseudoglandular phase the preacinar branching pattern of airways and blood vessels is established (Jeffrey 1998). Many transcription factors are required for the development of the early foregut and are also later utilized in lung morphogenesis and maintenance. Among these, for example, deletion of *Nkx2.1, Foxa2, Catnb, Sox17, Gata-6* and *Stat3* genes leads to failure of normal embryonic patterning even before lung formation (Ang and Rossant 1994) (Huelsken, Vogel et al. 2000) (Kanai-Azuma, Kanai et al. 2002) (Morrisey, Tang et al. 1998) (Takeda, Noguchi et al. 1997). Before E15, lung cells are relatively undifferentiated as defined by cell-specific markers used to identify epithelial cell types. During canalicular period the airways epithelium goes into differentiation, later on in saccular and alveolar phases, which mainly take place during postnatal maturation, septae are forming in the terminal sacs leading to the expansion of the gas-exchange surface (Cardoso and Lu 2006). The adult lung is a very complex organ that includes over 40 different cell types. The most studied pulmonary epithelial cells include Clara cells and Bronchio-Alveolar Stem Cells (BASCs) which are localized in trachea, bronchi and bronchioli, and Type I and Type II cells which are situated in the alveoli (Cardoso and Lu 2006). Type II cells secrete surfactant proteins such as SP-C which have a pivotal role in maintaining lung integrity and function. Moreover, Type II cells are the precursor of Type I pneumocytes which are the cells lining the alveoli (Cardoso and Lu 2006). The SP-C protein is not only expressed in alveolar Type II cells but also in a rare population of cells which are localized at the bronchio-alveolar duct-junction that also express the Clara cell-specific protein (CC10). It has been initially proposed that these cells are Bronchio-Alveolar Stem Cells (BASCs) that give rise to both bronchiolar and alveolar cells *in vivo* (Kim, Jackson et al. 2005). However, more

recent work using lineage-tracing strategy did not support the model in which BASCs function as stem cells to maintain the postnatal bronchioles. Furthermore, BASCs do not contribute significantly to the alveoli (Rawlins, Okubo et al. 2009).

1.1.2 Lung defense mechanisms

Pulmonary defense involves a wide and complex range of mechanisms that are necessary to remove inhaled particles and microorganisms. The first protection of the upper airways and bronchi is the nasopharyngeal anatomic barrier which efficiently prevents the penetration of particles or microorganisms bigger then 2–3 µm into the lower airways (Nicod 1999). The vast majority of particles bigger then 2–3 µm is collected on the mucus overlaying the ciliated epithelium (Nicod 1999). Many important elements contributing to lung defense for their bactericidal properties are included in the mucus. Among them are the secretory IgA, lysozyme, lactoferrin or peroxydases (Puchelle 1992). The mucociliary clearance is altered in many lung diseases such as asthma, chronic bronchitis or cystic fibrosis. Airway epithelial cells also actively participate in host defense mechanisms by secreting surfactant proteins, which play a pivotal role in innate and adaptive immunity (Wright and Churg 2006). SP-C for example has a major role in leukocyte trafficking and lung remodeling. Moreover, airway epithelial cells recruit immune cells by secreting various chemokines and cytokines such as GM-CSF, IL1ß, IL8, TNFα and IFNγ (Nicod 1999). In the absence of inflammation the lung epithelium includes a small fraction (~ 1%) of CD4 and CD8 T-lymphocytes. These cells are likely to play an important role in lung immunity where they react to pathogens in the absence of preliminary priming (Nicod 1999). Bronchus-associated lymphoid tissues (BALT), which are agglomerates of T- and B-

lymphocytes, were originally described as submucosal lymphoid organs, found along the bifurcations of the upper bronchi directly beneath the epithelium (Sminia, van der Brugge-Gamelkoorn et al. 1989). Although some species appear to develop BALT independent from antigenic stimulation (Pabst and Gehrke 1990), most normal mice and humans have little evidence of BALT (Tschernig and Pabst 2000). However, lung infection or inflammation in mice leads to the development of lymphoid follicles that are not restricted to the upper airways and are termed *inducible BALT* (*iBALT*) (Moyron-Quiroz, Rangel-Moreno et al. 2004). Also pulmonary macrophages have a key role in defense against respiratory infection and are very important in both innate and acquired immunity (Gordon and Read 2002). Due to their position in the alveolar lumen, resident alveolar macrophages are continuously entering in contact with inhaled substances (Lambrecht 2006). In order to avoid collateral damage to pulmonary cells in response to harmless antigens, macrophages are normally kept in a quiescent state by closely adhering to alveolar epithelial cells and by producing little inflammatory cytokines (Lambrecht 2006). Alveolar macrophages play a critical role in the pathophysiology of inflammatory lung diseases such as Chronic Pulmonary Disease (COPD) (Barnes 2004). Macrophage numbers are markedly increased in the airway spaces of patients with COPD and are localized at the sites of alveolar destruction (Barnes 2004). Moreover, alveolar macrophages of patients with COPD display and increased baseline and stimulated secretion of inflammatory proteins, including certain cytokines, chemokines and reactive oxygen species (Barnes 2004).

1.2 Chronic Obstructive Pulmonary Disease (COPD)

1.2.1 Histopathology of COPD

COPD is a group of lung diseases that cause obstruction of the airways. This results in a reduction of airflow both into, and out, of the lungs. COPD encompasses two groups of lung diseases: emphysema and chronic bronchitis. Emphysema is defined as an abnormal, permanent enlargement of the airspaces distal to the terminal bronchiole accompanied by destruction of their walls´ and ´without obvious fibrosis´ (Wright and Churg 2006). Chronic bronchitis is characterized by inflammation of the bronchi which is accompanied by alteration of the epithelium with goblet cell hyperplasia and metaplasia coupled with an increase in fibrotic tissue and smooth muscles (Wright and Churg 2006).

According to the World Health Organization, COPD is the fourth leading cause of death in the world, with approximately 2.75 million deaths each year (Raherison and Girodet 2009). The projection for 2020 indicates that COPD will be the third leading cause of death worldwide (Raherison and Girodet 2009). There are currently no cures for COPD and no ways to reverse the damage to the airways and lungs that has already occurred.

1.2.2 COPD and lung cancer

In the mid-1980s, two groups independently demonstrated that lung cancer incidence increased in individuals with COPD (Tockman, Anthonisen et al. 1987) (Skillrud, Offord et al. 1986). However, it is difficult to imagine common molecular mechanisms between two diseases that seem to be diametrically opposed. COPD is specified by inflammation-mediated destruction of the extracellular

matrix, whereas lung cancer is characterized by an uncontrolled cell proliferation (Houghton, Mouded et al. 2008). In the past decades, very little has been done to explore the link between these two diseases. Nevertheless, by use of computer tomography chest imaging researchers could show that just the presence of emphysema predisposes an individual to lung cancer (de Torres, Bastarrika et al. 2007) (Wilson, Weissfeld et al. 2008). These important clinical findings will require new mechanistic hypothesis and molecular models to understand the connections between these related pathologies (Houghton, Mouded et al. 2008).

One hypothesis considers that the inflammation and the body´s attempt to repair emphysematous airspaces might link these diseases. Emphysema starts when inhaled particles, contained in cigarette smoke, induce a mild lung inflammation associated with matrix-degrading proteinases such as elstases (Shapiro 2005). Cell death is the first consequence of the tissue destruction caused by these proteinases (Shapiro 2005). Moreover, inflammatory cells like macrophages and neutrophils can at this site secrete pro-tumorigenic factors (Coussens, Tinkle et al. 2000). In the same time, it is likely that progenitor cells are under constant pressure to proliferate and repair the chronic damaged areas of the lung (Houghton, Mouded et al. 2008). However, it could be that in this carcinogen-rich, inflammatory milieu, one of these progenitor cells start to proliferate in an uncontrolled manner and then give rise to lung cancer (Houghton, Mouded et al. 2008). In line with this hypothesis, it has been shown that in COPD patients the corticosteroids-mediated inhibition of inflammation reduced the lung cancer incidence (Houghton, Mouded et al. 2008).

1.3 Lung cancer

1.3.1 Histopathology of lung cancer

Lung cancer is the first cause of cancer related death worldwide. During the past 20 years many efforts have been made to reduce the mortality of lung cancer patients (Carney 2002). Traditional treatments comprise surgery, radiotherapy, chemotherapy or most often a combination of those. Recently, small molecule inhibitors and monoclonal antibodies have been developed to specifically target key molecules in cancer initiation and progression. However, despite all improvements, patients are usually diagnosed at late stages and therefore the five-year survival rate is less than 15% (Carney 2002).

Based on size and morphology of the cells, lung cancer has been divided into two major categories: Small Cell Lung Cancer (SCLC) and Non-Small Cell Lung Cancer (NSCLC). SCLC accounts for ~20% of lung cancer and arises from neuroendocrine cells. NSCLC, which account for ~80% of lung cancer, originates from epithelial cells and it is divided into four subcategories: Squamous cell carcinoma, Adenocarcinoma, Bronchioalveolar carcinoma and Large-cell undifferentiated carcinoma (Brambilla, Travis et al. 2001). Adenocarcinoma, which account for 30-40% of NSCLC, is the most common type of lung cancer (Brambilla, Travis et al. 2001).

1.3.2 Genetic of lung cancer

Molecular genetic studies have demonstrated that lung cancer tissues display multiple genetic and epigenetic abnormalities, including DNA sequence alterations, copy number changes, and aberrant promoter hypermethylation

(Sato, Shames et al. 2007). The most frequent aberrations found in human NSCLC and SCLC are reported in the Table 1.1 [modified from (Meuwissen and Berns 2005)].

Gene	Aberration	NSCLC frequency	SCLC frequency
MYC	Amplification	5%-20%	20%-35%
RAS	Mutations	15%-20%	<1%
EGFR	Mutations	20%	-
INK4a	LOH	70%	50%
$p16^{INK4a}$	Mutations	20%-50%	<5%
$p14^{ARF}$	Mutations	20%	65%
TP53	LOH	60%	75%-100%
TP53	Mutations	50%	75%
RB	LOH	30%	70%
RB	Mutations	15%-30%	90%
FHIT	Mutations	40%	80%
TSG101	Mutations	-	90%
DMBT1	Mutations	40%-50%	100%
LOH in various regions (3p, 4p, 4q, 8p)	LOH	10%-100%	50-100%
INK4a	Promoter Hm.	8%-40%	ND
RARβ	Promoter Hm.	40%	70%
RASSF1A	Promoter Hm.	30%-40%	90%-100%
CDH1	Promoter Hm.	55%	ND

Table 1.1. Major genetic aberrations in human NSCLC and SCLC (LOH indicates loss of heterozygosity, Hm.= hypermethylation, ND= not determined).

Notably, the Ras-mitogen-activated protein kinase (MAPK) pathway is deregulated in 50% of human lung cancer and the *Ras* GTPase is one of the most frequently mutated gene in NSCLC (Forbes, Bindal et al. 2011) (Ding, Getz et al. 2008).

1.4 Developmental syndromes of cancer related genes

RAS genes are well-studied cancer-related genes due to their frequent activation in human cancers and play a central role in the MAPK signaling cascade, which has a pivotal role in cell proliferation, differentiation, survival, and cell death (Barbacid 1987) (Malumbres and Barbacid 2003) (Giehl 2005). Studies on RAS and its downstream targets have been mainly focused on their role in tumor development although the function of the wild type form of these genes in humans has not been well elucidated. Recently, germline mutations in *H-RAS* and *K-RAS* and in genes encoding other molecules in the Ras–RAF–MEK–ERK cascade were shown to underlie cases of Noonan, Costello syndromes and Cardio-facio-cutaneous syndrome (CFC) (Table 1.2) (Schubbert, Bollag et al. 2007) (Tidyman and Rauen 2009).

Syndrome	MAPK pathway gene	Protein
Noonan	PTPN11	SHP2
	SOS1	SOS1
	RAF1	C-RAF
	KRAS	KRAS
Leopard	PTPN11	SHP2
	RAF1	C-RAF
Costello	HRAS	HRAS
CFC	B-RAF	B-RAF
	MAP2K1	MEK1
	MAP2K2	MEK2
	KRAS	KRAS

Table 1.2. Genetic syndromes of the Ras/MAPK pathway [modified from (Tidyman and Rauen 2009)].

These syndromes are autosomal dominant multiple congenital anomaly syndromes characterized by a distinctive facial appearance, heart defects, musculocutaneous abnormalities, and mental retardation (Schubbert, Shannon et al. 2007). Notably, although many of the mutated genes encode for proteins with an increased kinase activity, malignant tumors are relatively uncommon in patients affected by these disorders (Schubbert, Shannon et al. 2007).

1.5 The MAPK cascade

1.5.1 Ras/RAF-signalling

The MAPK pathway is a key signalling pathway that is involved in the regulation of normal cell proliferation, survival, growth, differentiation, and apoptosis (Roberts and Der 2007) (Robinson and Cobb 1997) (Wellbrock, Karasarides et al. 2004). Mutations or over expression of the components of this signalling network are hallmark of several human cancers and other human diseases (Roberts and Der 2007).

As described in the figure 1.2 (Rapp, Fensterle et al. 2003), the binding of growth factors and/or hormones to cell-surface receptor tyrosine kinases and G-protein-coupled receptors, respectively, leads to Ras activation (McCubrey, Steelman et al. 2007). This initiates membrane recruitment and activation of RAF, which leads to the activation of the dual-specificity mitogen-activated protein kinase (MAPK) and extracellular signal-regulated kinase (ERK) kinases (MEK) 1 and/or MEK2 and, subsequently, ERK1 and/or ERK2 (Wellbrock, Karasarides et al. 2004). The

ERKs have many cytosolic and nuclear substrates (Wellbrock, Karasarides et al. 2004).

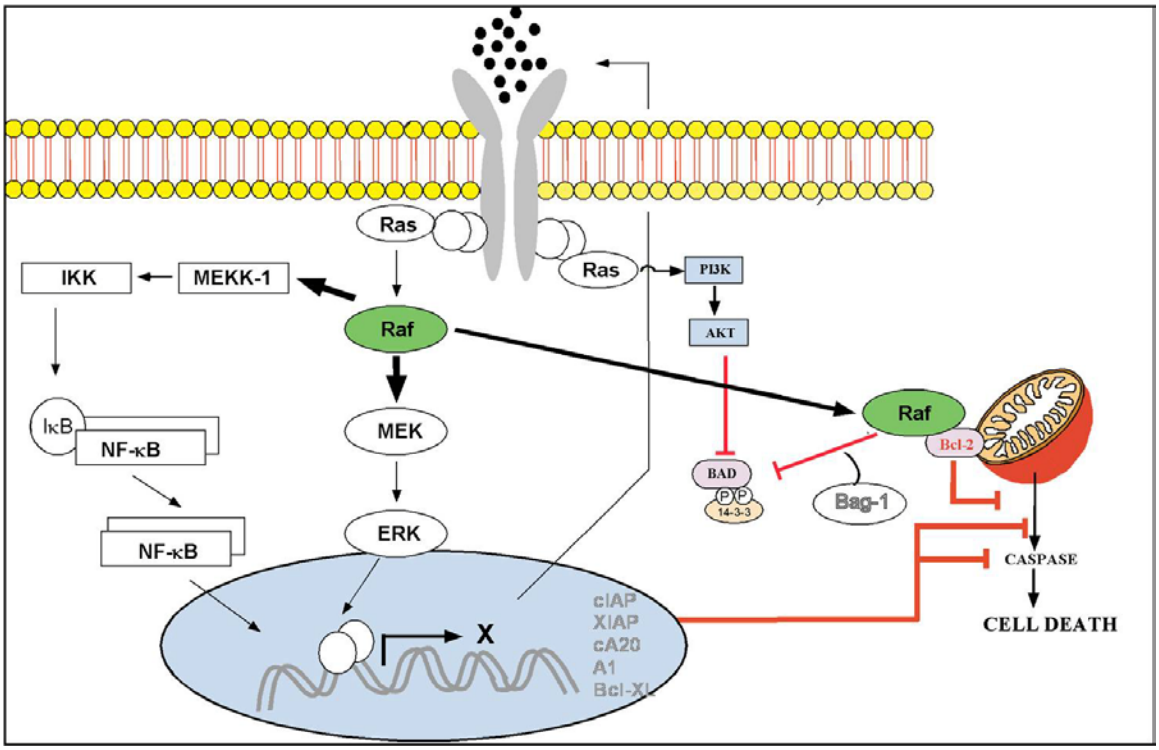

Figure 1.2. Overview of the Ras/MAPK pathway (Rapp, Fensterle et al. 2003).

Although the Ras/MAPK pathway is traditionally drawn as a linear, unidirectional cascade of protein kinases, the more appropriate depiction of this cascade is that it is a key core element of a complex signalling network, with many other interactions (Kolch 2005). RAF proteins have, indeed, different MEK/ERK independent functions. RAFs have been shown to inhibit apoptosis by interacting with proteins localized at mitochondria such as Bcl-2 and BAD (Wang, Rapp et al. 1996) (Panka, Wang et al. 2006) (Kebache, Ash et al. 2007) (Polzien, Baljuls et al. 2009) (Polzien, Baljuls et al.). Moreover, RAFs stimulate survival programs by activating the NFkB pathway through interaction with the membrane shuttle kinase MEKK1 (Li and Sedivy 1993) (Baumann, Weber et al. 2000).

1.5.2 RAF isoforms

Lower organisms, like *Drosophila melanogaster* or *Caenorhabditis elegans* have only one *RAF* gene, mammals have instead three functional *RAF* genes (*A*-, *B*- and *C-RAF*) (Galabova-Kovacs, Kolbus et al. 2006). B-RAF is the most similar to the RAFs of lower organisms (Galabova-Kovacs, Kolbus et al. 2006). Although they differ in size and for basal enzymatic activity all RAFs contain three highly conserved regions (figure 1.3) (Wellbrock, Karasarides et al. 2004) (Baljuls, Schmitz et al. 2008). The first two (CR1 and CR2) conserved regions are localized in the N terminus, the third (CR3) in the C terminus where also the kinase domain is localized (Wellbrock, Karasarides et al. 2004).

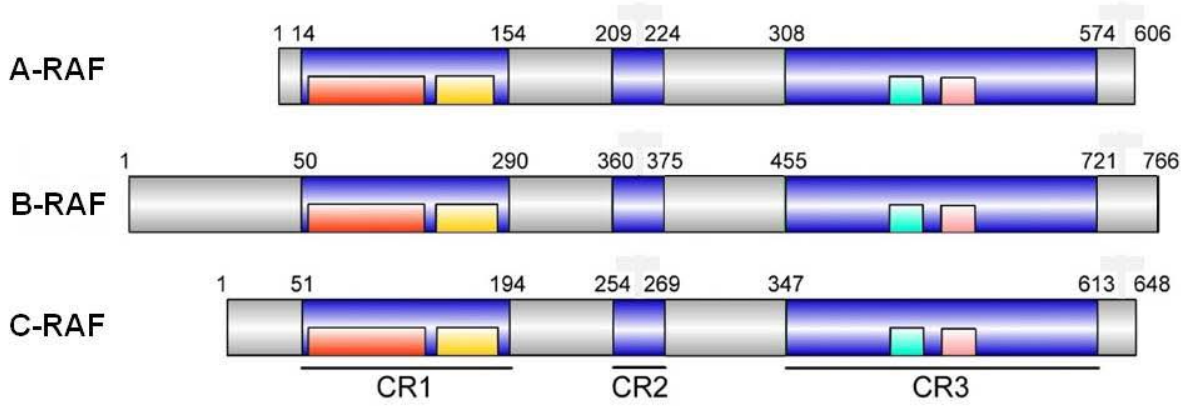

Figure 1.3. Schematic representation of human RAF kinases [modified from (Baljuls, Schmitz et al. 2008)]. A-, B- and C-RAF share three highly conserved domains (blue). In the CR1 region are situated the Ras binding domain (red) and the cysteine-rich domain (yellow) which are necessary for membrane recruitment. The CR2 domain is another important regulatory domain which contains a 14-3-3 binding site. The CR3 domain contains the catalytic domain that includes the MEK binding site (light blue) and the activation segment (pink) (Baljuls, Schmitz et al. 2008).

Genetic studies of mice with inactivated *Raf* genes have shown that Raf proteins signal non-redundant functions during development (Pritchard, Bolin et al. 1996) (Wojnowski, Zimmer et al. 1997) (Wojnowski, Stancato et al. 1998) (Mikula, Schreiber et al. 2001). *A-raf -/-* mice survive to birth but they die after 7-21 days due to gastrointestinal and neurological defects (Pritchard, Bolin et al. 1996). *B-raf -/-* and *c-raf -/-* embryos die between day 10.5 and 12.5 days post-coitum. *B-raf -/-* embryos show vascular defects with endothelial cell death and growth retardation (Wojnowski, Zimmer et al. 1997). *C-raf -/-* embryos are growth retarded and die at midgestation with anomalies in the placenta and in the fetal liver caused by massive apoptosis of hepatocytes (Mikula, Schreiber et al. 2001).

The activity of RAF protein kinases is tightly regulated by multiple phosphorylation events to direct ERK MAPK signalling to distinct subcellular compartments in response to growth factor stimulation (Nekhoroshkova, Albert et al. 2009). The formation of RAFs homo- and heterodimers, that is necessary for kinase activity, is mainly mediated by scaffold proteins such as 14-3-3 and Kinase-Suppressor-of-Ras (KSR) (Roskoski 2010).

1.5.3 RAF and cancer

The first *Raf* gene was described as retroviral oncogene, *v-raf*, transduced by a murine sarcoma virus (Rapp, Goldsborough et al. 1983). This transforming retrovirus encoded the first oncogene with serine/threonine kinase activity (Moelling, Heimann et al. 1984). After the cellular proto-oncogene homologs, C-raf and the other RAF isoforms, had been cloned, the majority of the studies focused on elucidating the function of RAF proteins. For almost two decades research concentrated on RAF proteins as the critical effector of Ras (Matallanas,

Birtwistle et al. 2011). Recently, this changed when B-RAF mutations were found in several human cancers, particularly melanoma (30–60%), thyroid cancer (30–50%), colorectal cancer (5–20%) and ovarian cancer (~30%), but also at a low frequency (1–3%) in a number of other cancers (Davies, Bignell et al. 2002).

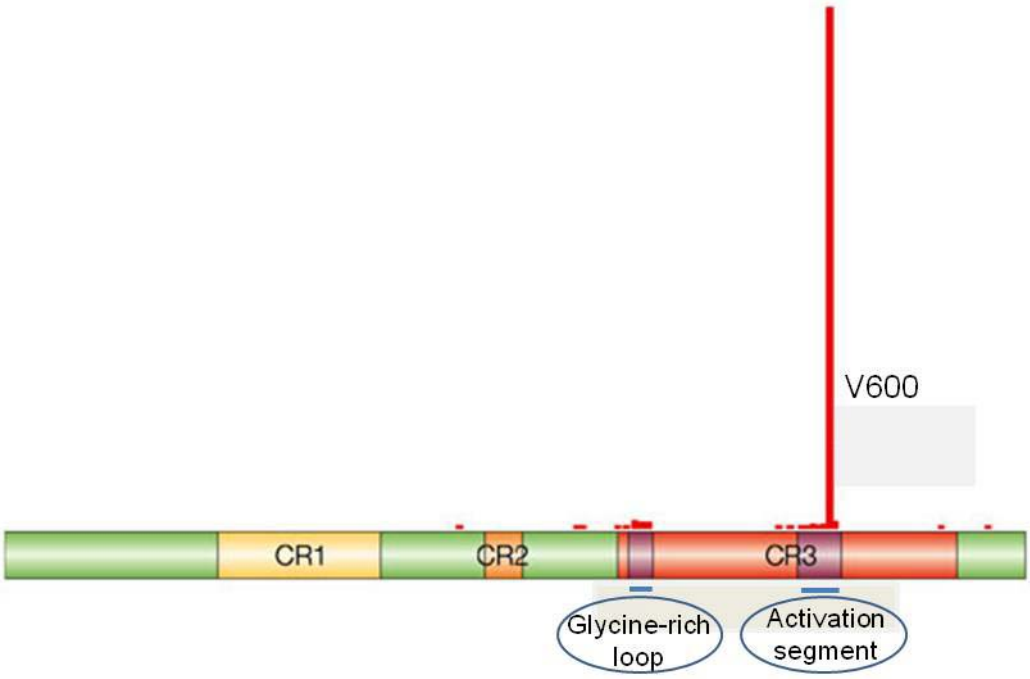

Figure 1.4. Schematic representation of the human B-RAF kinase with its mutations [modified from (Wellbrock, Karasarides et al. 2004)]. The majority of B-RAF mutations are localized in the kinase domain (C3). In the C3 domain there are two main clusters of mutations: one in the Glycine-rich loop, the other in the Activation-segment where the V600 aminoacid is situated. The V600 is the most frequently mutated B-RAF site.

The majority of mutations are single non-sense substitutions that render the kinase constitutively active (Davies, Bignell et al. 2002). ~90% of all B-RAF mutations consist of a single substitution of a valine residue at position 600 for glutamic acid (figure 1.4) (Davies, Bignell et al. 2002) (Wellbrock, Karasarides et al. 2004). The B-RAF V600E mutant, which is the most important human RAF

oncogene, display a 700 fold increased kinase activity compared to the wild type B-RAF (Wan, Garnett et al. 2004). In regard to the other RAFs, detailed analysis of the mutational status of *A-RAF* and *C-RAF* in several cancer cell lines and primary human samples showed that mutations in these *RAF* genes are very rare or nonexistent events (Fransen, Klintenas et al. 2004) (Lee, Soung et al. 2005) (Emuss, Garnett et al. 2005).

Although point mutations are the most common, *RAF* genes can be mutationally activated by chromosome translocations, as observed in thyroid cancer and pilocytic astrocytoma (Ciampi, Knauf et al. 2005) (Jones, Kocialkowski et al. 2008) (Jones, Kocialkowski et al. 2009). More recently, Palanisamy *et al.* identified chromosomal translocations involving either B- or C-RAF in a small percentage of prostate and gastric cancers and melanoma (Palanisamy, Ateeq et al. 2010) (McMahon 2010). Notably, these gene fusions encode for RAF proteins retaining the kinase domain but losing the N-terminal RAS-binding domain, suggesting that the mutant proteins may be constitutively active (Palanisamy, Ateeq et al. 2010).

1.5.4 RAFs driven mouse lung tumor models

In recent years, several mouse models have been developed to establish a causal relationship between MAPK mutations found in human lung cancer and tumor development (Karreth and Tuveson 2009). These models have contributed significant insights into the mechanisms of tumor formation and progression and are indispensable tools for preclinical testing of new therapeutic drugs (Schreck and Rapp 2006).

The first transgenic lung tumor models expressing RAF kinases were established in our lab by overexpression of wild type or constitutive active C-RAF (C-RAF BxB) under the control of the human Surfactant Protein-C promoter in lung alveolar epithelial type II cells (Kerkhoff, Fedorov et al. 2000). All mice expressing oncogenic C-RAF BxB develop benign adenomas within two weeks of age (Kerkhoff, Fedorov et al. 2000) (Rapp, Korn et al. 2009). RAF-induced lung tumors expand continuously without any sign of apoptosis (Schreck and Rapp 2006) (Kerkhoff, Fedorov et al. 2000) and are highly dependent on MEK activity as treatment of mice with the CI-1040 (MEK) inhibitor led to reduced lung adenoma formation (Kramer, Gotz et al. 2004). More recently, based on the occurrence of B-RAF V600E mutations in NSCLC patients, many efforts were made to evaluate the role of this type of B-RAF mutation (B-RAF V600E) in lung tumor initiation and progression using mouse models. One of these models employed a knock-in strategy in which the oncogenic B-RAF allele is activated by infection of lungs with adenovirus expressing Cre-recombinase (Dankort, Filenova et al. 2007). These mice developed benign neoplastic adenomas in the lung that show some signs of senescence in the course of disease progression. However, in this study the tumor-initiating cell could not be identified due to the promiscuous target cell specificity of the activating virus (Dankort, Filenova et al. 2007). In a second study Ji et al. used an inducible rat specific CCSP promoter that targets both bronchiolar Clara cells as well as a fraction of type II cells (Perl, Wert et al. 2005) for expression of B-RAF V600E. However, lung tumor formation in this model was only achieved in an *Ink4A/Arf*-/- background (Ji, Wang et al. 2007).

1.6 Experimental design and aim of the project

1.6.1 Lung-targeted expression of oncogenic B-RAF V600E

Tissue- or cell-type-specific promoters allow restriction of the expression of the gene of interest to a tissue type in which the gene is known or suspected to be involved in transformation. In this project we aimed to evaluate the role of B-RAF V600E in lung tumor initiation and progression *in vivo*. For this purpose we have generated a novel transgenic mouse in which we have employed the Surfactant Protein C (SP-C) promoter to drive B-RAF V600E expression in epithelial type II pneumocytes, hypothetical cells of origin of NSCLC (figure 1.5). Using a similar strategy we have previously shown that lung alveolar type II cells respond to oncogenic C-RAF mediated activation of the mitogenic cascade with benign adenoma formation in the absence of additional genetic lesions (Kerkhoff, Fedorov et al. 2000).

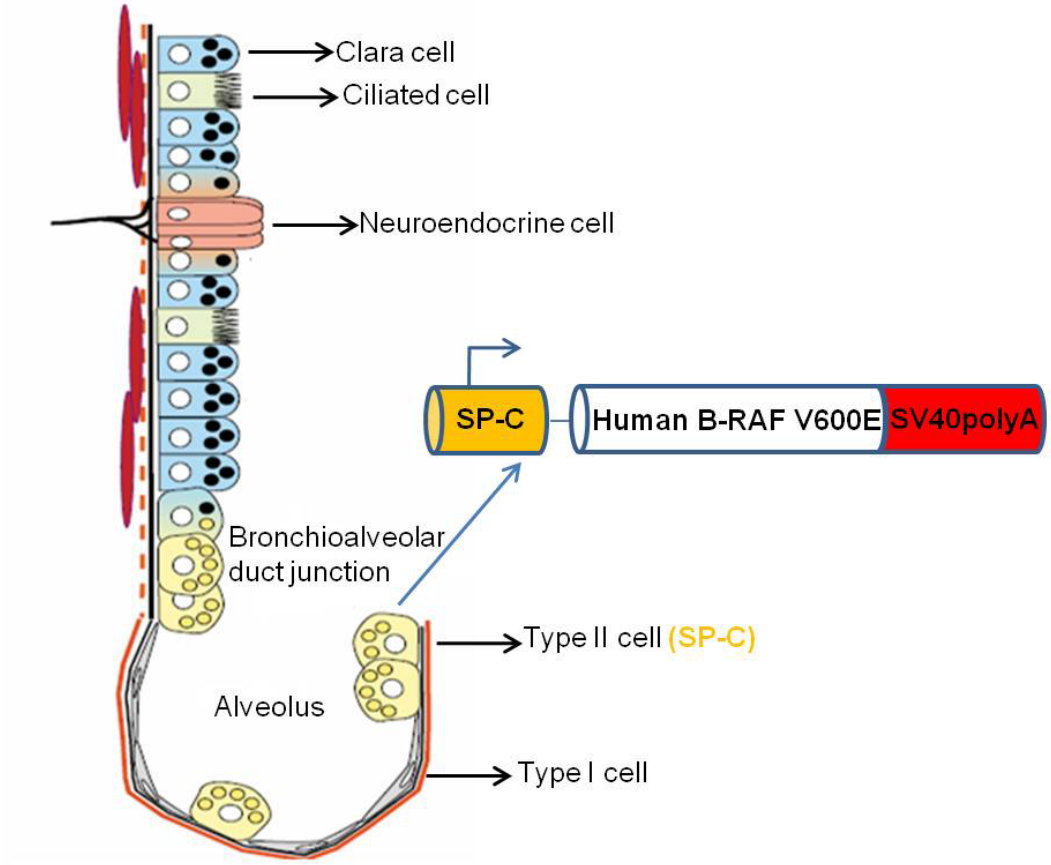

Figure 1.5. Experimental strategy for lung-targeted expression of B-RAF V600E [modified from (Rawlins and Hogan 2006)]. Cartoon of a distal lung with a schematic representation of the targeting vector in which the Surfactant Protein C (SP-C) promoter drives the expression of oncogenic B-RAF V600E in alveolar epithelial type II cells.

1.6.2 Elimination of B-RAF in a mouse model for NSCLC

Conditional gene-targeting technology, in conjunction with regulatable systems, enables gene deletion in tissues of interest at specific times and eliminates concerns about potential embryonic lethality (O'Hagan, Wu et al. 2005). This analysis can be limited to selected tissues with appropriate engineering of the gene-targeting system (O'Hagan, Wu et al. 2005). Such knockout models can be interbred with cancer models to determine whether conditional gene deletion prevents tumor formation, inhibits progression, or causes regression of established tumors (Zambrowicz and Sands 2003).

Our lab has previously generated a mouse model for lung tumor development by expressing in type II pneumocytes an oncogenic N-terminal deleted form of C-RAF (C-RAF BxB**)** (Kerkhoff, Fedorov et al. 2000). *In vitro* experiments have shown that B-RAF constitutively heterodimerize with C-RAF BxB by targeting its kinase domain and by activating it in the cytoplasm (Weber, Slupsky et al. 2001) (Garnett, Rana et al. 2005). Thus, B-RAF might be an important factor for the oncogenic activity of C-RAF BxB. In this project, we aimed to evaluate *in vivo* whether B-RAF is necessary for the transformation and/or growth of C-RAF BxB-driven lung tumors. However, as already described, *b-raf -/-* mice die between embryonic day 11.5 (E11.5) and E12.5. Therefore, our laboratory has generated floxed-B-RAF mice to conditionally knock-out B-RAF in a tissue specific and in a time dependent manner. Conditional inactivation of B-RAF in lung tumors expressing oncogenic C-RAF was carried out by doxycyclin-induction of quadruple transgenic mice *SpC-C-RAF BXB23/SpC- rtTA/Tet-O-cre/B-RAF* $^{flox/flox}$ (figure 1.6).

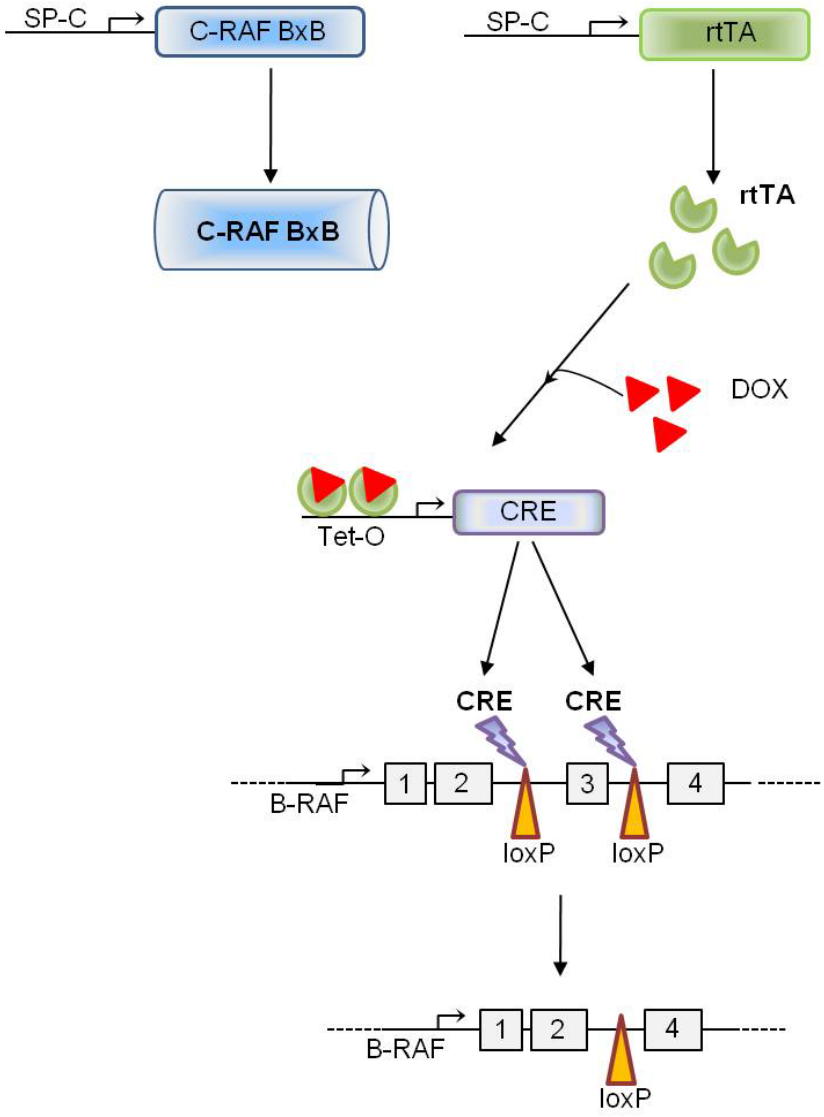

Figure 1.6. Experimental strategy for conditional elimination of B-RAF in C-RAF BxB mediated lung tumors. In this system the SP-C promoter, which is active in type II cells, drives expression of both oncogenic C-RAF and the reverse tetracycline-controlled transcriptional activator (rtTA). When doxycyclin (DOX) is present the rtTA binds to the tetracycline response element (Tet-O) that leads to CRE-loxP-mediated deletion of the exon 3 of B-RAF and therefore absence of B-RAF protein.

2. Results (Lung-targeted expression of oncogenic B-RAF V600E)

2.1 Generation of transgenic mice with lung-targeted expression of B-RAF V600E

2.1.1 Construction of SpC-B-RAF V600E plasmid

SpC-B-RAF V600E plasmid was generated by releasing the 2,5 Kb human B-RAF V600E cDNA from pKS-h B-RAF V600E (unpublished) by digestion with *NotI* restriction enzyme and inserted into SPC/SV40 plasmid (kindly obtained from Jeffrey Whitsett) that was previously digested with *Bam HI* endonuclease (figure 2.1). Prior to ligation, both vector and insert were blunt-ended with T4 DNA polymerase.

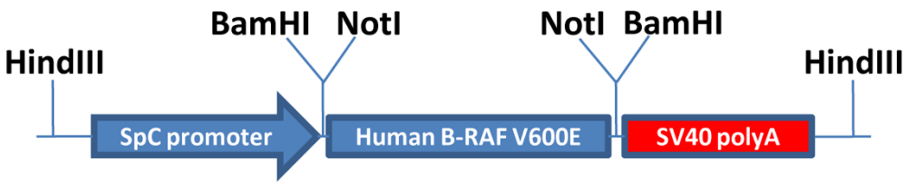

Figure 2.1. Schematic representation of the SpC-B-RAF V600E targeting vector.

Correct orientation of the insert was tested by digestion with *XhoI* and *SalI* endonucleases and gel electrophoresis analysis. SpC-B-RAF V600E expression cassette (6,2 Kb) was resolved in a low melting agarose gel after digestion with *Hind III* restriction enzyme. The purified fragment was then injected into the

pronucleus of fertilized eggs of FVB/n mice. Dr. Rudolf Götz constructed the SpC-B-RAF V600E plasmid. Hildegard Troll carried out the pronuclear injection.

2.1.2 Generation of SpC-B-RAF V600E transgenic mice

We have generated three transgenic mouse founders for the expression of human B-RAF V600E under the control of the human SpC promoter. SpC-B-RAF V600E transgenic mice were born in the expected mendelian ratios, were fertile and did not show any gross morphological or behavioral abnormalities. Analysis of transgene expression levels among the founders showed comparable results (figure 2.2).

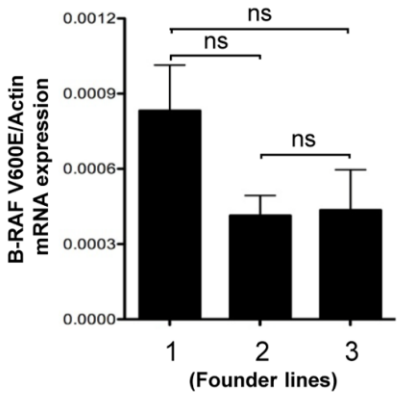

Figure 2.2. Comparable levels of B-RAF V600E transgenic expression in the lung of the transgenic mouse founders. Analysis of B-RAF V600E mRNA levels between the founders (2 weeks old) by Real-time PCR, data represent mean + SEM, (*t*-test ns= not significant, *n*= 3).

Histopathological analysis of lung sections from adult mice revealed airspace enlargements with various degrees in all the founders compared to control animals (figure 2.3). Interestingly lung tumor formation was not detected in any of

these founders (figure 2.3). Based on the highest penetrance of alveolar enlargements, we have selected the founder line number 3 for further studies.

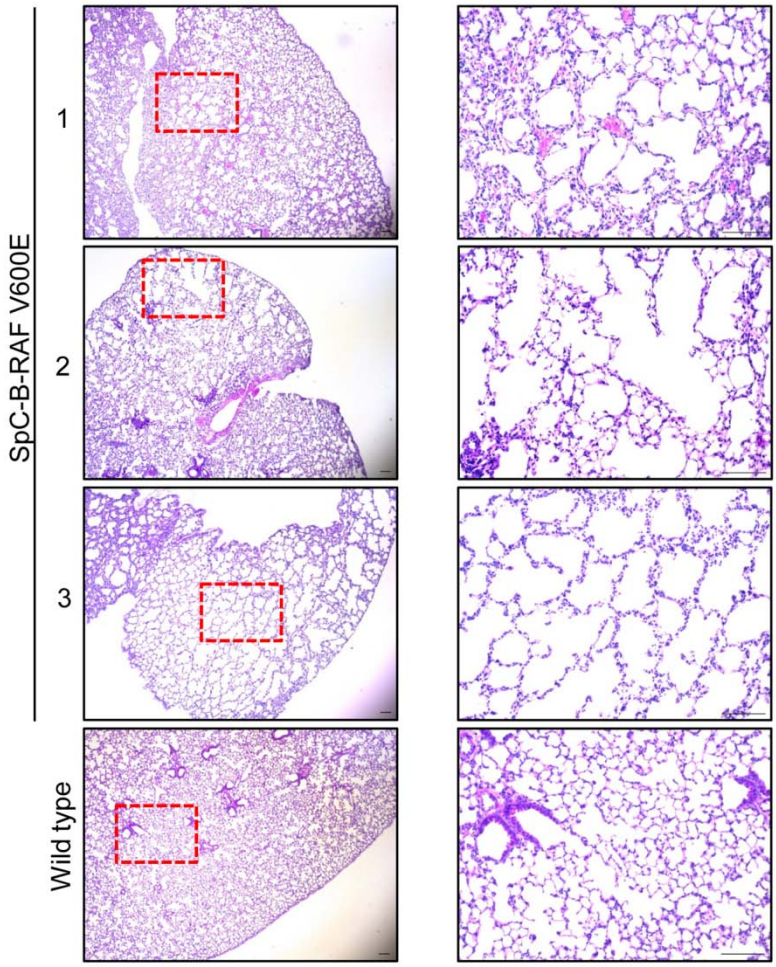

Figure 2.3. Comparable formation of alveolar enlargements in SpC-B-RAF V600E transgenic founder lines. Representative paraffin embedded H&E stained lung sections from wild type and transgenic mice (2 months old), right panel pictures are high magnification of the red inserts, scale bar = 100 µm.

2.2 Characterization of SpC-B-RAF V600E transgenic mice

2.2.1 Expression of B-RAF V600E in alveolar type II cells leads to airway enlargements in mice

Consistent with the early expression of the transgene (figure 2.4A), we found airspace enlargements in the embryonic lung sections (figure 2.4B) that persisted in both post-natal and adult lungs of the transgenic animals (figure 2.4B). Some of these alveolar disruptions increased in size over time forming macroscopic air-filled structures reminiscent of human bullous-emphysema (figure 2.4B-2.4C). The presence of these lesions affected the life span of animals (figure 2.4D).

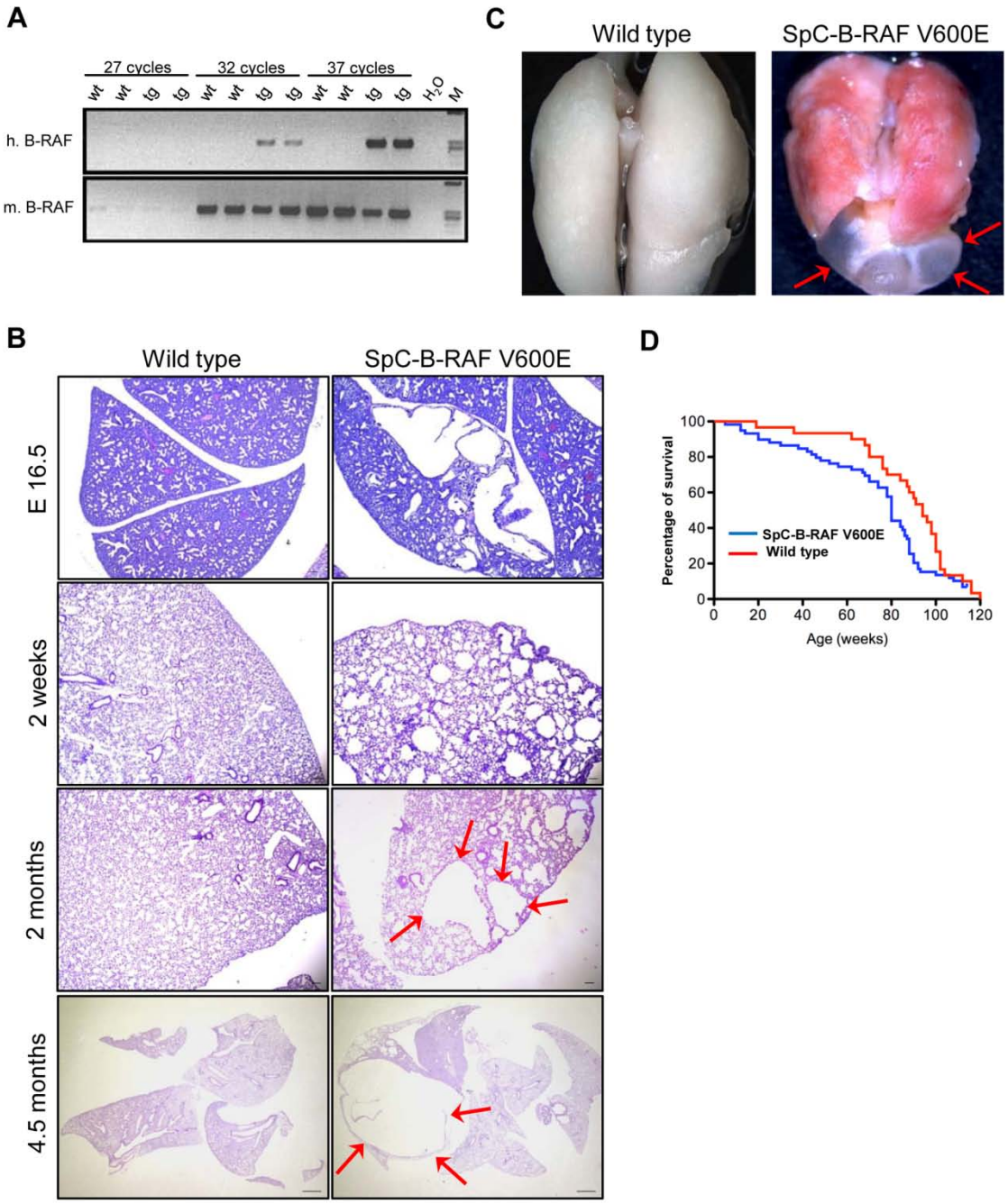

Figure 2.4. Induction of airspace enlargements in mice with targeted expression of mutant B-RAF (V600E) in lung alveolar type II cells. (A) Semi-quantitative RT-PCR using species-specific primers shows transgenic- and endogenous- B-RAF expression in lungs of two wild type and transgenic embryos (E16.5), (cycles=PCR cycle; M=marker; h=human; m=mouse). (B) Paraffin embedded hematoxylin and eosin (H&E) stained lung sections from mice of different ages show airspace enlargements (arrows) in transgenic animals, (scale bar = 100 μm for the first, second and third panel; 1 mm for the forth panel). (C) Whole lung photographs of 4.5 months old wild type and transgenic mice

show macroscopic blebs (arrows). (D) Kaplan-Meier survival curves, (log-rank analysis $P < 0.05$; SpC-B-RAF V600E $n = 59$; wild type $n = 30$).

For analysis of airspace enlargements, lungs from wild type and SpC-B-RAF V600E transgenic mice were evaluated blindly by two independent examiners. Tissue samples were graded in the following manner: 1) Micro- and macroscopically normal; 2) Macroscopically normal, but microscopically abnormal [airspace enlargement]; 3) Macroscopic abnormalities [bulb formation] (figure 2.5A). From all animals analyzed, only ~50% of SpC-BRAF V600E transgenic mice displayed grade 2 and grade 3 lesions (~25% each group), respectively (figure 2.5A-2.5B). The lungs of all wild type mice analyzed were graded as 1(figure 2.5A-2.5B). However, ~50% of the transgenic mice analyzed were apparently similar to wild type (figure 2.5A-2.5B). All immunohisopathological analysis that will be described in the following chapters were performed on lung sections of transgenic animals carrying grade 2 and grade 3 lesions.

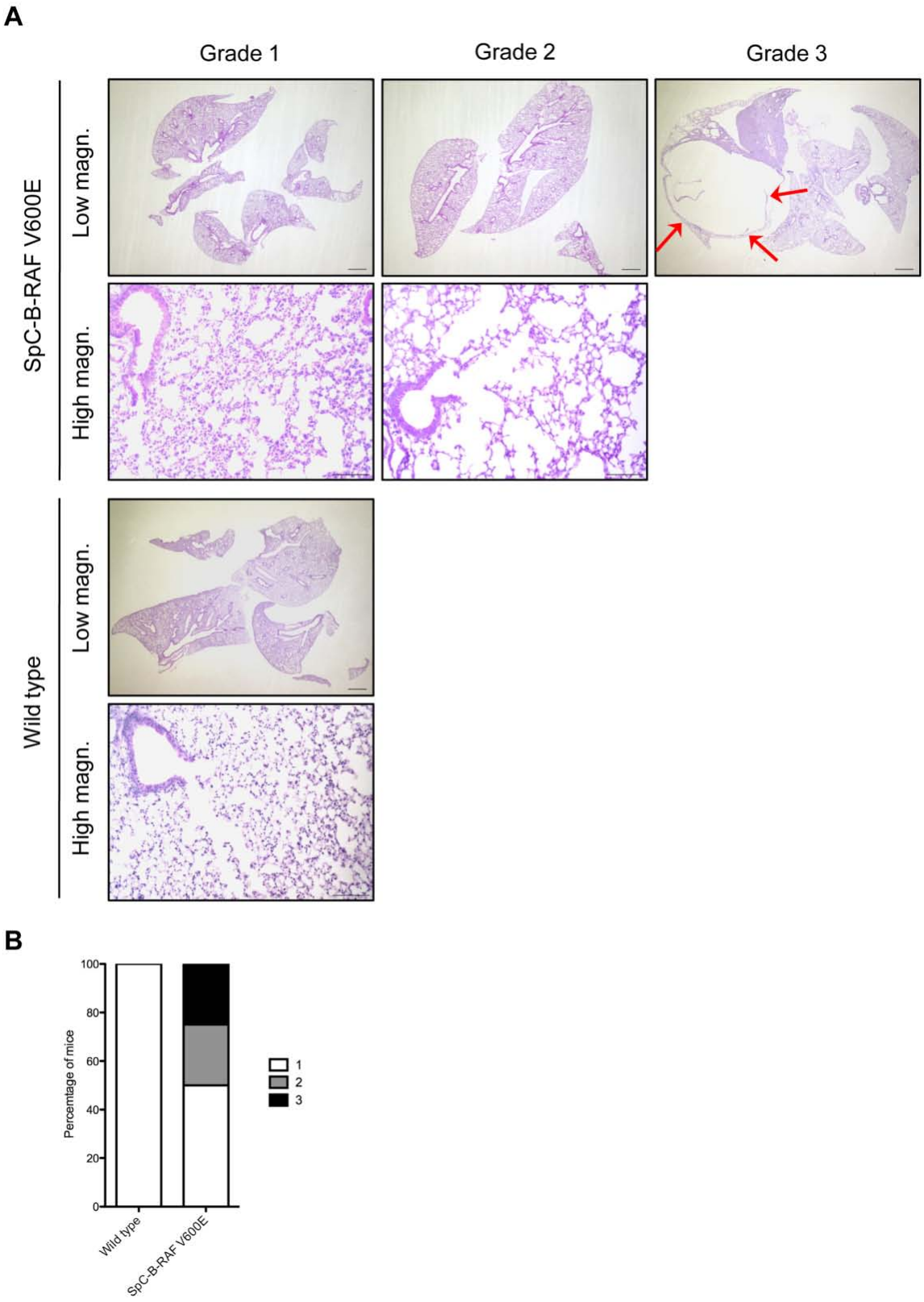

Figure 2.5. Scoring of B-RAF V600E induced lung lesions in transgenic mice. (A) Representative pictures of H&E stained lung sections from wild type and transgenic mice show airspace enlargements with different grades. The scoring was performed as

follows: 1) Micro- and macro-scopically normal**;** 2) Macroscopically normal, but microscopically abnormal [airspace enlargement]; 3) Macroscopic abnormalities [bulb formation, pointed by arrows]. Scale bar= 1 mm for low magn. and 100 μm for high magn. pictures. (B) Incidence of the lung lesions with different grades, (*n*=59 for wild type, *n*=102 for SpC-B-RAF V600E).

2.2.2 Increased apoptosis and absence of MAPK signaling activation

To characterize the observed defect in lung development at the molecular and cellular level, we first examined the apoptotic and proliferative rate of the lung epithelium. We therefore screened lung sections from SpC-B-RAF V600E transgenic mice of different ages for apoptosis and proliferation markers. We found increased active caspase 3 staining in lung sections from transgenic mice only at postnatal day 1 (figure 2.6A-2.6B). There was no change in cell proliferation assessed by Ki67 immunostaining at this age (figure 2.6C-2.6D). However we found a significant increased in cell proliferation in lungs of transgenic mice at postnatal day 14 (figure 2.6C-2.6D).

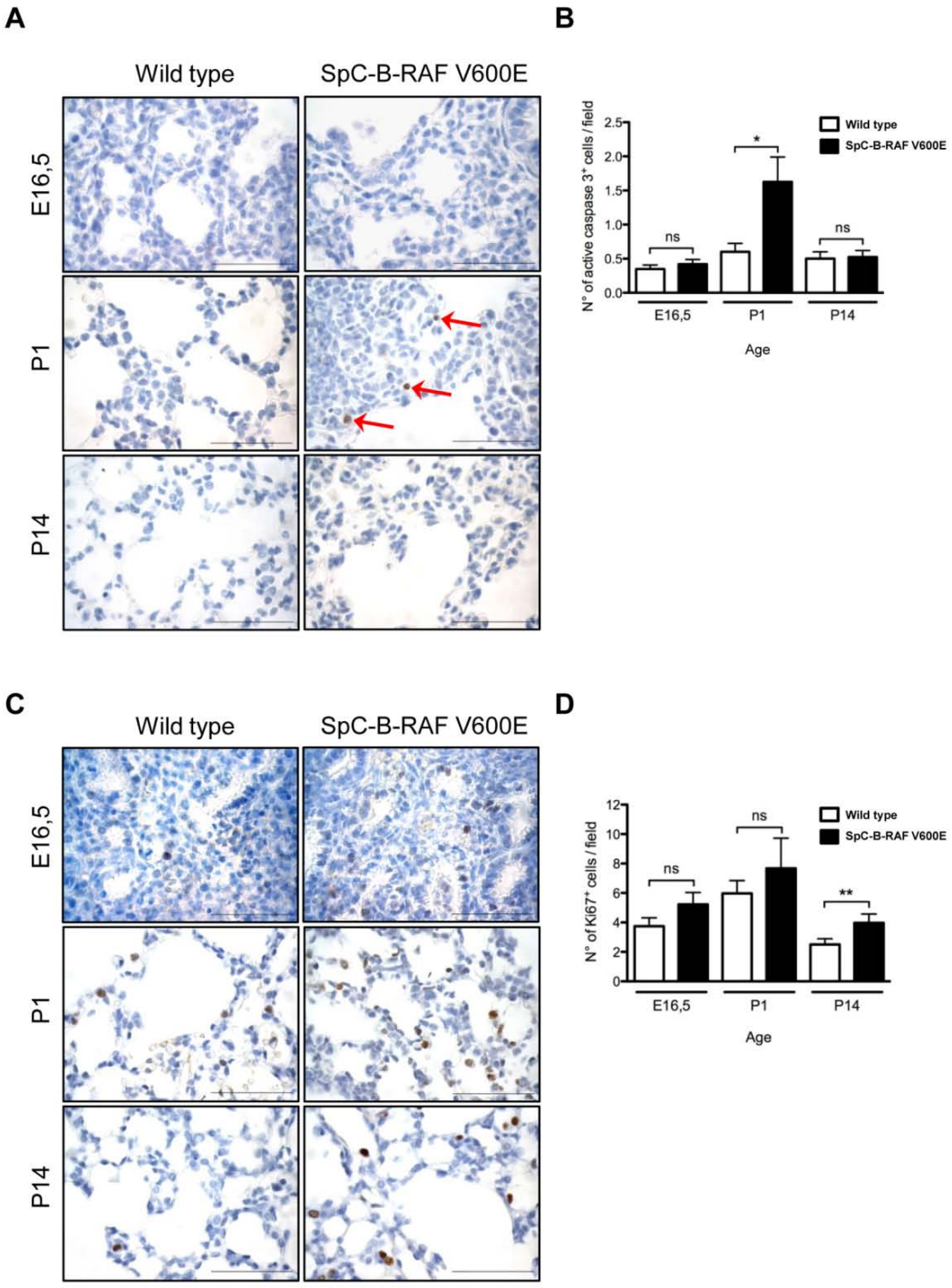

Figure 2.6. Analysis of cell death and cell proliferation in transgenic mice. (A) Active caspase 3 staining of control and transgenic animals, (arrows indicate positive cells), (E= embryonic, P=post-natal), (hematoxylin was used as a counterstain); scale bar= 50 µm. (B) Quantitation of active caspase 3 staining. (C) Ki67 staining (brown) of control and transgenic animals, (E= embryonic, P= post-natal), (hematoxylin was used as a counterstain); scale bar= 50 µm. (D) Quantitation of Ki67 staining. For quantitation

of apoptosis and cell proliferation, at least 4 mice were used for each time point. Values represent mean + SEM, (*t*-test *= $P < 0.05$, ns= not significant).

Consistent with the increased rate of apoptosis we observed diminished levels of transgene expression in adult mice (figure 2.7A). Furthermore, neither total B-RAF nor phospho-ERK protein levels altered between the wild type and transgenic mice (figure 2.7B).

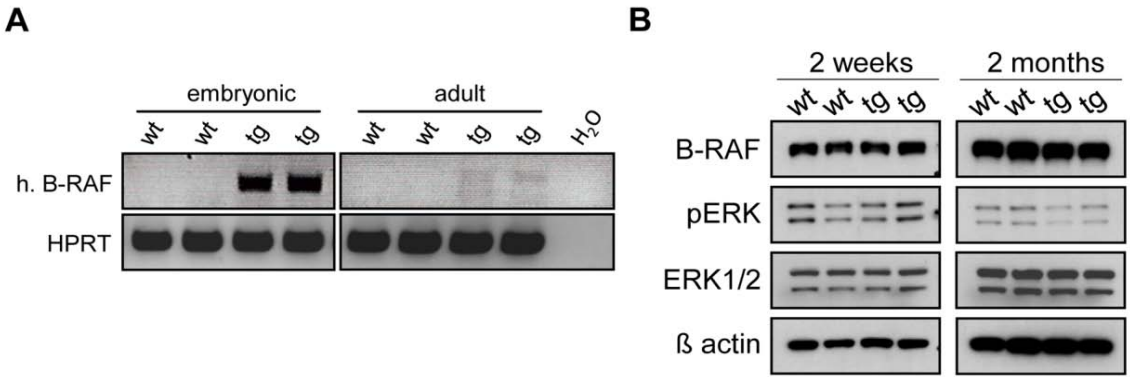

Figure 2.7. Diminished transgene expression and lack of phospho-ERK upregulation in SpC-B-RAF V600E mice. (A) Semi quantitative RT-PCR analysis total lung RNA samples from wild type (wt) and transgenic (tg) animals shows different levels of transgene expression between embryonic and adult mice, HPRT was used as an internal control, (h.=human). (B) Total lung protein lysates from two wild type (wt) and transgenic (tg) littermates were gel separated and immunoblotted; ages and antibodies are as indicated.

Immunohistochemical analysis of lung sections for lung differentiation markers showed the presence of epithelial cell types from the distal lung, including Clara cells, type I and type II pneumocytes (figure 2.8). Notably, the lung lesions were often found to be continuous with bronchio-alveolar junctions (figure 2.8). Moreover we found a significant fraction of proliferating cells (figure 2.8).

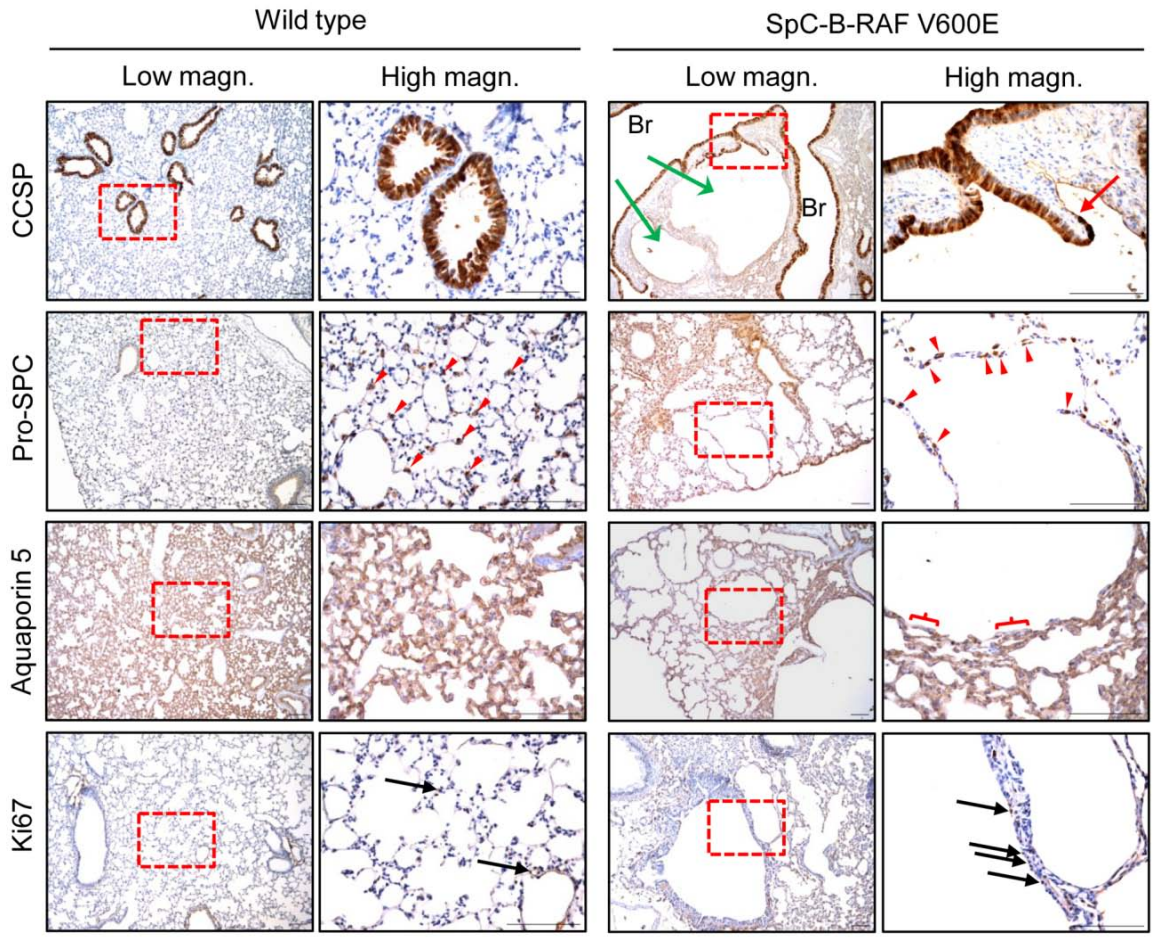

Figure 2.8. Immunohistochemical analysis of lung lesions for lung differentiation markers. Paraffin embedded lung sections from wild type and transgenic mice at 2 months of age were stained for indicated markers; (green arrows point out airspace enlargements), (the red arrow marks the bronchio-alveolar junction), (red-parenthesis indicates a AQP5 negative sector), (red arrowheads point to Pro-SPC expressing cells), (black arrows highlight Ki67 positive cells), (Br= bronchiole), (hematoxylin was used as a counterstain), (right panel pictures are high magnification of the red insets); scale bar = 100 µm.

2.2.3 Signs of tissue remodeling

Airway and lung tissue remodeling and fibrosis play an important role in the development of symptoms associated with lung function loss such as bronchopulmonary dysplasia and COPD (Postma and Timens 2006). Since SpC-

B-RAF V600E animals display some features of these diseases such as airspace enlargements, we thought to search for fibrosis marker in the lung of our transgenic mice. Interestingly, we found progressive deposition of collagen (figure 2.9*)* in non-epithelial lining sectors of the emphysematous lesions (figure 2.8, red parenthesis) indicating an ongoing tissue remodeling.

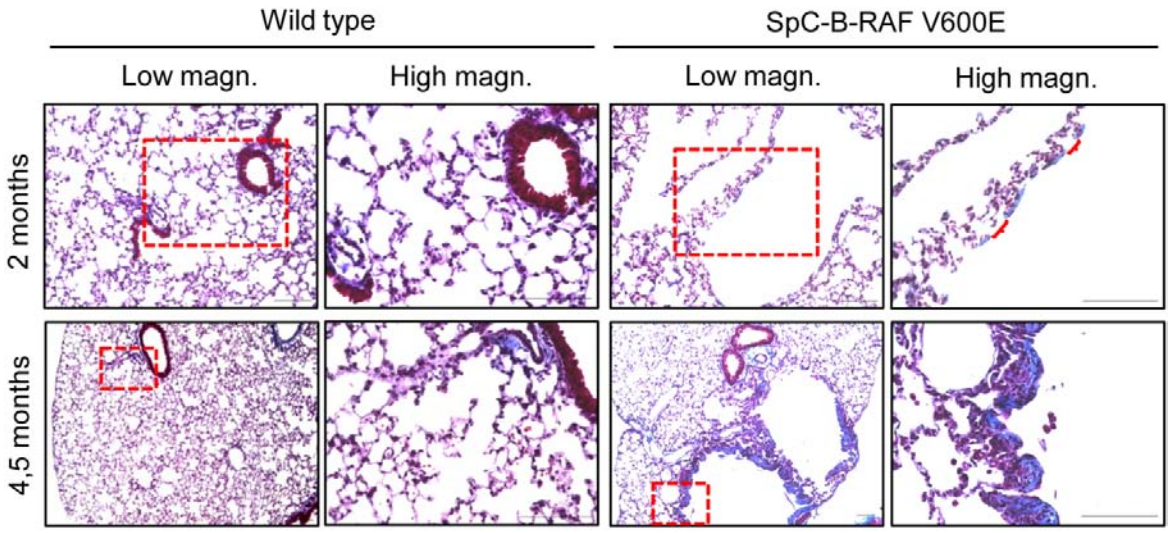

Figure 2.9. Masson´s Trichrome staining shows progressive collagen (blue) accumulation in the lung of SpC-B-RAF V600E transgenic mice, red-parenthesis indicates Masson´s Trichrome negative parts, (the right panel pictures are high magnification of the red inserts); scale bar = 100 µm.

Bronchiolar hypertrophy and mucus hypersecretion are other prominent features of various human lung disease (Barnes 2000); we therefore stained lung sections from wild type and SpC-B-RAF V600E transgenic mice with Alcian Blue pH 2.5 solution for the detection of acidic mucins. Interestingly, we found an age-related increase in mucus secretion in transgenic mice (figure 2.10).

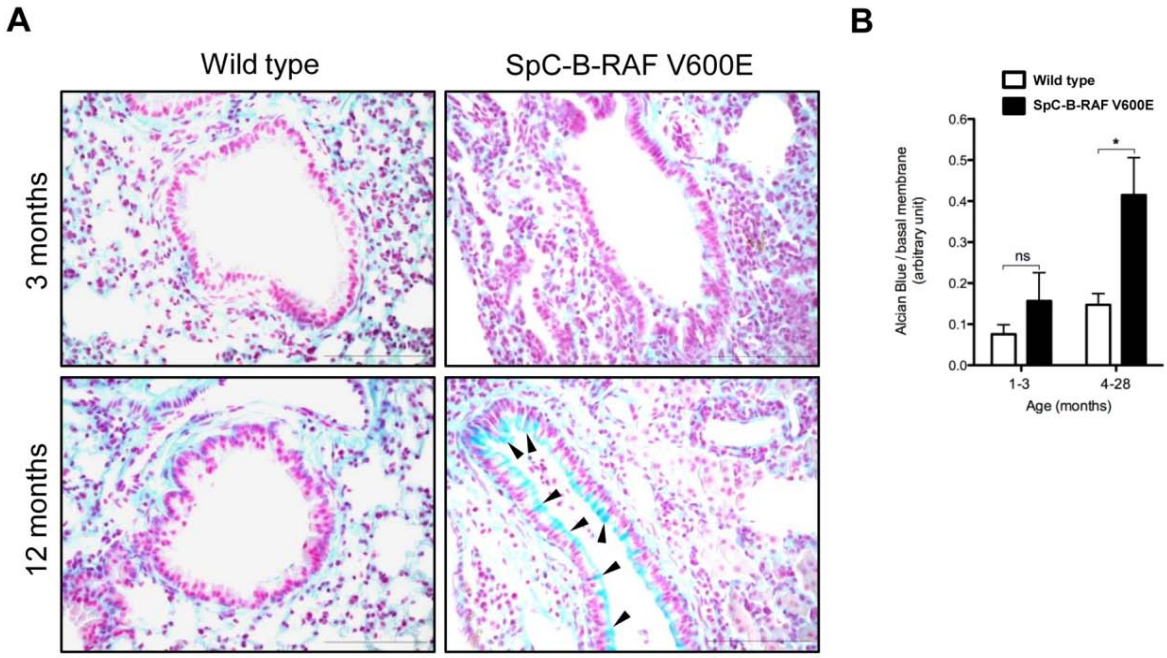

Figure 2.10. Goblet cell hyperplasia in aged SpC-B-RAF V600E transgenic mice. (A) Representative pictures of Alcian blue stained paraffin embedded lung sections from wild type and transgenic mice at 3 and 12 months of age, respectively, black arrowheads denote Alcian Blue-positive (blue) regions indicative of increased mucus production; scale bar = 100 µm. (B) Quantification of Alcian Blue positive bronchiole in wild type (*n*= 6-8) and SpC-B-RAF V600E (n= 7-8) transgenic mice at young (1-3 months) and older (4-28 months) ages (*t*-test *= $P < 0.05$, ns= not significant).

Epithelial-Mesenchymal-Transition (EMT) was often shown to be associated with chronic human lung diseases such as COPD and pulmonary fibrosis (Holgate, Davies et al. 2000; Flanders 2004; Willis and Borok 2007; Lee, Walser et al. 2009). We therefore analyzed total lung tissue lysates of SpC-B-RAF V600E transgenic mice, which harbored macroscopic lung lesions (grade 3) with known EMT markers. We found reduced expression of E-cadherin, ß-catenin and increased expression of Vimentin, indicating EMT induction (figure 2.11A), although we cannot rule out the induction of an alveolar maintenance program in alveolar type II cells (Yildirim, Muyal et al. 2010). Expression of Vimentin was not

solely localized next to the emphysemic lesions but also abundantly found in fibrotic lung parenchyma (figure 2.11B). Since the transgenic lungs show airspace enlargement and inflammation, these results could simply reflect the relative changes in cell populations in the lung rather than an EMT phenomenon. We therefore analyzed the same markers in isolated alveolar type II cells from mice that in this case did not show macroscopic lesions by Real-Time PCR and immunoblotting. We found significantly reduced E-cadherin and increased Vimentin mRNA levels in isolated type II cells from SpC-B-RAF V600E mice (figure 2.11C). Different from the mRNA data, we detected equal to mildly decreased levels of E-cadherin in protein lysates of type II cells from transgenic animals (figure 2.11D). In contrast, variable levels of vimentin expression were detected between the samples (figure 2.11D). As in the case of the total lung lysates we observed strongly reduced levels of ß-catenin in type II cells from mutant mice (figure 2.11A and 2.11D). In addition to ß-catenin, the levels of $p120^{ctn}$ were also reduced (figure 2.11D). ß-catenin is a key signaling mediator of the canonical WNT signaling (Mucenski, Wert et al. 2003). Interestingly, in both total lung and isolated type II cells protein lysates from SpC-B-RAF V600E mice we detected diminished levels of active ß-catenin expression suggesting an inhibition of the canonical WNT signaling pathway (figure 2.11A and 2.11D).

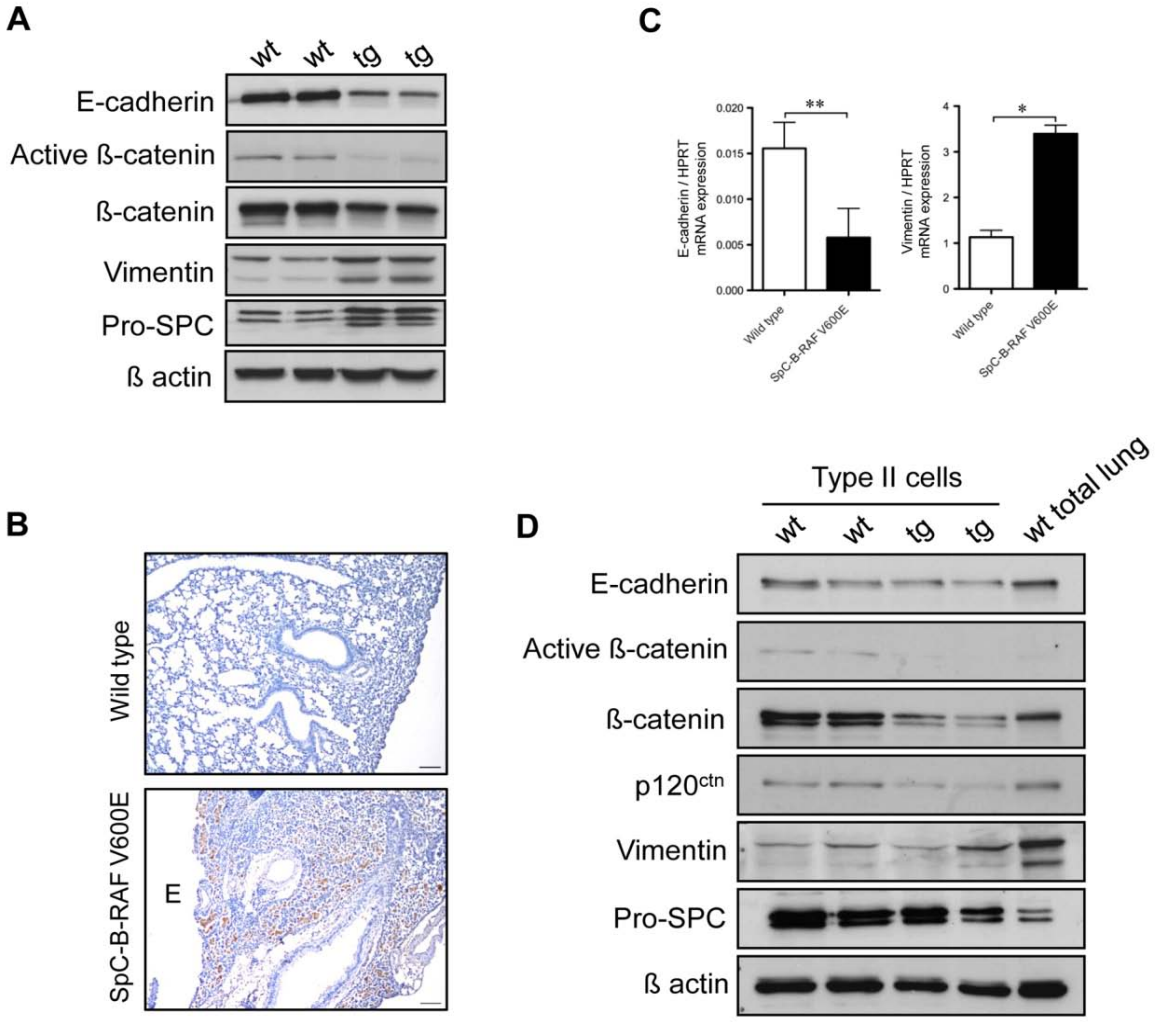

Figure 2.11. Analysis of Epithelial-Mesenchymal-Transition (EMT) in SpC-B-RAF V600E transgenic mice. (A) Total lung protein lysates from two wild type (wt) and transgenic (tg) littermates (17 and 21 months old) were gel separated and immunoblotted with the indicated antibodies. (B) Immunostaining of lung sections from wild type and SpC-B-RAF V600E transgenic mice for Vimentin (brown), (E= airspace enlargement), hematoxylin was used as a counterstain, scale bar = 100 µm. (C) Analysis of E-cadherin and Vimentin mRNA levels in alveolar type II cells isolated from wild type and SpC-B-RAF V600E transgenic mice (5 months old) by Real time PCR, data represent mean + SEM, (*t*-test *= $P < 0.05$, **= $P < 0.01$, *n*= 3-4). (D) Protein lysates of isolated type II cells from two wild type (wt) and transgenic (tg) littermates (20 months old) were gel separated and immunoblotted with the indicated antibodies.

2.2.4 Induction of inflammation

Chronic inflammation is a prominent feature of degenerative lung diseases in human (Qu, Roberts et al. 2009). In order to assess the infiltration of immune cells, we screened lung sections from young (1-3 months) and aged (4-28 months) mice using different immune cell markers. Progressive accumulations of infiltrating macrophages were observed in the vicinity of the lung lesions (figure 2.12A and 2.12B). In extreme cases, these massive accumulations led to the formation of granulomas that filled almost the whole lung parenchyma (figure 2.12A, 12 months).

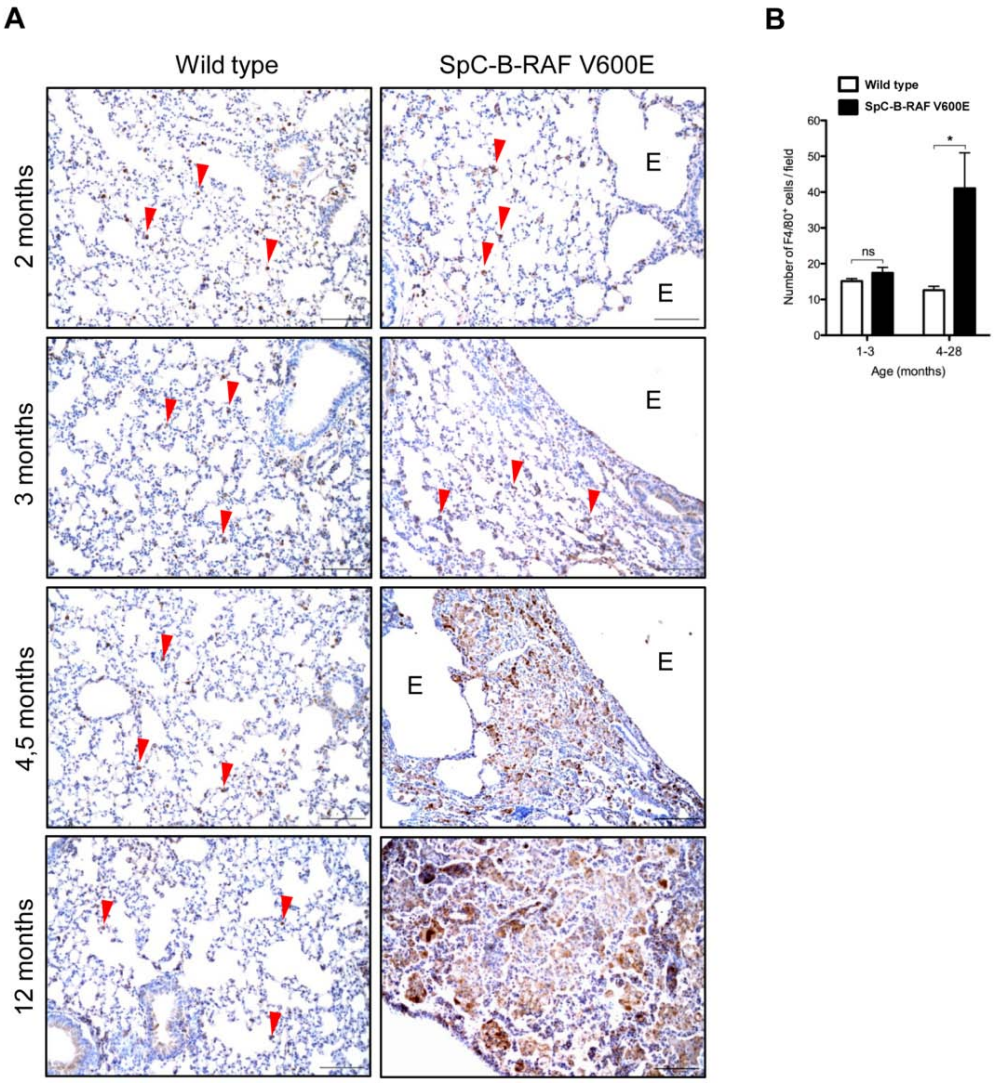

Figure 2.12. Progressive accumulation of macrophages in the lung of SpC-B-RAF V600E transgenic mice as a function of age. (A) Paraffin embedded lung sections from mice with indicated genotypes and ages stained for F4/80 (brown), E= airspace enlargement, arrowheads show scattered alveolar macrophages, hematoxylin was used as counterstain, scale bar = 100 µm. (B) Quantification of F4/80 positive macrophages in wild type (*n*= 9) and SpC-B-RAF V600E (n= 9) transgenic mice at young (1-3 months) and older (4-28 months) ages (*t*-test *= $P < 0.05$, ns= not significant).

Interestingly mast cells were detected in the walls lining the enlarged air spaces (figure 2.13A). Moreover, we found an increased incidence of lymphoid aggregates in SpC-B-RAF V600E transgenic mice (figure 2.13B and 2.13C).

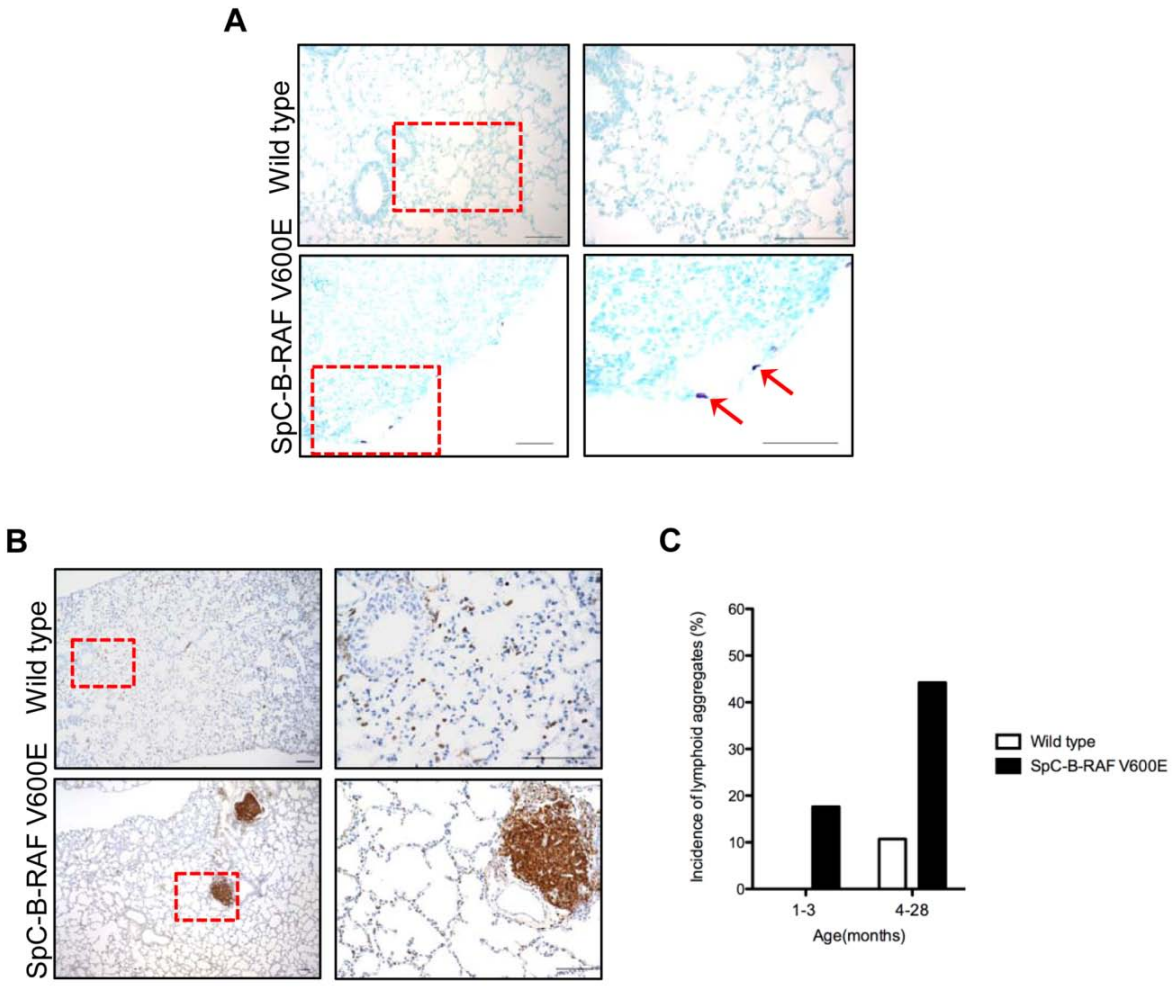

Figure 2.13. Infiltration of immune cells in emphysema-like lesions. (A) Toluidine blue staining identifies mast cells (purple) in the epithelial lining of a lesion. (B) Staining of paraffin embedded lung sections from wild type and transgenic mice for CD45 (brown), hematoxylin was used as counterstain, the right panel pictures are high magnification of the red insets; scale bar = 100 μm. (C) Lymphoid aggregate incidence in lung sections from wild type (1-3 months *n*=16, 4-28 months *n*=28) and SpC-B-RAF V600E (1-3 months *n*=17, 4-28 months *n*=52) transgenic mice.

Immunohiostochemical analysis of lung sections with lymphoid clusters from SpC-B-RAF V600E transgenic mice revealed that these follicles are mostly composed of T- and B-lymphocytes (figure 2.14).

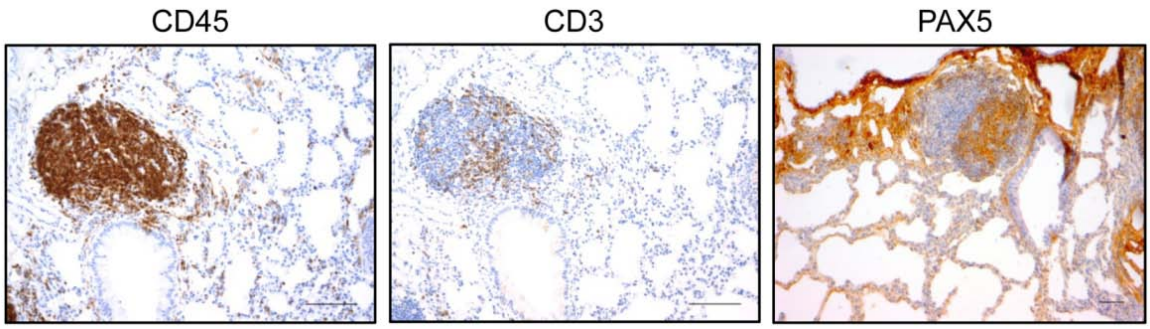

Figure 2.14. Presence of T- and B- cells in CD45 positive clusters. Lung sections from SpC-B-RAF V600E transgenic mice were stained for CD3 and PAX5 to identify T- and B- cells, respectively; hematoxylin was used as a counterstain; scale bar= 100 μm.

Interestingly, in rare extreme cases, these lymphoid aggregates reached very large sizes occupying most of the air exchange space of the entire lung (figure 2.15A). Moreover, these CD45 positive clusters were found to be surrounded by intense collagen accumulations (figure 2.15B).

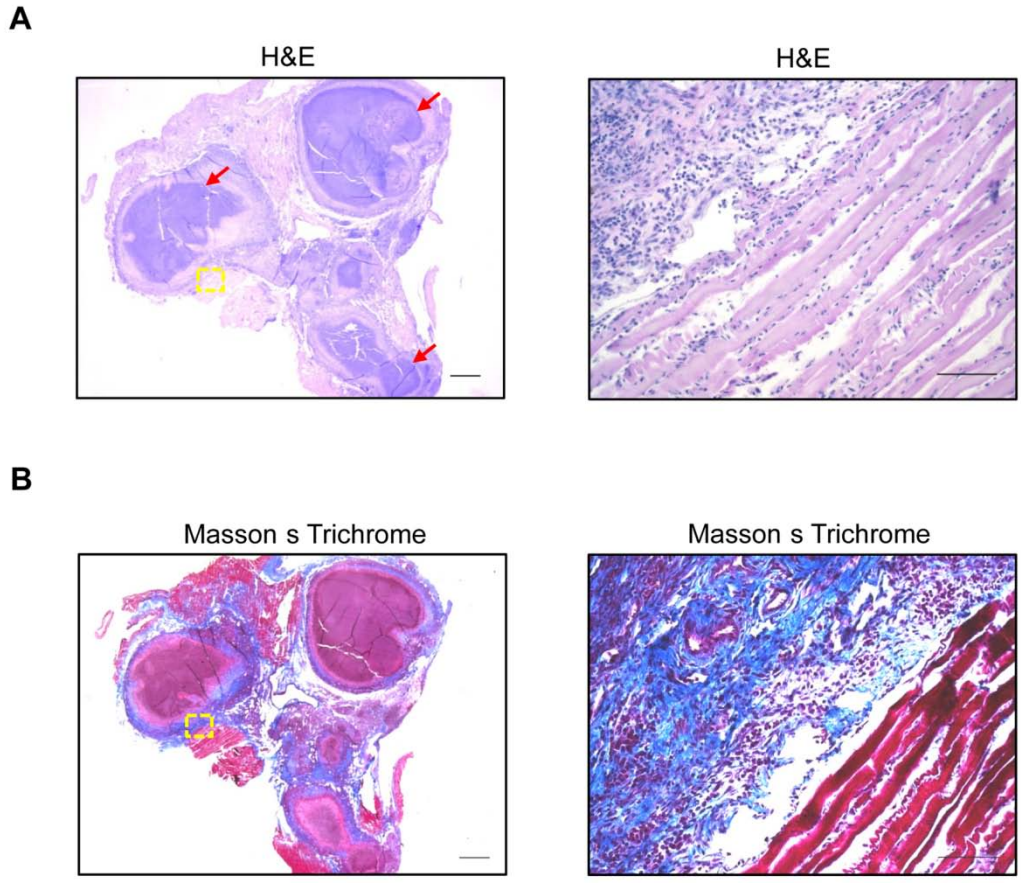

Figure 2.15. Severe lung degeneration in an aged (17.5 months) mouse transgenic for B-RAF V600E. (A) H&E staining of a lung section shows massive infiltration of leukocytes (red arrows). (B) Masson´s Trichrome staining of the consecutive lung section reveals collagen-enriched regions (blue), the right panel pictures are high the magnification of the yellow inserts; scale bar=1 mm for the left and 100 µm for the right panel.

In order to identify the mechanisms by which B-RAF V600E triggers inflammation, IL-6/signal transducer and activator of transcription 3 (STAT3), a well known inducer of inflammation (Jarnicki, Putoczki et al. 2010), was studied. Western blot analysis of lung protein lysates showed up-regulation of phospho-STAT3 in transgenic animals (figure 2.16A). Immunostaining of lung sections with

phospho-STAT3 specific antibody showed similar results indicating the activation of STAT3 signaling in SpC-B-RAF V600E mice (figure 2.16B).

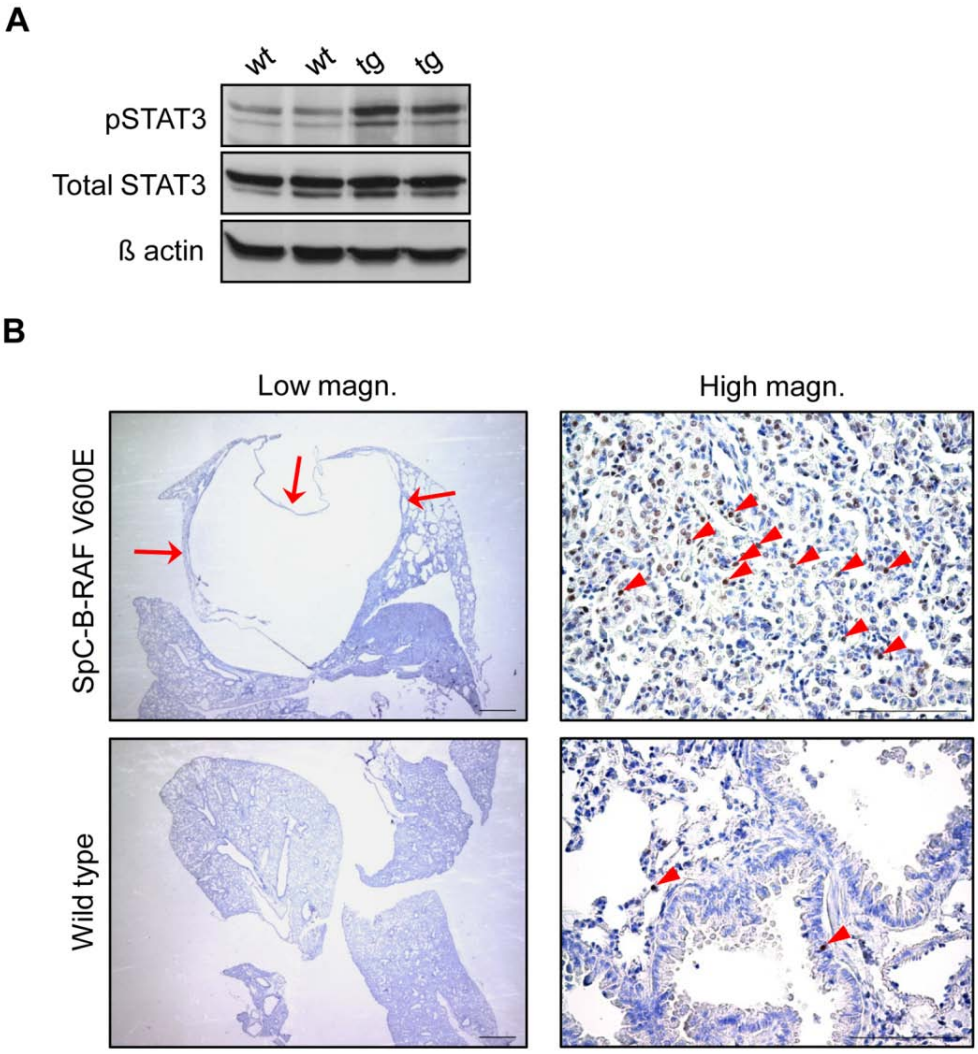

Figure 2.16. Activation of STAT3 signaling in SpC-B-RAF V600E transgenic mice. (A) Total lung protein lysates from two wild type (wt) and transgenic (tg) littermates (17 and 21 months old) were gel separated and immunoblotted with the indicated antibodies. (B) Phospho-STAT3 immunostaining of lung sections shows accumulation of pSTAT3 positive cells in transgenic mice (arrows point to a macroscopic bleb, arrowheads point to pSTAT3 positive cells), hematoxylin was used as a counterstain, scale bar = 1 mm in the right and 100 µm in the left panel pictures.

2.2.5 Synergistic effect of oncogenic B- and C-RAF in SpC-B-RAF V600E/SpC-C-RAF BxB 23 compound mice

In order to test whether the lack of early adenoma formation in our SpC-B-RAF V600E transgenic mouse is a consequence of an acquired tumor resistance in the founders, the mice were crossed with transgenic animals that develop oncogenic-C-RAF driven adenomas originating in type II pneumocytes (Kerkhoff, Fedorov et al. 2000).

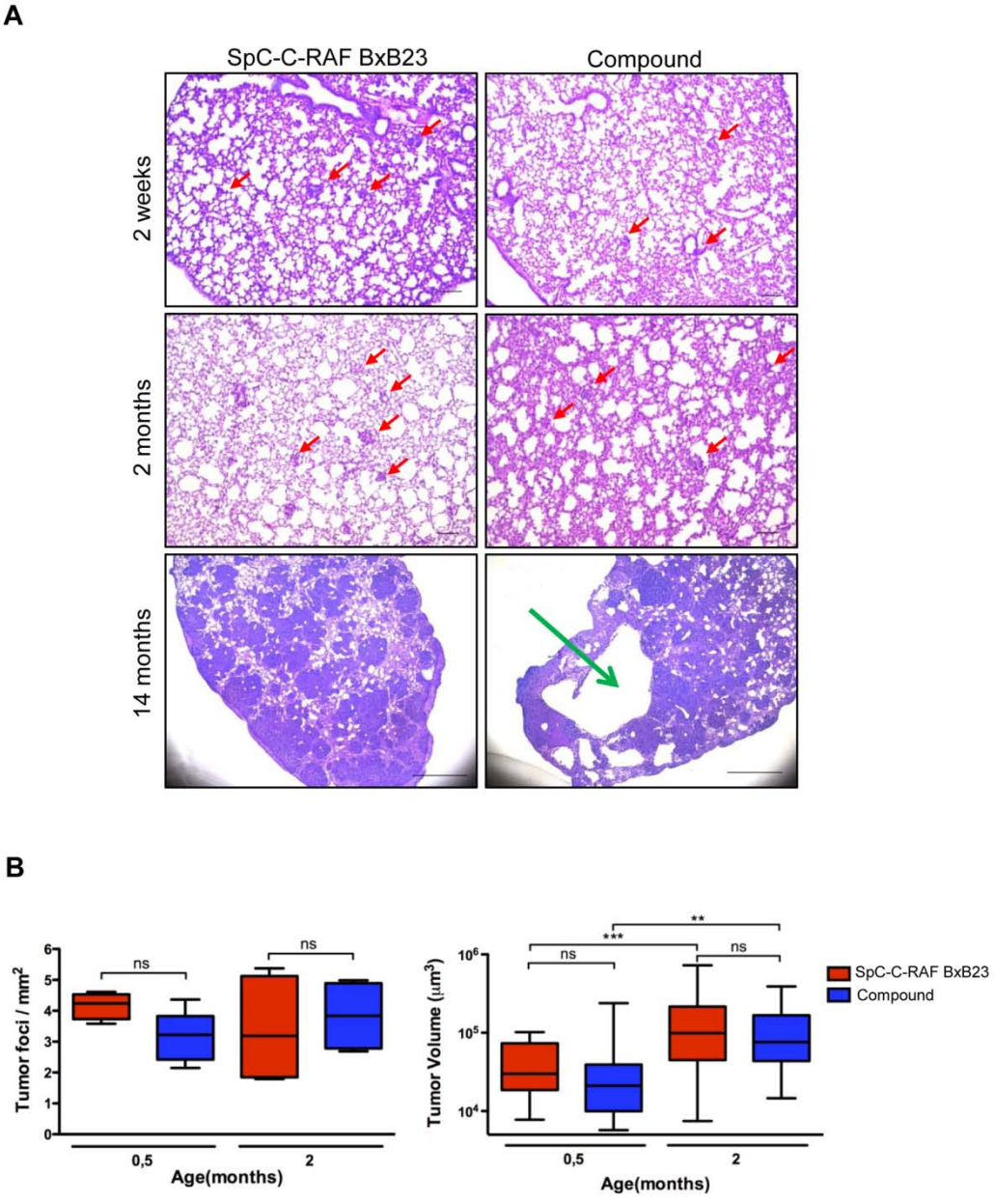

Figure 2.17. Independence of emphysema-like lesions and adenoma-formation in SpC-B-RAF V600E / SpC-C-RAF BxB23 compound mice. (A) H&E staining of lung sections reveal both types of pathology. (Red arrows indicate individual adenomas; green arrow indicates emphysema-like lesions; genotype and ages are as indicated; scale bar= 100 μm). (B) Quantitation of tumor load and tumor size as a function of age. (Mean values are ± SEM; ns= not significant; **= *P*<0.005; ***=*P*<0.0005).

As reported in figure 2.17, coexpression of oncogenic B- and C-RAF transgenes showed that the two transgene-driven lesions are co-dominant (figure 2.17A). Indeed, tumor load and tumor size are indistinguishable between SpC-C-RAF BxB 23 single and compound double transgenic animals (figure 2.17B). B-RAF V600E is a very potent activator of the mitogenic cascade; we therefore compared nuclear pERK levels and found no differences between lung tumors in single and compound transgenic mice (figure 2.18A and 2.18B). Finally, we found no difference in the life span between single transgenic and compound mice (figure 2.18C). Altogether these data indicate that oncogenic B- and C-RAF do not cooperate during disease progression.

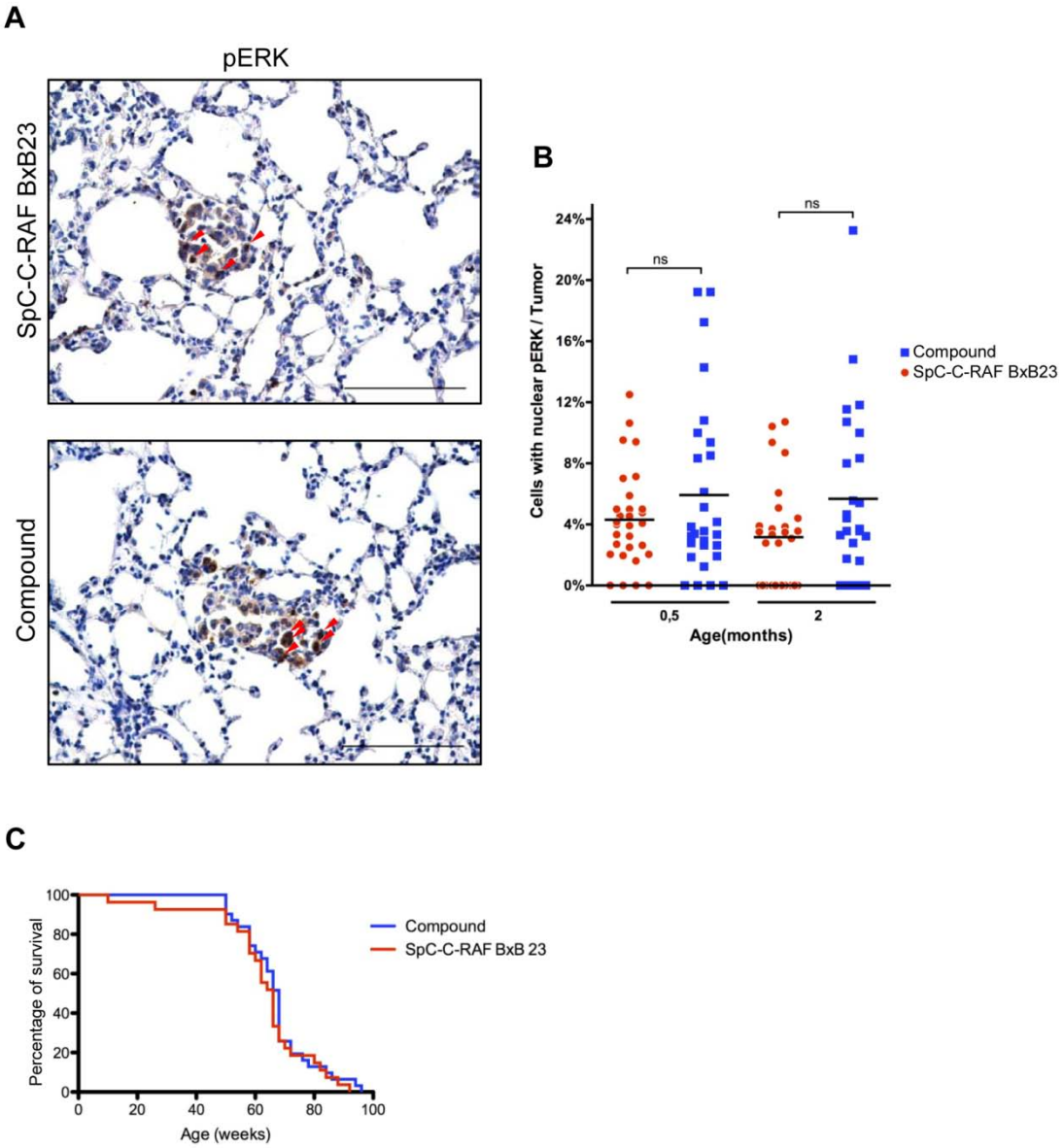

Figure 2.18. Presence of B-RAF V600E transgene does not alter phospho-ERK levels in SpC-C-RAF BxB23 driven adenomas. (A) phospho-ERK immunostaining for the indicated genotypes. (Compound= SpC-B-RAF V600E / SpC-C-RAF BxB23 double transgenic mice; red-arrowheads marks cells with high nuclear pERK; hematoxylin was used as counter stain; scale bar= 100 μm). (B) Quantitation of nuclear pERK staining. (Mean values are ± SEM; ns= not significant). (C) Kaplan-Meier survival curves, (log-rank analysis $P > 0.05$; Compound $n = 32$; SpC-C-RAF BxB23 $n = 27$).

2.2.6 Delayed tumor formation in SpC-B-RAF V600E transgenic

As there is a large body of clinical evidence that human chronic lung diseases may be linked with the late onset of lung cancer (de Torres, Bastarrika et al. 2007) (Wilson, Weissfeld et al. 2008), we looked at a cohort of aged mice for lung tumor formation. In comparison to wild type control littermates, we detected single focal lung tumors with low incidence (~10%) in SpC-B-RAF V600E transgenic mice (figure 2.19A and 2.19B). Notably, tumors were always found in lungs with airspace enlargements (figure 2.19B). Lung tumors stained positive for TTF-1, Pro-SPC, and Aquaporin-5 and negative for CCSP indicating a type II pneumocyte origin (figure 2.19C). Immunohistochemical analysis of tumors with the components of mitogenic cascade signaling showed positive staining for both B-RAF and phospho-ERK1/2 but not for C-RAF (figure 2.19C).

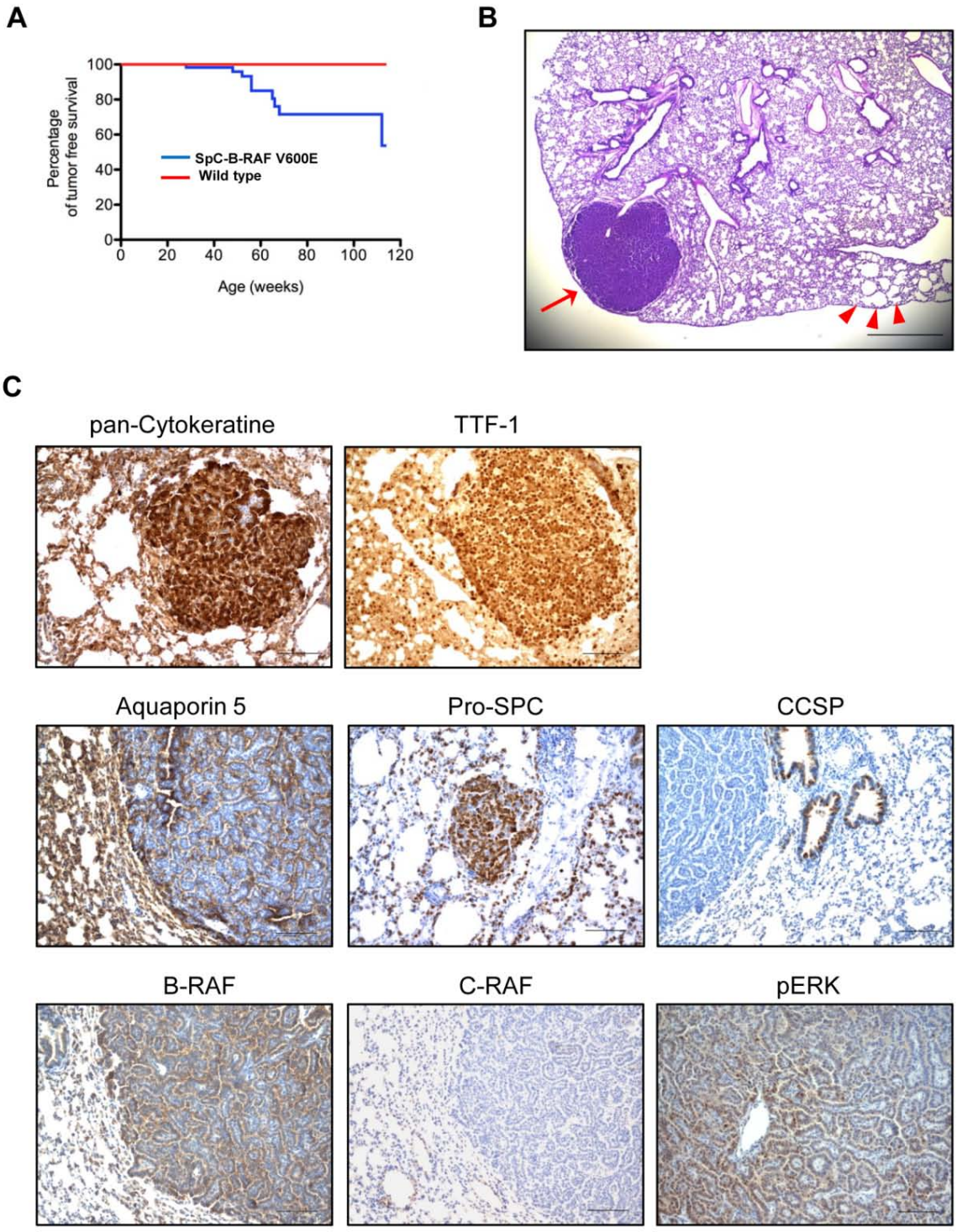

Figure 2.19. Lung tumor formation in SpC-B-RAF V600E transgenic mice. (A) Tumor incidence as a function of age, log-rank analysis for wild type (*n* = 59) and SpC-B-RAF V600E (*n* = 102) transgenic mice, $P < 0.05$. (B) H&E staining of lung section from a one year old SpC-B-RAF V600E transgenic mouse shows coexistence of the lung lesions (arrowheads) with a lung tumor (arrow); scale bar= 500 µm. (C) Tumor bearing

lung sections were stained with the indicated markers, hematoxylin was used as counterstain; scale bar = 100 µm.

Low incidence and late latency of lung tumors from SpC-B-RAF V600E mice are in the favor of a spontaneous origin. We therefore screened tumor samples for somatic mutations that are commonly found in human and mouse NSCLC (Forbes, Bindal et al. 2011). Interestingly the majority of the tumors were negative for these mutations (figure 2.20).

	EGFR			K-ras		CDKN2A				P53			LKB1		
ID Number	Exon 19	Exon 20	Exon 21	Exon 1	Exon 2	ARF Exon 1	INK4a Exon 1	Exon 2	Exon 3	Exon 5	Exon 7	Exon 8	Exon 1	Exon 2	Exon 6
11019	wt	wt	wt	wt	wt	wt	wt			wt	wt	wt		wt	wt
11018			wt	wt	wt		wt	wt	wt	wt	wt	wt	CGC>CGT (R74R) Homo	wt	wt
9842			wt	wt	wt	wt	wt	wt	wt	wt	wt	wt	wt	wt	ACG>ACA (T250T) Homo
9849		wt		wt	wt		wt		wt		wt	wt		wt	wt
10296				wt	wt		wt				wt	wt		wt	
23876	wt	wt	wt	wt	wt	GCG>ACG (A14T) Hetero	wt	wt	wt	wt	wt	wt	wt	wt	wt
16207	wt	wt	wt	wt	wt	wt	wt		wt	wt	wt	wt	wt	wt	wt
19482	wt	wt	wt	wt	wt	wt	wt	wt		wt	wt	wt	wt	wt	wt
30478				wt		wt	wt	wt	wt	wt	wt	wt			
80711				wt	CAA>CGA (Q61R) Hetero										

Figure 2.20. Lung tumors found in SpC-B-RAF V600E transgenic mice in general do not harbor mutations frequently present in human and mouse NSCLC. Genomic DNA from both lung tumors and matched histological normal lung tissue of SpC-B-RAF V600E transgenic mice were screened for the indicated genes, individual animal (ID) and Exon numbers are as indicated, wt= wild type, Hetero=heterozygous, Homo=homozygous, empty boxes represent untested samples.

2.2.7 T- and B-lymphocytes are not involved in the development of COPD-like lesion and lung tumor

In order to evaluate the potential role of the adaptive immunity in the development of COPD-like lesions, SpC-B-RAF V600E single transgenic mice were crossed with *RAG1*-null mice that lack mature T- and B- lymphocytes (Mombaerts, Iacomini et al. 1992). Histological examination of lung sections from compound mice (SpC-B-RAF V600E / RAG1 KO) demonstrated persistence of COPD-like lesions indicating that T- and B- cells are not involved in the lung pathogenesis in our system (figure 2.21A and B).

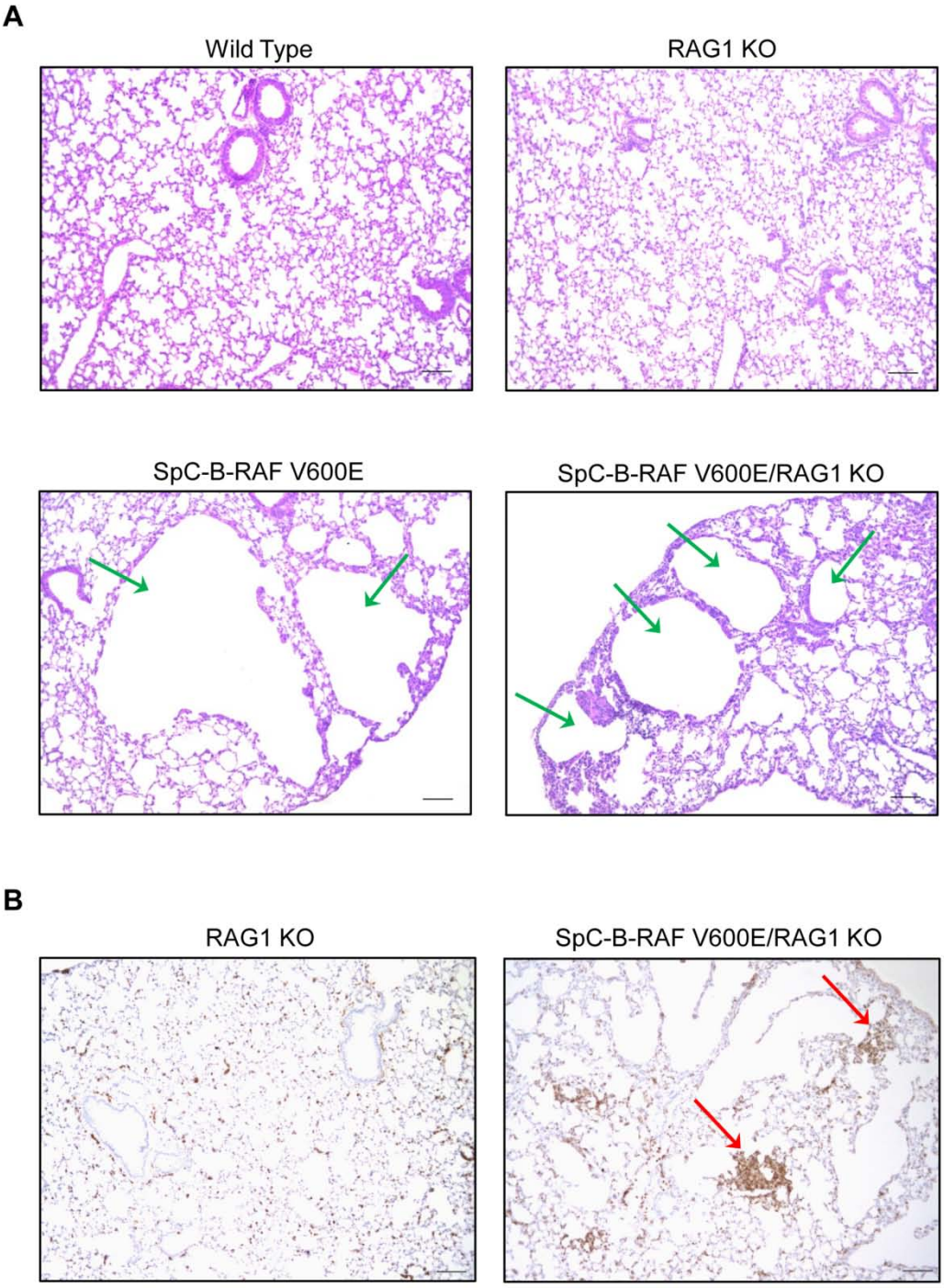

Figure 2.21. Mature T- and B- cells are not required for the formation of COPD-like lesions in SpC-B-RAF V600E transgenic mice. (A) H&E staining of lung sections from wild type, RAG1 knock out (KO), SpC-B-RAF V600E single transgenic and SpC-B-RAF V600E/RAG1 KO compound animals show persistence of lung lesions in SpC-B-RAF V600E single and compound mice, green arrows point to airspace enlargements. (B) Immunostaining of paraffin embedded lung sections from RAG1 KO single transgenic

and SpC-B-RAF V600E/RAG1 KO compound animals for CD45 (brown), red arrows point to CD45 positive clusters, hematoxylin was used as counterstain; scale bar= 100 µm.

Moreover, the late development of lung tumors with incomplete penetrance in compound animals supports this data (figure 2.22).

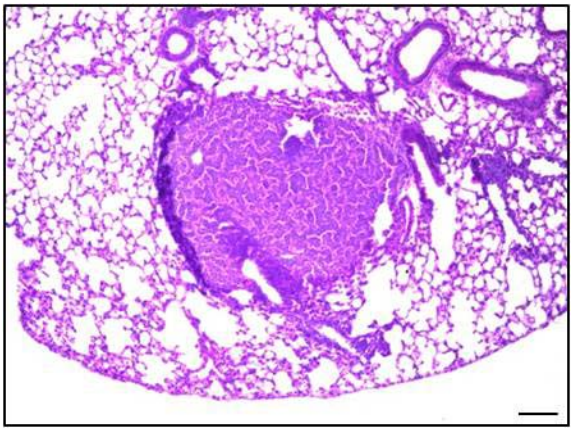

Figure 2.22. Delayed lung tumor formation in SpC-B-RAF V600E/RAG1 KO compound mice with incomplete penetrance. H&E staining of lung section from a 5 months old SpC-B-RAF V600E/RAG1 KO compound mouse shows an adenoma; scale bar= 100 µm.

3. Discussion (Lung-targeted expression of oncogenic B-RAF V600E)

Mutations in the components of the mitogenic cascade play an important role in both developmental syndromes and neoplastic diseases (Schubbert, Bollag et al. 2007). Individuals with these syndromes often have mutations in this signaling pathway that predisposes them to cancer too (Schubbert, Bollag et al. 2007). NSCLC is the leading cause of cancer related death worldwide and frequently

harbors activating mutations in the MAPK pathway (Ding, Getz et al. 2008). A fraction (~ 2%) of NSCLC patients harbor B-RAF mutations (Forbes, Bindal et al. 2011) and several previous studies attempted to model human NSCLC in mice. They have shown that conditional expression of B-RAF V600E rapidly induces lung adenoma formation (Dankort, Filenova et al. 2007; Ji, Wang et al. 2007). However, in our study, constitutive expression of this mutant B-RAF in type II pneumocytes did not elicit immediate tumor formation but predominantly caused airspace enlargements which were often associated with inflammation. Lack of tumor formation in SpC-B-RAF V600E transgenic mice in comparison to the SpC-C-RAF BxB mice (Kerkhoff, Fedorov et al. 2000) is intriguing, as both oncogenes are known to activate the mitogenic cascade. It is plausible that the diminished transgene expression caused by the induction of apoptosis during lung development precluded oncogenic transfomation of alveolar type II cells. The absence of elevated phospho-ERK levels in transgenic mice supports such a hypothesis. Alternatively, as reported previously, induction of cellular senescence program by oncogenic B-RAF may restrict expansion of transformed cells (Michaloglou, Vredeveld et al. 2005). However, we did not find detectable levels of $p16^{INK4a}$, $p21^{WAF1}$ and $p19^{ARF}$, the common oncogene-induced senescence markers, protein expression neither by immunoblotting nor by immunohistochemistry in transgenic mice from different ages (data not shown).

In the present study, the expression of B-RAF V600E specifically in alveolar type II cells during lung development affected alveolar formation. Earlier studies showed that the canonical WNT signaling plays a crucial role during lung development (Mucenski, Wert et al. 2003). Inhibition of WNT signaling by conditional knockout of ß-catenin in alveolar type II cells disrupted lung

morphogenesis and caused respiratory failure due to dilated terminal structures in their lungs (Mucenski, Wert et al. 2003). The airway space enlargements that we find in our transgenic mice may be related to the downregulation of WNT signaling that we detected in isolated type II pneumocytes. Interestingly, similar to oncogenic B-RAF, activation of oncogenic K-ras^{G12D}, the most frequent mutation found in human NSCLC, was shown to impair lung morphogenesis by up-regulating Ras/MAPK antagonist Sprouty-2 in the absence of apoptosis (Shaw, Meissner et al. 2007). It remains to be elucidated whether Sprouty-2 or other antagonists of the mitogenic cascade play a role in generation of developmental defects induced by B-RAF V600E in our transgenic model.

The airspace enlargements observed in embryonic lungs of SpC-B-RAF V600E transgenic mice were maintained in adult animals and were associated with tissue remodeling and chronic inflammation. Accumulations of collagen and mucus secretion that we found in transgenic lungs suggest that there is an ongoing tissue repair. However, persistence of the lung lesions throughout the lifetime of the animals indicates that there is an inefficient recovery of the lung epithelium. Inhibition of canonical WNT signaling as well as absence of full EMT in lungs of transgenic animals may account for incomplete repair. Chronic inflammation plays also an important role in tissue remodeling by promoting the release of cytokines by immune cells (Curtis, Freeman et al. 2007). STAT3, a cytokine-induced gene related to pulmonary inflammation in human COPD, has been shown to be required for alveolar structure maintenance and function (Li, Du et al. 2007). Persistent activation of the STAT3 signaling in murine respiratory epithelial cells was also shown to induce pulmonary inflammation and tumor formation in the lung (Li, Du et al. 2007). Moreover STAT3 is a potent mediator of

pro-inflammatory interleukin 6 (IL-6) that was shown to induce EMT phenotype in human breast cancer cells (Sullivan, Sasser et al. 2009). Abundant expression of activated STAT3 that we found in lungs of SpC-B-RAF V600E transgenic mice may indicate a role for STAT3 in the promotion of tissue remodeling and inflammation in our system.

Histopathological analysis of the infiltrating immune cells present in SpC-B-RAF V600E transgenic mice demonstrated the recruitment of inflammatory cells from both innate and adaptive immune system. The increase in occurrence of lymphoid aggregates consisting of T- and B-cells raises the question whether there was a specific immune response to B-RAF V600E. We have previously described a T-cell specific epitope of B-RAF V600E (Andersen, Fensterle et al. 2004) that could be involved in immune selection, suggesting that the immune response might be the driving force behind the development of these lesions in the transgenic animals. However, lack of immune cells in embryonic lungs with airspace enlargements and persistence of these lesions in lungs from SpC-B-RAF V600E / RAG1-null compound mice suggest that cells of the adaptive immune system are dispensable in the course of the disease. In fact, cells from the innate immune system; such as macrophages and mast cells were abundantly found in the lung of our transgenic animals. The progressive accumulation of macrophages as well as lymphoid aggregates might contribute to an elevated mucus production and increased damage observed in these lesions. In addition to macrophages, mast cells have important roles in innate immunity and tissue remodeling but so far, they have been poorly studied in human COPD (Andersson, Mori et al. 2010). Our data suggest that mast cells might play a role

in the progression of chronic lung degeneration and therefore should be examined in more detail in future.

It has been previously shown that the expression of B-RAF V600E in lung epithelial cells induced lung tumor formation. In contrast to these previous studies, we found that the early expression of mutant B-RAF in alveolar type II cells caused airspace enlargements in the absence of lung tumors. The differences between these models might result from a different targeting strategy, as well as different timing of oncogene induction (Dankort, Filenova et al. 2007) (Ji, Wang et al. 2007). Nevertheless we detected lung tumors with low incidence only in aged transgenic animals. The presence of single focal tumors with low penetrance in transgenic mice suggests a spontaneous origin. However, the rate of spontaneous tumor formation in transgenic mice was significantly higher than in C57BL/6 mice (Krupke, Begley et al. 2008). Consistent with the link between inflammation and cancer, the increased number of spontaneous lung tumors found in SpC-B-RAF V600E mice might be due to inflammation that was often associated with the airspace enlargements.

4. Results and discussion (Elimination of B-RAF in a mouse model for NSCLC)

4.1 Rationale

Tumors often are highly dependent on signaling pathways promoting cell growth or survival and may become hypersensitive to downregulation of key components within these signaling cascades (Gotz, Kramer et al. 2004). RAF and Ras mutations found in human malignancies convey constitutive activity to these signaling molecules thereby converting them into an oncogenic state (Davies, Bignell et al. 2002). Non-sense point substitutions are the most frequent type of RAF mutations in human cancer. Recently, chromosomal translocations involving either B- or C-RAF in a small percentage of several type of cancers were found (Palanisamy, Ateeq et al. 2010) (McMahon 2010). Notably, these gene fusions encode for RAF proteins retaining the kinase domain but losing the N-terminal RAS-binding domain, suggesting that the mutant proteins may be constitutively active (Palanisamy, Ateeq et al. 2010).

Previously, our lab has generated a mouse lung tumor model by targeting an active C-RAF (C-RAF BxB) to type II cells using the SP-C promoter. C-RAF BxB lacks the regulatory NH_2-terminal sequences including the Ras interaction domain (Kerkhoff, Fedorov et al. 2000). Cell culture experiments showed that C-RAF BxB constitutively associates with B-RAF in a Ras-independent manner (Weber, Slupsky et al. 2001). These data may suggest that the C-RAF BxB/B-RAF heterodimerization is necessary for the oncogenic properties of C-RAF BxB.

4.2 Oncogenic C-RAF cooperates with B-RAF in lung tumor growth

In order to evaluate *in vivo* the role of B-RAF in oncogenic-C-RAF mediated lung tumorigenesis, conditional *B-RAF* gene inactivation using a DOX inducible Cre/*loxP* site-specific recombination system was employed (figure 1.6). Lung specific ablation of *B-RAF* was detected in *SpC-C-RAF BXB/SpC- rtTA/Tet-O-cre/B-RAF* $^{flox/flox}$ compound mice that were induced with doxycyclin (DOX) throughout gestation and until the day of sacrification (figure 4.1).

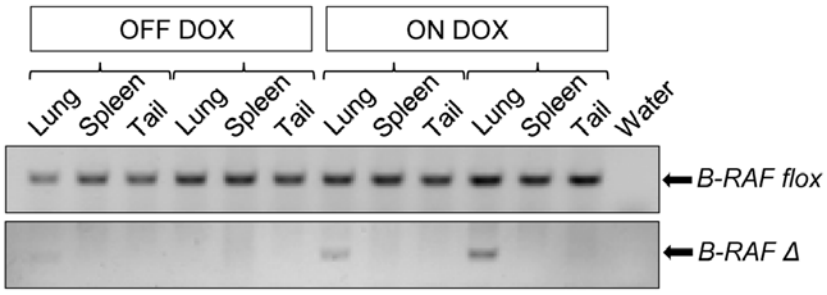

Figure 4.1. Specific recombination of the conditional *B-RAF* allele in the lung of DOX-induced compound mice. DNA was extracted from the indicated tissues of two months old animals and subjected to PCR using primers that detect the conditional *B-RAF* allele in the germline (*B-RAF flox*) or recombined (*B-RAF Δ*) state. PCR products were resolved on agarose gel electrophoresis and photographed.

In order to assess the effect of *B-RAF* loss on lung tumorigenesis, compound mice were DOX-treated throughout gestation until 2, 7 and 12 months respectively; and subsequently examined by histology. Interestingly, all compound animals displayed lung tumors (figure 4.2A and B). We found no difference in the tumor incidence of DOX-induced *SpC-C-RAF BXB/SpC-rtTA/Tet-O-cre/B-RAF* $^{flox/flox}$ compound mice and aged-matched controls at 2 and

7 months of age (figure 4.2B). However, we observed a significant reduction in the lung tumor growth only in DOX-induced compound animals (figure 4.2C).

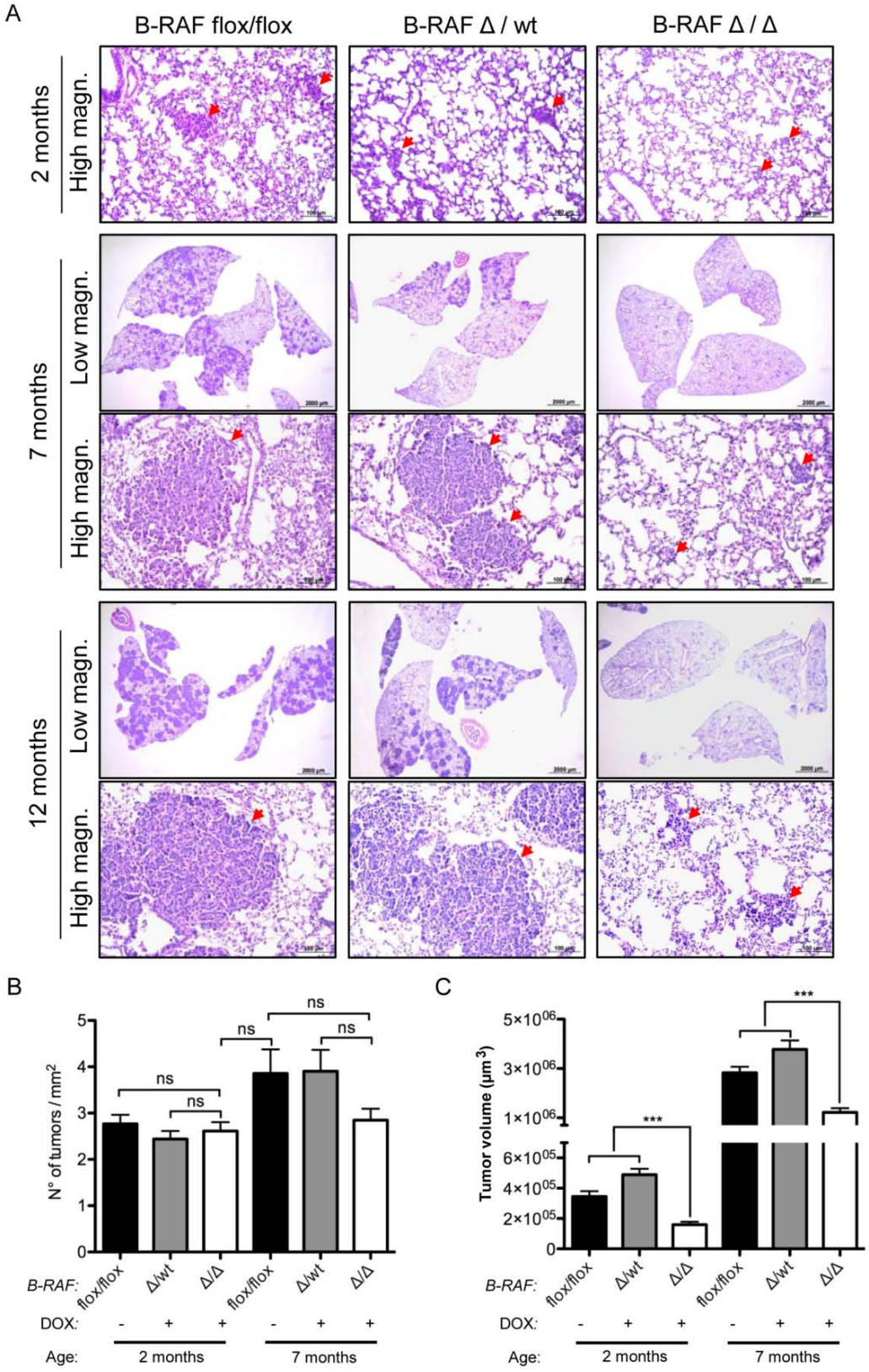

Figure 4.2. Oncogenic C-RAF BxB cooperates with B-RAF in lung tumor growth but not in tumor incidence. (A) Representative pictures of H&E stained lung sections from DOX-induced (*SpC-C-RAF BXB/SpC- rtTA/Tet-O-cre/B-RAF* $^{flox/flox}$) compound mice and aged-matched controls, genotypes and ages are as indicated, red arrows point to lung adenomas. (B and C) Analysis of tumor incidence and tumor volume in compound mice; genotypes, induction status and ages are as indicated; tumor volume was calculated by assuming a spherical shape (for details on quantification methods see material and methods section). (Mean values are + SEM; *t*-test ns= not significant; ***= *P*<0.0005).

Although reduced in size, the tumors of DOX-induced compound animals were well differentiated as judged by their cell morphology and immunostaining of two tumor markers (pan-Cytokeratine and Pro-SPC) (figure 4.3).

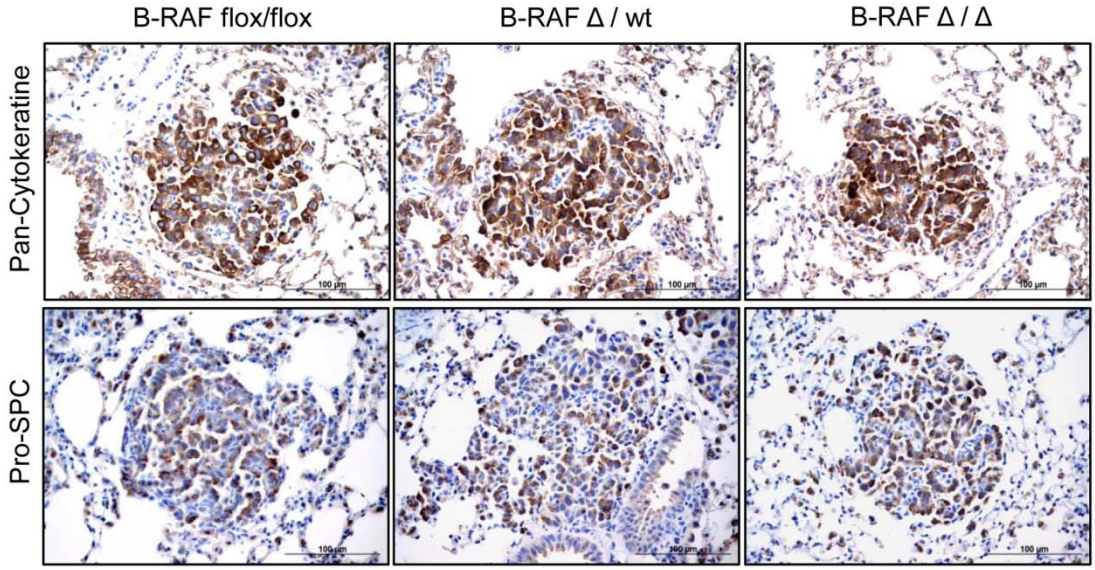

Figure 4.3. **Pan-Cytokeratine and Pro-SPC expression in lung tumors of DOX-induced and controls compound mice.** Representative pictures of paraffin embedded lung sections from 7 months old DOX-treated (*SpC-C-RAF BXB/SpC- rtTA/Tet-O-cre/B-RAF* $^{flox/flox}$) and controls animals that were stained with the indicated markers (brown). The genotypes are as indicated.

4.3 Reduced cell proliferation in lung tumors lacking B-RAF

The reduced tumor growth in oncogenic-C-RAF driven lung tumors, which lack B-RAF, could be either a consequence of reduced cell proliferation or an increase in apoptosis or even a combination of both. We therefore screened tumor bearing lung sections from DOX-induced *SpC-C-RAF BXB/SpC- rtTA/Tet-O-cre/B-RAF* $^{flox/flox}$ and aged-matched compound mice with markers of both proliferation and apoptosis. Ki67 and phospho-H3 stainings clearly showed a strong reduction of cycling cells upon B-RAF ablation in C-RAF BxB induced lung tumors (figure 4.4A and B). TUNEL and active caspase 3 stainings instead did not exhibit any difference between DOX-induced and control animals (figure 4.4C and D). No decrease in the number of lung tumors between 2 and 7 months and the absence of apoptosis argue against cell death mechanisms as responsible for the slow tumor growth after B-RAF elimination (figure 4.2A and B) (figure 4.4C and D).

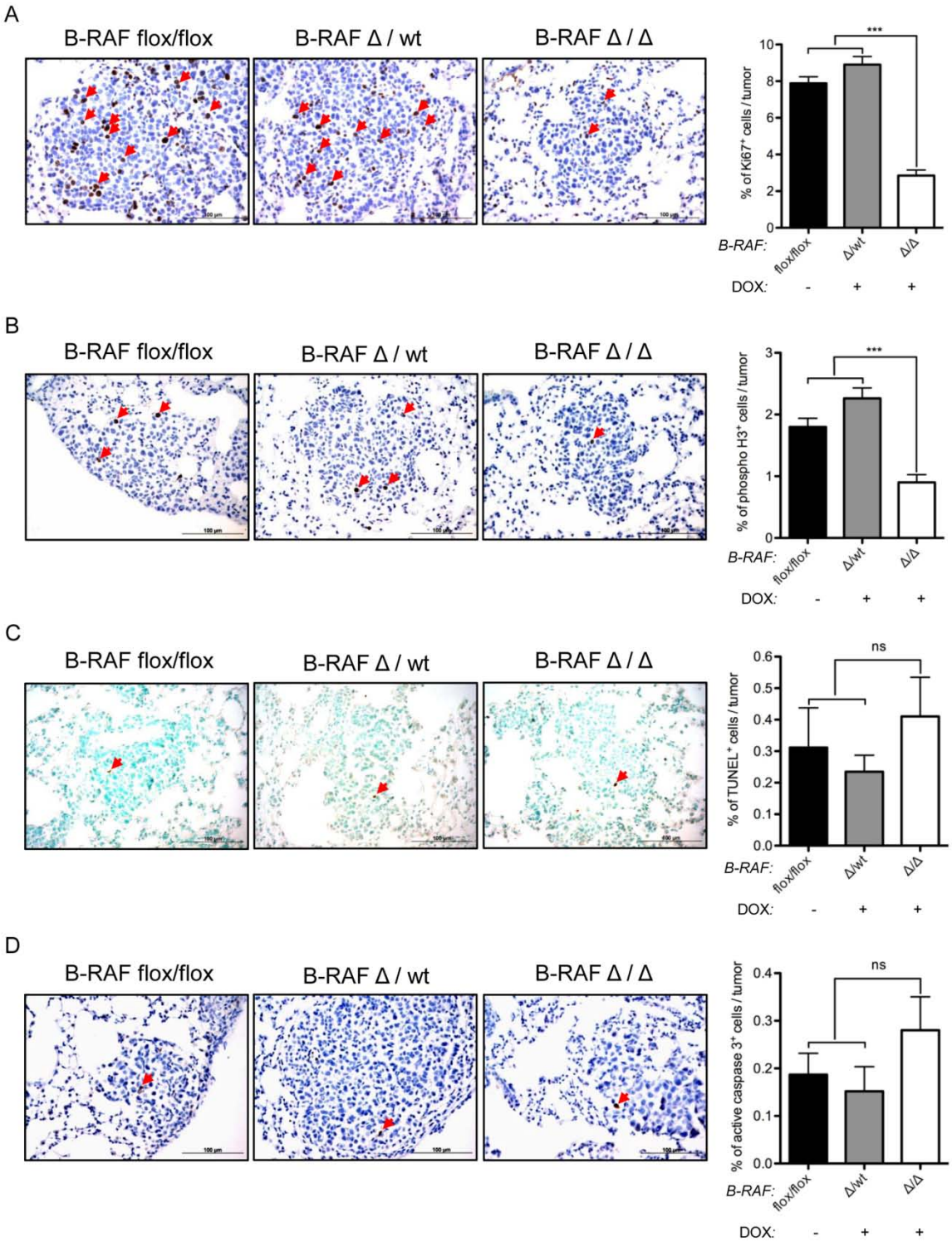

Figure 4.4. Reduced proliferation and absence of apoptosis in C-RAF BxB driven lung tumors lacking B-RAF. *SpC-C-RAF BXB/SpC- rtTA/Tet-O-cre/B-RAF* $^{flox/flox}$ compound mice were DOX-induced for 7 months and compared to aged-matched controls. Representative pictures and quantification of Ki67 (A), phospho-H3 (B), TUNEL (C) and active caspase 3 (D) staining (brown) of paraffin embedded lung sections.

Genotype and induction status are as indicated, red arrows point to positively stained cells. (*n*=75, mean values are + SEM; *t*-test ns=not significant, ***=*P*<0.0005).

4.4 B-RAF cooperates with oncogenic C-RAF in the activation of the MAPK cascade

In line with recombination of the *B-RAF* allele (figure 4.1), immunohistochemical analysis of tumor bearing lung sections showed the loss of B-RAF protein only in adenomas of DOX-induced *SpC-C-RAF BXB/SpC- rtTA/Tet-O-cre/B-RAF* $^{flox/flox}$ compound mice (figure 4.5A). Not all tumors of DOX-induced compound mice displayed the loss of B-RAF expression indicating that these tumors were "escapers" of the cre-mediated recombination (data not shown). Reduction of tumor growth in DOX-induced compound animals could be a consequence of transgene shutdown upon B-RAF ablation. However, staining of lung sections with a C-RAF antibody showed the transgene expression (figure 4.5A). Nevertheless, the levels of nuclear phospho-ERK were reduced in lung tumors of DOX-induced compound mice indicating that B-RAF cooperates with C-RAF BxB in the activation of the mitogenic cascade (figures 4.5A and B). Immunoblotting experiments using protein lysates from total lung of 7 months old DOX-induced *SpC-C-RAF BXB/SpC- rtTA/Tet-O-cre/B-RAF* $^{flox/flox}$ and 2 months control mice confirmed these findings (figure 4.5C). These results are in line with previous biochemical data showing that B-RAF heterodimerize with C-RAF by targeting its kinase domain and by activating it in the cytosol in a RAS-independent manner (Garnett, Rana et al. 2005).

It is conceivable that the reduced tumor growth in oncogenic-C-RAF driven lung cancer that lack B-RAF is caused by a reduction in signaling through the

mitogenic cascade. However, since all DOX-induced compound mice that we analyzed developed lung tumors we can speculate that *in vivo* B-RAF is a dispensable factor in the oncogenic properties of C-RAF BxB.

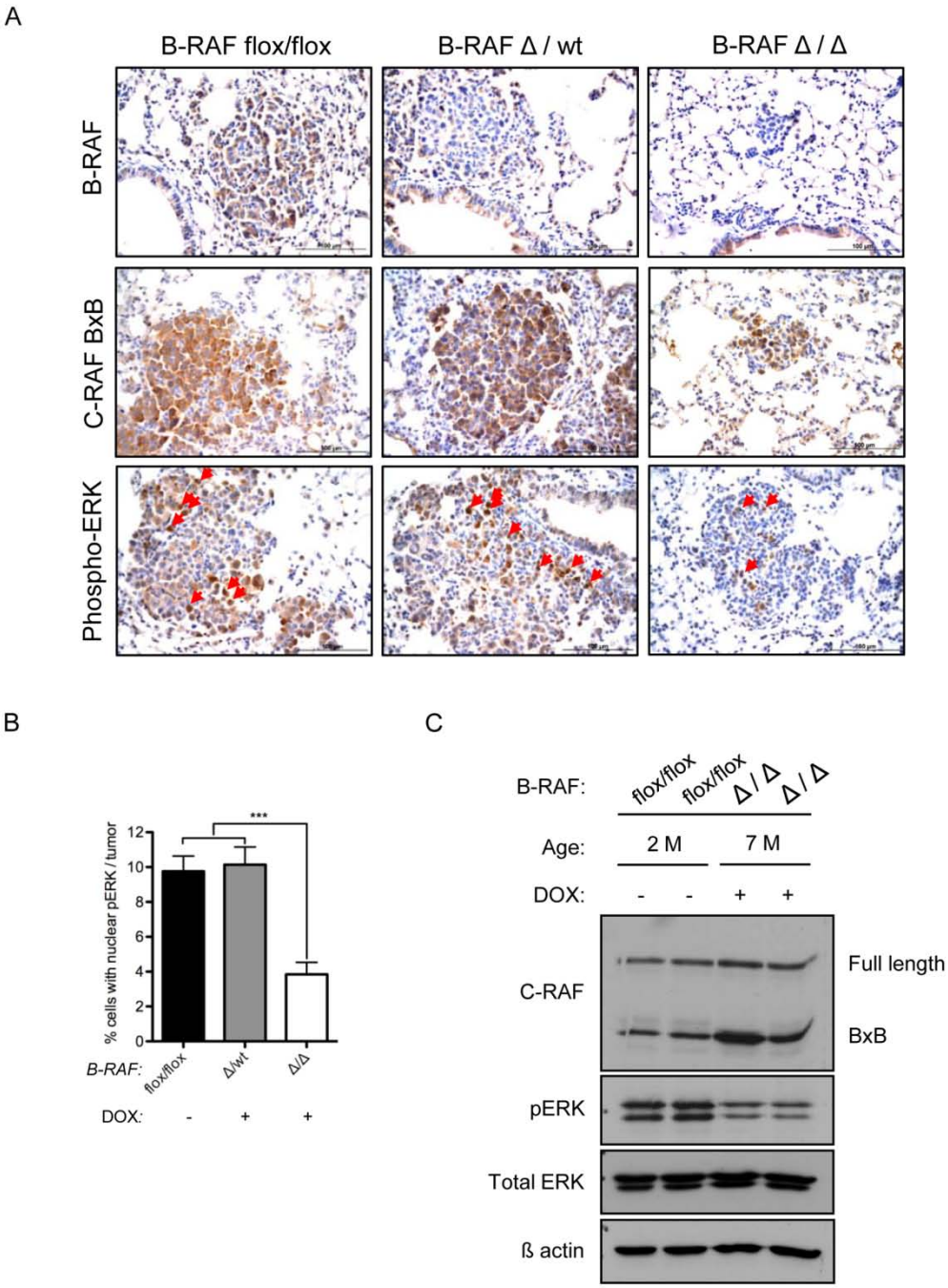

Figure 4.5. B-RAF cooperates with C-RAF BxB in the activation of the MAPK cascade. (A) Paraffin embedded lung sections from 7 months old DOX-treated and controls (*SpC-C-RAF BXB/SpC- rtTA/Tet-O-cre/B-RAF* $^{flox/flox}$) compound mice were stained with the indicated markers (brown), red arrows point to tumors cells which

display nuclear phospho-ERK staining (brown), hematoxylin was used as counterstain. (B) Quantification of nuclear phospho-ERK staining shown in A, genotypes and induction status are as indicated. (*n*=40, mean values are + SEM; *t*-test ***=*P*<0.0005). (C) Total lung protein lysates from 7 months DOX-treated and 2 months control compound mice were gel separated and immunoblotted with the indicated antibodies; age, genotype and induction status are as indicated.

Recently, Blasco *et al.* demonstrated in mouse models that C-RAF, but not B-RAF, is essential for the development of oncogenic-K-Ras-driven NSCLC (Blasco, Francoz et al. 2011). Interestingly, in this work, the elimination of B-RAF expression had no effect on the levels of MEK and ERK phosphorylation suggesting that other RAF proteins can maintain mitogenic signaling (Blasco, Francoz et al. 2011). Instead, our data underline the importance of B-RAF in C-RAF BxB-mediated neoplastic transformation. B-RAF/C-RAF BxB heterodimerization seems to be necessary for the full activation of the mitogenic cascade.

Our lab has previously shown that the RAF inhibitor BAY 43-9006 was not efficient in the inhibition of lung adenomas in SpC-C-RAF BxB23 transgenic mice (Kramer, Gotz et al. 2004). Several biochemical assays have shown that the BAY 43-9006 is a very potent inhibitor of the catalytic domain of C-RAF, wild type B-RAF, B-RAF V600E and also different receptor tyrosine kinases (Wilhelm, Carter et al. 2004). Recently, many novel data on a new and more specific RAF inhibitor (PLX4032) have shown that although this inhibitor is active against tumors with mutant RAFs (such as B-RAF V600E), it does not suppresses the growth of tumors with mutant Ras or wild type B-RAF. Indeed, this inhibitor can activate the MAPK cascade through homo- or heterodimerization mechanisms of B- and C-RAF in a Ras-dependent manner (Poulikakos, Zhang et al. 2010) (Heidorn,

Milagre et al. 2010) (Hatzivassiliou, Song et al. 2010). So why is the BAY 43-9006 inhibitor not active in our RAF dependent lung tumor mouse model (Kramer, Gotz et al. 2004)? Why, instead, as presented in this work, the specific elimination of B-RAF leads to a reduced lung tumor growth? It is conceivable that the BAY 43-9006 inhibitor treatment did not block or even did induce B-RAF/C-RAF BxB heterodimerization and therefore had no effects on the mitogenic signal intensity (Kramer, Gotz et al. 2004). In the present work instead, the complete ablation of the B-RAF protein renders RAFs heterodimerization not possible. Indeed, C-RAF BxB lung tumors lacking B-RAF showed a reduced intensity in mitogenic signal.

5. Materials and Methods

5.1 Materials

5.1.1 Instruments

Supply	Manufacturer
100/40/20 µm cell strainer	BD Falcon
Cell culture hood	Heraeus Instrument
Cell culture incubator	Heraeus Instrument
Cryo microtome	Leica
Developing machine	Agfa
Electrophoresis power supply	Bio-Rad
Electrophoresis unit, small	Bio-Rad Mini-Protean II
Fine scale	Scaltec SBC 21
Fluroscence Microscope (CCD)	Leica (Hamamatsu Orca)
Glass coverslip	Leica
Heat block	Liebisch, Type 2099-DA
Homogenizer	Ultra-Turrax®
Horizontal electrophoresis gel	PEQLAB
Incubator (37 °C)	Heraeus B 6200
Inverted microscope	Olympus
Laser microdissection microscope	Leica
Mini centrifuge	Eppendorf; Biofuge 15, Heraeus
Mega centrifuge	J-6B, Beckman; Megafuge 1.0 R
Microlumat	EG&G, Berthold
Microscope Slides, Super Frost® Plus	Menzel-Gläzer
Microtome (rotating/sliding)	Leitz Wetzlar
Paraffin embedding machine	Leica
pH meter	Microprocessor, WTW
Roto-Gene 2000	Corbett Research

Scale	BP2100S, BP310S, Sartorius
Shaker	New Brunswick Scientific
Sonicator	Sono Plus HD 70
Spectrophotometer	Ultraspec 3000, Pharmacia Bio.
Thermocycler	PE9600, Perkin Elmer ; T3, B.M.
Vortex	Scientific Industries Genie-2
Water bath	GFL 1083, Amersham-Buchler

5.1.2 Disposable materials

Supply	Manufacturer
Cell culture dish (6- well)	Nunc Brand Products
Cell culture dish (12- well)	Nunc Brand Products
Cell culture dish (24- well)	Nunc Brand Products
Cell culture dish (96- well)	Nunc Brand Products
Cell culture dish (6 cm)	Corning
Cell culture dish (10 cm)	Corning
Cell strainer (100 µm)	Falcon
Cell strainer (40 µm)	Falcon
Conical tubes (15 ml)	Falcon
Conical tubes (50 ml)	Falcon
Cover slips	Menzel-Gläser
Embedding cassettes	Simport
Fast Optical 96-Well Reaction Plate	Applied Biosystems
Object slides SuperFrost	Thermo Scientific
Optical Adesive Film	Applied Biosystems
Thermo-strip (0,2 ml)	Thermo Scientific
Whatman paper	Protran
X-ray film	Fujifilm

5.1.3 Chemicals

Supply	Manufacturer

1 kb and 100 bp DNA ladder	Fermentas
Acrylamide (30%)/Bisacrylamide (0.8%)	Roth
Adenosin-5'Triphosphate (ATP)	Sigma
Agarose, ultra pure	Roth
Ammonium peroxydisulfate (APS)	Sigma
Ampicillin	Sigma
Bacto-Agar	Roth
BCP	Molecular Research Center Inc.
Bovine serum albumin (BSA)	Sigma
Bromodeoxyuridine (BrdU)	Sigma
Bromophenolblue	Sigma
β-Mercaptoethanol	Roth
Chloroform	Roth
Diaminobenzidine (DAB)	Sigma
DAPI	Sigma
Diethyl pyrocarbonate (DEPC)	Merck
Dimethylsulfoxide (DMSO)	Sigma
Dithiothreitol (DTT)	Sigma
DNase I (for type II cell isolation)	Sigma
dNTPs	MBI
Doxycycline	Sigma
ECL-System	Amersham
EDTA	Sigma
Entellan	Merck
Eosin	Merck
Ethanol	Roth
Ethidiumbromide	Invitrogen
Formaldehyde	Roth
Glycerol	Sigma
Guanidine thiocyanate	Roth
Haematoxylin	Merck
HEPES	Roth

Hydrochloride (HCl)	Roth
Hydrogen Peroxide (30 %)	A. Hartenstein
IGEPAL (NP-40)	Sigma
Isopropanol	Merck
Ketamin (10%)	Bela-pharm
SeaPlaque agarose (LMP)	Lonza
Magnesiumchloride	Sigma
Methanol	A. Hartenstein
Mowiol	Calbiochem
Paraffin wax (Histosec Pastillen)	Merck
Paraformaldehyde (PFA)	Sigma
Phenol	Roth
Phenol:Chloroform:Isoamylacohol	Roth
Phenol/Chloroform (TE saturated)	Roth
Ponceau S	Sigma
Protein ladder, BenchMark^{TM}	Invitrogen, MBI
Rnase-free water	Fermentas
Rompun (2%)	Bayer
SDS ultra pure	Roth
Serum (goat)	Chemicon
Serum (rabbit)	Chemicon
Serum (donkey)	Chemicon
Sodium citrate	Merck
Sodium Chloride	Roth
Sucrose	Fluka
TEMED	Roth
Cryomatrix (OCT)	Thermo Scientific
Trizol Reagent	Invitrogen
Triton-X100	Sigma
Tween 20	Sigma
Xylen	J. T. Baker

5.1.4 Antibodies

5.1.4.1 Primary antibodies

Antibody	Catalog Nr.	Manufacturer
anti-actin (I19)	sc-1616-R	Santa Cruz
anti-Aquaporin 5 (rabbit)	AQP-005	Alomone Labs
anti-B-RAF (H145) rabbit	sc-9002	Santa Cruz
anti-B-RAF (C19) rabbit	sc-166	Santa Cruz
anti-ß-catenin (mouse)	610154	BD Transduction Lab
anti ß-catenin (rabbit)	06-734	Upstate
anti-CCSP (Goat)	sc-9772	Santa Cruz
anti-CD3 (rabbit)	SP-7	Lab Vision
anti-CD45 (rat)	553076	Pharmingen
anti-CD45 (rat)	550539	Pharmingen
anti-CD16/CD32 (Rat)	553142	Santa Cruz
anti-cleaved caspase 3 (rabbit)	9664	Cell Signaling
anti-C-RAF (C12) rabbit	sc-133	Zymed Lab
anti-C-RAF (E10) mouse	sc-7267	Santa Cruz
anti cow cytokeratin (rabbit)	Z0622	DAKO
anti-E-cadherin (rabbit)	3195	Cell Signaling
anti-ERK 1/2 (rabbit)	4695	Cell Signaling
anti-F4/80 (rat)	ab6640	Abcam
anti-Ki67 (VPK452)	MM1	Vector laboratories
anti-$p120^{ctn}$ (6H11) (mouse)	sc-23873	Santa Cruz
anti-Pax5 (mouse)	610863	BD Transduction Lab
anti-phospho-ERK (rabbit)	4376	Cell Signaling
anti-phospho H3 (S10) (rabbit)	9701	Cell Signaling
anti-phospho-Stat3 (rabbit)	D3A7	Cell Signaling
anti-pro-SPC (rabbit)		Gift from J. Whitsett
anti-pro-SPC (rabbit)	AB 3786	Chemicon
anti-Stat3 (rabbit)	124H6	Cell Signaling
anti-Vimentin (C20) (rabbit)	sc-7557	Santa Cruz

anti-Vimentin (rabbit)	3932	Cell Signaling
anti-TTF-1 (Rat)	8G7G3/1	Imgenex

5.1.4.2 Secondary antibodies

Antibody	**Catalog Nr.**	**Manufacturer**
anti-Mouse IgG HRP conjugated	NA931 V	Amersham
anti-Rabbit IgG HRP conjugated	NA934	Amersham
anti-Rat IgG HRP conjugated	NA935	Amersham
anti-cow biotinylated (Rabbit)	Z0622	Dako
anti-goat biotinylated (Rabbit)	E0466	Dako
anti-mouse biotinylated (Rabbit)	E0354	Dako
anti-mouse biotinylated (Goat)	EO433	Dako
anti-rabbit biotinylated (Goat)	EO32	Dako

5.1.5 Plasmids

Vector	**Source**
SpC-B-RAF V600E	Rudolf Götz
SpC/SV40 polyA	Jeffrey A. Whitsett

5.1.6 Oligonucleotides

Mouse genotyping primers

Transgene	**Oligo Sequences**	**Annealing T.**
SpC-B-RAF V600E	S 5'- GGA GGA GGT GTG GAA TAT CAA AC – 3´ AS 5´- CCA ACA CTT CCA CAT GCA ATT C – 3´	60°C
SpC-C-RAF	S 5´- AAA GAC TCA ATG CAT GCC ACG – 3´ AS 5´- GCT GGT GTT CAT GCA CTG CAG – 3´	60°C

BXB 23		
RAG1	RAG4 5´- AGA CAC AAC GGC TTG CAA CAC AG – 3´ RAG5 5´- TGC CGA GAA AGT CCT TCT GCC AG – 3´ RAG6 5´- GTG GAA TGA GTG CGA GGC CAG A – 3´	63°C
SpC-rtTA	S 5´- CTC CAG GAA CCC ACT CTC TG – 3´ AS 5´- TCC TGG CTG TAG AGT CCC TG – 3´	60°C
Tet-O Cre	S 5´- GAG GAG GAT GAG GGT GTC TAT AGG T – 3´ AS 5´- GTG ATC AGC TCC AGG TTT GAC TT – 3´	60°C
B-RAF floxed allel	S 5´- TGT AGC CTC GGC TGT GGA ACT C – 3´ AS 5´- GAG ACC AAA CCA AGG ACC TCT G – 3´	60°C
B-RAF wt allel	S 5´- TGT AGC CTC GGC TGT GGA ACT C – 3´ AS 5´- GAG ACC AAA CCA AGG ACC TCT G – 3´	60°C
B-RAF deleted allel	S 5´- CCT GAA AGC TGC TAG TAG AAG AC – 3´ AS 5´- GAG ACC AAA CCA AGG ACC TCT G – 3´	60°C

Primers for RT-PCR

Gene	**Oligo Sequences**	**Annealing T**
Human B-RAF	S 5'- GTC ATC TTC ATC CTC AGA AG – 3´ AS 5´- TTC AAC ATT TTC ACT GCC AC- 3´	60°C
Mouse B-RAF	S 5'- CAT CTT CTT CCT CAT CCT CG – 3´	60°C

	AS 5´- TTC AAC ATT TTC ACT GCC AC- 3´	
Mouse E-cadherin	S 5'- GCTGGACCGAGAGAGTTA – 3´ AS 5´- TCGTTCTCCACTCTCACAT – 3´	60°C
Mouse HPRT	S 5'- TCAGTCAACGGGGGACATAAA – 3´ AS 5´- GGGGCTGTACTGCTTAACCAG – 3´	60°C
Mouse Vimentin	S 5´- GTGCGCCAGCAGTATGAAAG – 3´ AS 5´- GCATCGTTGTTCCGGTTGG -3´	60°C
ß actin	S 5'- GTCGTACCACAGGCATTGTGATGG – 3´ AS 5'- GCAATGCCTGGGTACATGGTGG – 3´	60°C

Primers for amplification of genomic DNA

Gene	**Oligo Sequences**	**Annealing T**
EGFR exon 19	S 5'- CCAGCTCACAAGGCAACATG – 3´ AS 5'- CCCACGTCCCTATAAGCAGA – 3´	55°C
EGFR exon 20	S 5'- AAGGGATATGCGTGCCTCTC – 3´ AS 5'- GGGTACTTCAGTGGACAGAC – 3´	55°C
EGFR exon 21	S 5'- ACCCTGTGTTCAGGTGCATG – 3´ AS 5'- CTGGGCTGTCAGGAAAATGC – 3´	55°C

K-Ras *exon 1*	S 5'- ATGACTGAGTATAAACTTGT – 3´ AS 5'- TCGTACTCATCCTCAAAGTG – 3´	55°C
K-Ras *exon 2*	S 5'- TACAGGAAACAAGTAGTAATTGATGGAGAA – 3´ AS 5'- ATAATGGTGAATATCTTCAAATGATTTAGT – 3´	50°C
$p19^{ARF}$ *exon 1*	S 5'- TTGTCACAGTGAGGCCGCCG – 3´ AS 5'- GCACCTGTGCGTGCAGCTTC – 3´	54°C
$p16^{INK4a}$ *exon 1*	S 5'- GCGAACTCGAGGAGAGCCAT – 3´ AS 5'- TTACCCGACTGCAGATGGGACAC – 3´	53°C
$p16^{INK4a}$ *exon 2*	S 5'- CTGGCCGTGATCCCTCTACT – 3´ AS 5'- GAGTGTCAGAAGCTTTTGGACCAA – 3´	53°C
$p16^{INK4a}$ *exon 3*	S 5'- CTGGCACCTAGGACAGCTTTATA – 3´ AS 5'- GAAAAAGGCGGGCTGAGGCC – 3´	53°C
p53 *exon 5*	S 5'- GCTTGTCCCCGACCTCCGTT – 3´ AS 5'- GGCTGCCAGTCCTAACCCCAC – 3´	55°C
p53 *exon 7*	S 5'- CCACAGGTCTCCCCAAGG – 3´ AS 5'- TGGCAAGTGGCTCCTGAC – 3´	55°C
p53 *exon 8*	S 5'- TCTTACTGCCTTGTGCTGGTCC – 3´ AS 5'- AGGCTCCTCCGCCTCCTT – 3´	55°C

LKB1 *exon 1*	S 5'- GCTCCCGAAGGGGACGAGGA – 3´ AS 5'- AGGAAGGGCTGCCCAAGGAG – 3´	50°C
LKB1 *exon 2*	S 5'- CAGCAGGCAGGGTCAGCTAA – 3´ AS 5'- CCAGCCCACTCCACCCACAG – 3´	50°C
LKB1 *exon 6*	S 5'- ACCCTGTAGCGGGGGG – 3´ AS 5'- CCTCCCATCCGGACAA – 3´	50°C

5.1.7 Enzymes

Enzyme	Catalog Nr.	Manufacturer
Collagenase	C0130-100MG	Sigma Aldrich
Dispase	17105-041	Gibco
DnaseI (for cloning)	EN0521	Fermentas
DnaseI (for type type II cell isolation)	04 716 728 001	Roche
Klenow fragment	EP0051	Fermentas
Proteinase K (for tail lysate)	7528.3	Roth
Proteinase K (for histology)	P5568-1ML	Sigma Aldrich
Shrimp Alkaline Phosphatase	EF0511	Fermentas
Taq-Polymerase	GC-002-0500	Genecraft
T4 DNA ligase	EL0011	Fermentas

5.1.8 Kits

Product	Catalog Nr.	Manufacturer
Dead End Fluorometric TUNEL Kit	TB235	Promega
First Strand cDNA Synthesis Kit	K1612	Fermantas

Pierce ECL Western Blotting Substrate	32106	Thermo Scientific
Pierce® BCA Protein Assay Kit	23227	Thermo Scientific
QIAGEN Plasmid Maxi Kit	12163	Qiagen
QIAprep Spin Miniprep Kit	27104	Qiagen
QIAquick PCR purification kit	28104	Qiagen
QIAquick Gel Extraction Kit	28706	Qiagen
REDTaq® ReadyMix™ PCR Reaction Mix	2523-100RXN	Sigma-Adrich
Trichrome stain (Masson)	HT15	Sigma-Adrich
Vectastain® ABC-peroxidase kit	PK6100	Vector laboratories

5.1.9 Bacterial strains and Mouse lines

Bacterial strains

Bacterial strains	**Source**
DH5α	New England Biolabs

Mouse lines

Mouse lines	**Source**
floxed B-RAF	MSZ
LC1 (Tet-o-Cre)	Gift from Hermann Bujard
Rag1 -/-	Jackson Laboratory
SpC-B-RAF V600E	This work
SpC-C-RAF BxB23	MSZ
SpC-rtTA	Gift from Jeffrey A. Whitsett

5.2 Methods

5.2.1 Bacterial manipulation

5.2.1.1 Transformation of competent bacteria

Competent E. Coli DH5α strain was transformed with plasmid DNA using the Heat Shock transformation protocol. Briefly, 50 µl of competent bacteria were mixed with ~100 ng plasmid DNA and incubated for 15 minutes on ice. The mix was placed for 45 seconds at 42°C and subsequently put on ice for 2 minutes. After adding 200 µl of LB medium without antibiotics the bacteria were incubated for 1 hour at 37° C. 100 µl of the culture were spread on LB agar plate supplied with required antibiotics and placed overnight at 37°C.

LB-Medium

1.0 % Trypton

0.5 % Yeast Extract

1.0 % NaCl

pH 7.2

For preparation of LB-plates, 1.5 % of agar was added.

Antibiotic concentrations were 100 µg/ml for Ampicillin and 70 µg/ml for Kanamycin.

5.2.1.2 Purification of plasmid DNA

For mini or maxi plasmid DNA purification, a single colony of previously transformed E coli was inoculated in 5 or 100 ml LB medium, respectively,

supplemented with required antibiotics and grown overnight at 37°C, 200 rpm in an shaking incubator. DNA isolation was achieved using QIAGEN Plasmid Kits following the manufacturer's instructions.

5.2.2 DNA analysis

5.2.2.1 Measurement of DNA concentration

DNA concentration was determined by measuring the absorbance at 260 nm using the NanoDrop ND 1000 spectrophotometer (Thermo Scientific). The DNA purity was controlled by the ratio of absorbance values at 260 nm and 280 nm (A_{260}/A_{280}) which should be between 1.8 and 2. If the ratio A_{260}/A_{280} is lower than 1.8 indicates protein contamination in the sample.

5.2.2.2 Enzymatic digestion of DNA with restriction enzymes

DNA molecules were digested according to the following protocol: 1-3 µg DNA, 10 unit of enzyme, 1X enzyme buffer and water up to 10 or 20 µl of final volume. Reactions were incubated at 37 °C for 1-2 hours. Enzyme´s activity was normally stopped by thermal inactivation according to the instructions of the supplier.

5.2.2.3 Ligation of DNA fragments

Sticky-end ligation was carried out by mixing, in a total volume of 20 µl, vector and insert (in a molar ratio of 1:3), 2 µl T4 DNA ligase buffer and 1 µl T4 DNA ligase (Fermentas). The reaction was incubated for 1 h at 22°C. T4 DNA ligase was inactivated by heating at 65°C for 15 minutes.

Blunt-end ligation was essentially carried out as previously described except that 2 µl of PEG 50% solution were added to the ligation mix.

5.2.2.4 Polymerase-Chain-Reaction (PCR)

Amplification of DNA fragments was achieved via PCR method in automated thermo cyclers (Biometra). Usually, the reaction was carried out in a 30 µl mix which comprised 2 µl DNA sample, 0.5 µl (10 pmol) primers forward and reverse, 3 µl 2 mM dNTPs mix (Fermentas), 3 µl 10X Taq polymerase buffer (Fermentas) and 0.2 µl Taq polymerase (Supplied by the Max Planck Institute of Biochemistry).

In some cases the REDTaq ReadyMix PCR Reaction with $MgCl_2$ (Sigma, R2523) was used according to the manufacturer´s instructions.

The following PCR cycling protocol was adjusted to each specific application:

3 min 95°C (initial denaturation)

30 cycles:

1 min 95°C (denaturation)

1 min T°C (appropriate annealing temperature according to the primers)

1-3 min 72°C (extension)

5 min 72°C (final extension)

4°C end

PCR products were resolved on 1-3 % agarose gel or digested with restriction enzymes for other applications.

5.2.2.5 Agarose gel electrophoresis

Agarose gels were prepared by mixing agarose in TAE buffer to a final concentration of 0.8-3 %. Each solution was boiled in a microwave oven until the agarose was completely dissolved. Ethidium bromide was added (0.5 µg/ml final concentration) and the solution was poured in a horizontal chamber. After the gel has become solid DNA samples were loaded onto the gel with an appropriate amount of 6x gel loading buffer and electrophoresis was performed in TAE at 120 V for 25-35 minutes. DNA fragments were visualized under UV light and photographs were taken.

TAE buffer:

40 mM Tris/Acetate pH 8.0

1 mM EDTA

5.2.2.6 DNA fragment extraction from agarose gel

DNA fragments separated by gel electrophoresis were extracted under UV light with a scalpel. Agarose was dissolved and the DNA was isolated using the QIAquick Gel Extraction Kit (Qiagen) according to the supplier´s instructions.

5.2.2.7 DNA sequencing

DNA sequencing was performed in an ABI 3730 sequencer. 10 µl sequencing mix included: ~ 300ng plasmid DNA or ~100 ng PCR product, 10 pmol primers, 1.5 µl BigDye Mix 3.1 (ABI) and 1 µl 5x-buffer. Sequences were visualized with Chromas Lite program.

5.2.3 RNA analysis

5.2.3.1 RNA isolation from cells and tissues

RNA isolation from cells or tissues was performed using TRIzol Reagent (Invitrogen) according to the manufacturer's instructions. Briefly, ~100 mg frozen tissue was homogenized in 1 ml TRIzol solution with an Ultra-Turrax (IKA) in cold environment. Phase separation was carried out by adding either 100 µl of BCP reagent (MCP) or 200 µl Chloroform. Probes were vortexed for 15 seconds, incubated at room temperature for 2-5 minutes and then centrifuged for 5 minutes at full speed at 4°C. RNA contained in the upper aqueous phase was precipitated by adding 500 µl isopropanol and centrifuged for 10 min at full speed at 4° C. Pellet containing RNA was washed with 70 % ethanol, air dried and dissolved in DEPC water.

5.2.3.2 Measurement of RNA concentration

RNA concentration was determined by measuring the absorbance at 260 nm using the NanoDrop ND 1000 spectrophotometer (Thermo Scientific). The RNA quality was estimated by the ratio of absorbance values at 260 nm and 280 nm (A_{260}/A_{280}). Only RNA with a ratio between 1.8 and 2 was used for further experiments.

5.2.3.3 cDNA synthesis

cDNA was made from total RNA by using the First Strand cDNA Synthesis Kit (Fermentas) according to the manufacturer´s instructions. To avoid genomic DNA contaminations, ~1 µg of total RNA was incubated for 30 minutes at 37°C with 1 µl RNase-free DNase I (Fermentas) in presence of 1 µl DNase I buffer

(Fermentas) in 10 µl total volume. Dnase I was inactivated by adding 1 µl EDTA and incubating for 10 minutes at 65°C. cDNA synthesis was carried out by directly using Dnase I treated RNA and oligo d(T) primers (First Strand cDNA Synthesis Kit, Fermentas).

5.2.3.4 Real-Time PCR

Quantitative Real-Time PCRs were performed in a Rotor-Gene 2000 detection system (Corbett Research). Each 20 µl PCR mix included 2 µl pre-diluted cDNA (1:10 or 1:20), 10 µl SYBR green PCR master mix (F-410S/L, DyNAmo HS SYBR Green qPCR Kit), 0.4 µl dye ROX and 10 pmol forward and reverse primers, respectively. The PCR program was as follows: 5 minutes Taq activation and initial denaturation at 95° C followed by 40 cycles with 15 seconds of denaturation at 95° C, 15 seconds annealing at 61° C and 15 seconds elongation at 72°C. Primers specificity was evaluated by melt curve analysis. To calculate the transcript levels of the genes of interest, the amplification efficiency was raised to the power of the threshold cycle (Ct-value). The Ct-value is defined as the number of cycles that are necessary for the fluorescence signal to exceed the background levels. In each sample all values were normalized to housekeeping genes such as β-actin or HPRT in order to obtain relative amount of target mRNA. All assays were performed in duplicate or triplicate.

5.2.4 Protein analysis

5.2.4.1 Preparation of whole protein lysates from cells and tissues

Tissues were lysed in ice-cold RIPA buffer with protease and 88hosphor88e88 inhibitor cocktails (Roche) using an Ultra-Turrax (IKA) homogenizer in a cold environment. After centrifuging for 10 minutes at full speed at 4°C, supernatant containing proteins was transferred into a new tube to measure the protein concentration.

RIPA buffer:

50 mM Tris-HCl, pH 8.0

150 mM NaCl

0.1 % SDS

0.5 % deoxycholate [DOC]

1 % Nonidet P-40

5.2.4.2 Measurement of protein concentration

Protein concentration was measured by using the BCA protein assay kit (#23225, Thermo Scientific) according to the supplier's instructions and using Bovine Serum Albumin (BSA) as standard control. 20-30 µg proteins were denatured by mixing with 3x laemmli buffer supplied with ß-Mercaptoethanol and heated for 10 minutes at 95 °C. Protein lysates were stored at -20°C prior to SDS-PAGE and immunoblot analysis.

3X laemmli buffer:

100 mM Tris/HCl pH 6.8

3 % SDS

45 % Glycerol

0.01 % Bromphenol blue

7.5 % ß-Mercaptoethanol

5.2.4.3 SDS-PAGE

SDS-PAGE was carried out using the Mini-PROTEAN Tetra Cell system from Bio-Rad (Catalog Number: 165-8000). Glass cassettes and electrophoresis modules were assembled according to the manufacturer's instructions. A resolving gel of 8 – 15 % acrylamide was prepared and poured between the two glass cassettes, leaving a space of about 1 cm for the staking gel. Isoparopanol was added on top of the solution. After the gel was polymerized the isopropanol was removed. A staking gel of 5 % acrylamide was prepared and poured on the resolving gel. Immediately, a comb with either 10 or 15 wells was inserted and the gel was allowed to polymerize. After polymerization the comb was removed and the wells were rinsed with water. The gel was placed in the electrophoresis module and the tank was filled with 1X SDS-PAGE running buffer. Protein samples were incubated at 95°C for 5 minutes and shortly centrifuged. Protein marker (6.5 µl/well) and protein samples (20 µl/well) were loaded on gel and the electrophoresis was run at 110 V by using a powerpac 300 power supply (Bio-Rad) for about 1.5 h. After electrophoresis the gel was removed from the glas cassettes and subjected to western blotting.

<u>Resolving gel:</u>

Tris 1M pH 8.8	1.25 ml

10 % SDS	50 µl
10 % APC	50 µl
30 % Acrylamide/Bisacrylamide	1.33-2.5 ml
Temed	3 µl
H_2O	up to 5 ml

Stacking gel:

Tris 1M pH 6.8	0.3125 ml
10 % SDS	25 µl
10 % APC	25 µl
30 % Acrylamide/Bisacrylamide	0.425 ml
Temed	2.5 µl
H_2O	up to 2.5 ml

10X SDS-PAGE buffer:

25 mM Tris/HCl pH 7.5

200 mM Glycine

0.1 % SDS

5.2.4.4 Immunoblotting

Western blot was carried out by using the Mini Trans-Blot Electrophoretic Transfer Cell system from BIO-RAD (Catalog number 170-3930) according to the manufacturer´s instructions. Briefly, the gel sandwich was prepared by placing in the following order: fiber pad, two Whatman filters, gel, nitrocellulose membrane, two Whatman filters and fiber pad. The sandwich gel was placed in the blotting

cassette and subsequently deposited in the blotting tank with a cold pack. The blotting tank was filled with SD-transblot buffer and run at 400 mA for 1 h. After blotting, the nitrocellulose membrane was incubated for 1 h at room temperature with 5% milk in NETG to block unspecific binding of the antibody. Primary antibodies were diluted in NETG and incubated overnight at 4°C. After incubation, the nitrocellulose membrane was washed 3x for 10 minutes with NETG and subjected to 91hosphor91e-conjugated secondary antibody (1:5000 diluted in NETG) for 1 h at room temperature. The nitrocellulose membrane was then washed 3x for 10 minutes with NETG and probed with the ECL chemiluminescence reaction (Thermo Scientific) according to the supplier´s instructions. Proteins were visualized by exposing the nitrocellulose membrane to an X-ray film that was subsequently developed in a PROTEC x-ray processor.

SD-transblot buffer:

50 mM Tris/HCl pH 7.5

40 mM Glycine

20 % Methanol

0.004 % SDS

1x NETG:

50 mM Tris/HCl pH 7.4

5 mM EDTA

0.05 % Triton X-100

150 mM NaCl

0.25 % Gelatine

5.2.4.5 Stripping of membrane

Stripping was carried out by incubating the nitrocellulose membrane with stripping buffer for 30 minutes at 54°C in a shaking incubator. The membrane was then washed 3x for 10 minutes with NETG, blocked with 5% milk in NETG for 1 h at room temperature and subsequently re-probed with other primary antibody as described in 5.2.4.4.

Stripping buffer:

62.5 mM Tris/HCl pH 6.8

2% SDS

100 mM β-Mercaptoethanol

5.2.5 Mouse work

All animal experiments were performed according to the regulations of the Bavarian State authorities. Mice were housed in air-filtered units with a 12-hour dark/light circle and with the access to food and water *ab libitum.*

5.2.5.1 Generation of transgenic mice

For generation of transgenic mice constitutively expressing B-RAF V600E in lung alveolar type II cells, the SpC-B-RAF V600E expression cassette (6,2 Kb) was resolved in a low melting agarose gel after digestion with *Hind III* restriction enzyme. The purified fragment was then injected into the pronucleus of fertilized eggs of FVB/n mice. Three positive founders that showed germ line transmission

were obtained. All founders were backcrossed to C57Bl/6 for more than six generations before experiments.

5.2.5.2 Breeding of mice

Mating was started when female and male mice were at least 4 and 6 weeks old, respectively. Often two females were bred together with one male. Matings were stopped by separating males from the pregnant female after ~2 weeks. Pups were separated from the mother at the age of 3-4 weeks, at this point each mouse was marked by an earmark and a tail biopsy was taken for genotyping.

5.2.5.3 Genotyping of mice

Tails were lysed overnight at 54°C in 190 µl lysis buffer and 10 µl proteinase K (0,4 mg/ml). Tail lysates were centrifuged at full speed for 10 minutes, diluted 1:10 or 1:40 with sterile water and used as template for PCR reaction as described in 5.2.2.4 using the genotyping primers reported in 5.1.6. In some cases a preliminary step of DNA isolation followed by PCR detection was necessary. DNA isolation was carried out by adding to tail lysates 250 µl lysis buffer and 250 µl of saturated NaCl (~5M NaCl). The mixture was mixed by inversion ~10 times, incubated 5 minutes at room temperature and centrifuged at full speed for 10 minutes. The supernatant was transferred into new 1.5 ml tube and DNA precipitation done by adding 600 µl isopropanol. The sample was mixed by inversion ~10 times, incubated 5 minutes at room temperature and centrifuged at full speed for 10 minutes. Supernatant was discarded and the DNA containing pellet was washed by adding 1 ml of 100% ethanol and centrifuging at full speed for 5 minutes. Finally, pellet was air-dried for 10-15 minutes at room temperature and resuspended with 50-100 µl sterile water. This DNA solution

was diluted 1:10 or 1:40 with sterile water and used as template for PCR reaction as described in 5.2.2.4 using the genotyping primers reported in 5.1.6.

Tail lysis buffer

50 mM EDTA

50 mM Tris-HCl

0.5% SDS

pH 8.0

5.2.5.4 Sacrification of mice

Mice were euthanized with a lethal intraperitoneal injection of Ketamin and Rompun in PBS. After the loss of righting reflex, mice were perfused by intra-cardiac injection of PBS and organs were isolated.

For embryos isolation, pregnant females were sacrificed by cervical dislocation. The uterus of the mice was dissected and embryos were isolated from the yolk sac.

5.2.5.5 Lung type II cells isolation

At least 24 hours before cell isolation, 10 cm dishes were coated with 6 ml PBS containing 42 µg anti-mouse CD45 (84 µl) (Pharmingen #553076) and 16 µg anti-mouse CD32 (41 µl) (Pharmingen #553142).

For lung type II cells isolation mice were euthanized and perfused as reported in 5.2.5.4. After intratracheal injection of 3-5 ml dispase (2,1 U/ml) followed by 0.5-1 ml of 1% low melting agarose, animals were covered with ice and incubated for ~2 minutes to harden the agarose. Lungs were dissected, placed in 15 ml tubes containing 3 ml collagenase (1 mg/ml) and incubated for 1 hour at 37°C. Excess

dispase was removed from 15 ml tubes and lungs were placed in 60 mm dishes containing 7 ml DMEM/HEPES and 100 U/ml DNaseI. By use of forceps, lungs were squeezed “like a tea bag” (for ~5 minutes) until only connective tissue was visible to move cells in suspension. Cell suspensions were filtered two times through a 100 µm cell strainer (Falcon), one time through a 40 µm cell strainer (Falcon) and placed in 50 ml tubes. After centrifugation at 130 g for 8 minutes at 4°C cell pellets were resuspended in 10 ml DMEM/HEPES containing 10% FBS. Antibody solution was discarded from coated plates and 10 cm dishes were gently washed with DMEM/HEPES. Cell suspensions were put on plates and incubated for 2 h at 37°C to allow the attachment of immune cells. Cell suspensions were collected from plates, placed in 50 ml tubes and centrifuged at 130 g for 8 minutes at 4°C. After gently removing the supernatant cell pellets were snap-frozen in liquid nitrogen.

5.2.6 Histological techniques

5.2.6.1 Paraffin-embedding and sectioning of tissue

Animals were sacrificed and lungs were fixed under 25 cm water pressure with 4 % buffered paraformaldehyde and paraffin embedded**.** Tissue was placed in proper embedding cassettes and paraffin embedding was carried out as follow. Paraffinization requires essentially three steps: dehydration, clearing and embedding. Dehydration process was achieved by passing the tissue through a series of increasing alcohol concentrations, the detailed steps were: 1 hour in 50% ethanol, 1 hour in 70% ethanol, 1 hour in 80% ethanol, 1 hour in 90%

ethanol and 2 times for 1 hour in 100% ethanol. Clearing refers to the use of an intermediate fluid that is miscible with ethanol and paraffin since these two substances are immiscible. This step was carried out by passing the tissue, twice for 30 minutes, through a 1:1 mixture of xylol and ethanol and subsequently 2 times for 30 minutes in xylol only. All these steps were performed at room temperature in an automated tissue processor (Shandon Citadel 2000). For embedding procedure the tissue was transferred into melted paraffin and incubated for 1 hour at 65°C and then in fresh paraffin for 2 hours or overnight at 65°C. Finally, the tissue was placed into an embedding mold and melted paraffin was poured into the mold to form a block. After cooling down the blocks were ready for sectioning. Tissue blocks were sectioned in 6 µm sections by using a manual rotary microtome (Leica RM2235).

Embedding of mouse embryos was essentially carried out as already described except that chloroform was used instead of xylol and that the last step of paraffin incubation was prolonged to 5-7 days. Embryos tissue blocks were sectioned in 10 µm microsections.

<u>4% PFA in PBS</u>

Place 37 g PFA in 850 ml H_2O

Add 2-3 drops of 1 N NaOH

Heat to 60°C and mix until the PFA is dissolved.

Add 100 ml 10X PBS and bring pH to 7.4.

Bring final volume to 1l with H_2O.

5.2.6.2 Optimal Cutting Temperature (O.C.T.)-embedding and cryosectioning of tissue

Freshly isolated tissue was fixed in 4% PFA at 4°C for 4 hours. After washing two times for 10 minutes in PBS, the tissue was transferred into 15% sucrose in PBS and incubated for 4 hours at 4°C. Subsequently, it was placed overnight at 4°C in 30% sucrose in PBS. Finally, the tissue was embedded on dry ice in OCT (Shandon Crymatrix) and stored at -80°C. Blocks were sectioned into 6-10 µm microsections that were either directly used for experiments or stored at -80°C.

5.2.6.3 Hematoxilin and Eosin staining of tissue (H & E staining)

H & E staining of paraffin embedded sections was carried out following the protocol reported below:

	Solution	Time
Deparaffinization and reydration	Xylol-I	10 minutes
	Xylol-II	10 minutes
	100% alcohol-I	5 seconds
	100% alcohol-II	5 seconds
	100% alcohol-III	5 seconds
	700% alcohol	10 minutes
	Water	5 minutes
	Haematoxylin	2 minutes
	Tape water	5 minutes
	Eosin	5 seconds
	Water	5 seconds
Dehydration	70% alcohol	5 seconds
	100% alcohol-I	5 seconds
	100% alcohol-II	5 seconds
	100% alcohol-III	10 minutes
	100% alcohol-III	10 minutes
	Xylol-I	10 minutes
	Xylol-II	10 minutes

After the last incubation in xylol the tissue sections were mounted in Entellan (Merck).

5.2.6.4 Immunostaining of tissue

For immunostaining of tissue, paraffin embedded tissue sections were deparaffinised and rehydrated as reported in the H&E staining protocol. Applied

antigen-retrieval methods were either heat- or enzymatic-mediated according to the antibodies that were used. In the heat-mediated antigen retrieval, tissue sections were placed in a microwavable vessel containing 10 mM Citrate buffer (pH 6) and heated in a microwave oven for 6-20 minutes. In the enzymatic-mediated antigen retrieval, proteinase K solution (20 µg/ml in TE buffer, pH 8) was pipetted onto the tissue slides and incubated for 7-20 minutes at 37°C. After cooling down for 30 minutes at room temperature, sections were washed with water and then three times for five minutes with PBS. Endogenous peroxidase activity was quenched by incubating the tissue slides with 0.3-3% H_2O_2 in PBS or methanol for 30 minutes at room temperature. After washing three times for five minutes, unspecific binding of the antibodies was blocked by incubating the tissue with a blocking solution containing 3-5 % normal serum which was prepared from the species in which the secondary antibody is made and 0.1 % TritonX-100 in PBS for 1 hour at room temperature. Primary antibody was diluted in blocking solution, applied on tissue sections and incubated overnight at 4°C. After washing three times for 10 minutes, tissue sections were incubated for 90 minutes at room temperature with biotinylated secondary antibody (DakoCytomation) 1:200 diluted in blocking solution. ABC reagent ((Vectastain Elite ABC Kit, Vector Labs) was prepared and applied to tissue sections according to the manufacturer´s instructions, and then developed in diaminobenzidine (DAB) (0.8% H_2O_2 in 1 ml DAB). The reaction was stopped with water for 5 minutes, subsequently tissue slides were counterstained with hematoxilin for 20 seconds, washed with tap water, dehydrated and mounted in Entellan (Merck) as reported in the H&E staining protocol.

Immunofluorescence staining was carried out essentially as previously described except that secondary antibody fluorochrome-conjugated, diluted (1:200) in blocking solution, was used. Moreover counterstaining was done by using 4'.6-diamidino-2-phenylindole (DAPI) and by mounting with Mowiol (Roth).

In the table below the antibody dilutions and antigen retrieval conditions applied to each immunostaining are reported:

Article	Company	Dilution	Antigen retrieval	Incubation
Aquaporin-5	Almone Labs	1:1000	Citrate buffer	6 min
B-RAF (H145)	Santa Cruz	1:250	Citrate buffer	10 min
CCSP (T18)	Santa Cruz	1:2500	Citrate buffer	12 min
CD3	Lab Vision	1:1000	Citrate buffer	10 min
CD45	Pharmingen	1:20	Proteinase K	20 min at 37°C
cleaved Caspase-3	Cell Signaling	1:200	Citrate buffer	20 min
C-RAF (E10)	Santa Cruz	1:100	Citrate buffer	10 min
Cytokeratin	Dako	1:400	Citrate buffer	10 min
F4/80	Abcam	1:100	Proteinase K	7 min at room temperature
Ki67	Vector laboratories	1:50	Citrate buffer	15 min
Pax5	BD Transduction laboratories	1:1000	Citrate buffer	6 min
Phospho-ERK (Thr202/Tyr204)	Cell Signaling	1:100	Citrate buffer	10 min
Phospho-H3 (Ser10)	Cell Signaling	1:200	Citrate buffer	15 min

Phospho-Stat3 (Tyr 705)	Cell Signaling	1:100	Citrate buffer	15 min
Pro-SPC	J. Whitsett	1:2000	Citrate buffer	10 min
Pro-SPC	Chemicon	1:500	Citrate buffer	10 min
TTF-1	Imgenex	1:100	Tris-EDTA	20 min
Vimentin (C20)	Santa Cruz	1:200	Citrate buffer	12 min

10 mM Citrate buffer (pH 6):

Stock solutions:

Solution A = 0.1 M citrate acid solution (21.01 g citric acid, monohydrate in 1 L H_2O)

Solution B = 0.1 M sodium citrate (29.49 g trisodium citrate dehydrate in 1 L H_2O)

Working solution (pH 6):

18 ml solution A

82 ml solution B

to 1 L with H2O

TE buffer:

50 nM Tris Base (pH 8.0)

1 mM EDTA

0.5% Triton X-100

5.2.6.5 Immunohistopathological analysis of tissue

For analysis of airspace enlargements lungs from wild type and transgenic mice were evaluated blindly by two independent examiners. Tissue samples were graded in the following manner: 1) Micro- and macro- scopically normal; 2)

Macroscopically normal, but microscopically abnormal [airspace enlargement]; 3) Macroscopic abnormalities [bulb formation].

For scoring of active caspase 3 and Ki67 immunostainings at least 10 randomly selected areas were counted from at least 4 mice for each time point. Collagen accumulation was detected by staining lung sections with Masson´s Trichrome stain kit (Sigma Aldrich). Lung Goblet cells hyperplasia and mucus production were assessed by calculating the fraction of Alcian Blue positive stain per length of basal membrane in 7-10 large and small bronchial airways (wild type [1-3 months] *n*= 6, [4-28 months] *n*= 8; SpC-B-RAF V600E [1-3 months] *n*= 7, [4-28 months] *n*= 8). Calculation of lymphoid follicles incidence was done by analyzing CD45 stained lung sections under the microscope for each mouse. Macrophages quantification was carried out by counting the number of F4/80 positive cells in 10 randomly selected pictures taken at 40X magnification per mouse lung section. 9 animals for each age and genotype were used.

Lung tumor load was determined by counting the number of tumors in 5-7 randomly selected pictures (taken at 10x magnification) in H&E or C-RAF stained lung sections. For each lung, two no consecutive slides (at least ~ 100 µm apart) were used for quantification. At least 5 mice for each genotype and age were analyzed. Tumor volume (in μm^3) was calculated in the same lung sections used to determine the tumor load by assuming a spherical form. For quantitation of active caspase 3, TUNEL, Ki67 and phosphoH3 immunostainings 15 randomly selected tumors were counted from 5 mice for each genotype. The intensity of the MAPK signal in tumor bearing lungs was assessed by estimating the percentage of tumor cells with 102hosphor-ERK nuclear staining. For each lung

at least 10 tumors were quantified and at least 5 mice for each genotype were analyzed.

5.2.6.6 PCR-amplification of genomic DNA from paraffin section

DNA of tumors was isolated from 6 µm H&E stained paraffin embedded lung sections by using a sterile scalpel. DNA was isolated after solubilisation of the pooled material in 30 µl of lysis buffer (10mM TrisHCl, 1 mM EDTA, 1% w/v Tween 20, 100µg/ml proteinase K) overnight at 37º C. Proteinase K was blocked by heating the samples to 95º C for 20 minutes. 1 µl of this sample was used for PCR amplification of genomic DNA following the protocol reported in 5.2.2.4 and using the oligos listed in 5.1.6

5.2.7 Statistical analysis

Data sets from independent experiments were pooled and the results were shown as means with SEM (standard error of the mean). All statistical analyses were performed using GraphPad Prism4 software. Log-rank analysis was used to compare the survival rate of different group of mice. Student's *t*-test (two-tailed) was used to compare two groups ($P<0.05$ was considered significant).

8. References

Andersen, M. H., J. Fensterle, et al. (2004). "Immunogenicity of constitutively active V599EBRaf." Cancer Res 64(15): 5456-60.

Andersson, C. K., M. Mori, et al. (2010). "Alterations in lung mast cell populations in patients with chronic obstructive pulmonary disease." Am J Respir Crit Care Med 181(3): 206-17.

Ang, S. L. and J. Rossant (1994). "HNF-3 beta is essential for node and notochord formation in mouse development." Cell 78(4): 561-74.

Baljuls, A., W. Schmitz, et al. (2008). "Positive regulation of A-RAF by phosphorylation of isoform-specific hinge segment and identification of novel phosphorylation sites." J Biol Chem 283(40): 27239-54.

Barbacid, M. (1987). "ras genes." Annu Rev Biochem 56: 779-827.

Barnes, P. J. (2000). "Mechanisms in COPD: differences from asthma." Chest 117(2 Suppl): 10S-4S.

Barnes, P. J. (2004). "Alveolar macrophages as orchestrators of COPD." COPD 1(1): 59-70.

Baumann, B., C. K. Weber, et al. (2000). "Raf induces NF-kappaB by membrane shuttle kinase MEKK1, a signaling pathway critical for transformation." Proc Natl Acad Sci U S A 97(9): 4615-20.

Blasco, R. B., S. Francoz, et al. (2011). "c-Raf, but not B-Raf, is essential for development of K-Ras oncogene-driven non-small cell lung carcinoma." Cancer Cell 19(5): 652-63.

Brambilla, E., W. D. Travis, et al. (2001). "The new World Health Organization classification of lung tumours." Eur Respir J 18(6): 1059-68.

Cardoso, W. V. and J. Lu (2006). "Regulation of early lung morphogenesis: questions, facts and controversies." Development 133(9): 1611-24.

Carney, D. N. (2002). "Lung cancer--time to move on from chemotherapy." N Engl J Med 346(2): 126-8.

Ciampi, R., J. A. Knauf, et al. (2005). "Oncogenic AKAP9-BRAF fusion is a novel mechanism of MAPK pathway activation in thyroid cancer." J Clin Invest 115(1): 94-101.

Coussens, L. M., C. L. Tinkle, et al. (2000). "MMP-9 supplied by bone marrow-derived cells contributes to skin carcinogenesis." Cell 103(3): 481-90.

Curtis, J. L., C. M. Freeman, et al. (2007). "The immunopathogenesis of chronic obstructive pulmonary disease: insights from recent research." Proc Am Thorac Soc 4(7): 512-21.

Dankort, D., E. Filenova, et al. (2007). "A new mouse model to explore the initiation, progression, and therapy of BRAFV600E-induced lung tumors." Genes Dev 21(4): 379-84.

Davies, H., G. R. Bignell, et al. (2002). "Mutations of the BRAF gene in human cancer." Nature 417(6892): 949-54.

de Torres, J. P., G. Bastarrika, et al. (2007). "Assessing the relationship between lung cancer risk and emphysema detected on low-dose CT of the chest." Chest 132(6): 1932-8.

Ding, L., G. Getz, et al. (2008). "Somatic mutations affect key pathways in lung adenocarcinoma." Nature 455(7216): 1069-75.

Emuss, V., M. Garnett, et al. (2005). "Mutations of C-RAF are rare in human cancer because C-RAF has a low basal kinase activity compared with B-RAF." Cancer Res 65(21): 9719-26.

Flanders, K. C. (2004). "Smad3 as a mediator of the fibrotic response." Int J Exp Pathol 85(2): 47-64.

Forbes, S. A., N. Bindal, et al. (2011). "COSMIC: mining complete cancer genomes in the Catalogue of Somatic Mutations in Cancer." Nucleic Acids Res 39(Database issue): D945-50.

Fransen, K., M. Klintenas, et al. (2004). "Mutation analysis of the BRAF, ARAF and RAF-1 genes in human colorectal adenocarcinomas." Carcinogenesis 25(4): 527-33.

Galabova-Kovacs, G., A. Kolbus, et al. (2006). "ERK and beyond: insights from B-Raf and Raf-1 conditional knockouts." Cell Cycle 5(14): 1514-8.

Garnett, M. J., S. Rana, et al. (2005). "Wild-type and mutant B-RAF activate C-RAF through distinct mechanisms involving heterodimerization." Mol Cell 20(6): 963-9.

Giehl, K. (2005). "Oncogenic Ras in tumour progression and metastasis." Biol Chem 386(3): 193-205.

Gordon, S. B. and R. C. Read (2002). "Macrophage defences against respiratory tract infections." Br Med Bull 61: 45-61.

Gotz, R., B. W. Kramer, et al. (2004). "BAG-1 haplo-insufficiency impairs lung tumorigenesis." BMC Cancer 4: 85.

Greenlee, K. J., Z. Werb, et al. (2007). "Matrix metalloproteinases in lung: multiple, multifarious, and multifaceted." Physiol Rev 87(1): 69-98.

Hatzivassiliou, G., K. Song, et al. (2010). "RAF inhibitors prime wild-type RAF to activate the MAPK pathway and enhance growth." Nature 464(7287): 431-5.

Heidorn, S. J., C. Milagre, et al. (2010). "Kinase-dead BRAF and oncogenic RAS cooperate to drive tumor progression through CRAF." Cell 140(2): 209-21.

Holgate, S. T., D. E. Davies, et al. (2000). "Epithelial-mesenchymal interactions in the pathogenesis of asthma." J Allergy Clin Immunol 105(2 Pt 1): 193-204.

Houghton, A. M., M. Mouded, et al. (2008). "Common origins of lung cancer and COPD." Nat Med 14(10): 1023-4.

Huelsken, J., R. Vogel, et al. (2000). "Requirement for beta-catenin in anterior-posterior axis formation in mice." J Cell Biol 148(3): 567-78.

Jarnicki, A., T. Putoczki, et al. (2010). "Stat3: linking inflammation to epithelial cancer - more than a "gut" feeling?" Cell Div 5: 14.

Jeffrey, P. K. (1998). "The development of large and small airways." Am J Respir Crit Care Med 157(5 Pt 2): S174-80.

Ji, H., Z. Wang, et al. (2007). "Mutations in BRAF and KRAS converge on activation of the mitogen-activated protein kinase pathway in lung cancer mouse models." Cancer Res 67(10): 4933-9.

Jones, D. T., S. Kocialkowski, et al. (2008). "Tandem duplication producing a novel oncogenic BRAF fusion gene defines the majority of pilocytic astrocytomas." Cancer Res 68(21): 8673-7.

Jones, D. T., S. Kocialkowski, et al. (2009). "Oncogenic RAF1 rearrangement and a novel BRAF mutation as alternatives to KIAA1549:BRAF fusion in activating the MAPK pathway in pilocytic astrocytoma." Oncogene 28(20): 2119-23.

Kanai-Azuma, M., Y. Kanai, et al. (2002). "Depletion of definitive gut endoderm in Sox17-null mutant mice." Development 129(10): 2367-79.

Karreth, F. A. and D. A. Tuveson (2009). "Modelling oncogenic Ras/Raf signalling in the mouse." Curr Opin Genet Dev 19(1): 4-11.

Kebache, S., J. Ash, et al. (2007). "Grb10 and active Raf-1 kinase promote Bad-dependent cell survival." J Biol Chem 282(30): 21873-83.

Kerkhoff, E., L. M. Fedorov, et al. (2000). "Lung-targeted expression of the c-Raf-1 kinase in transgenic mice exposes a novel oncogenic character of the wild-type protein." Cell Growth Differ 11(4): 185-90.

Kim, C. F., E. L. Jackson, et al. (2005). "Identification of bronchioalveolar stem cells in normal lung and lung cancer." Cell 121(6): 823-35.

Kolch, W. (2005). "Coordinating ERK/MAPK signalling through scaffolds and inhibitors." Nat Rev Mol Cell Biol 6(11): 827-37.

Kramer, B. W., R. Gotz, et al. (2004). "Use of mitogenic cascade blockers for treatment of C-Raf induced lung adenoma in vivo: CI-1040 strongly reduces growth and improves lung structure." BMC Cancer 4: 24.

Krupke, D. M., D. A. Begley, et al. (2008). "The Mouse Tumor Biology database." Nat Rev Cancer 8(6): 459-65.

Lambrecht, B. N. (2006). "Alveolar macrophage in the driver's seat." Immunity 24(4): 366-8.

Lee, G., T. C. Walser, et al. (2009). "Chronic inflammation, chronic obstructive pulmonary disease, and lung cancer." Curr Opin Pulm Med 15(4): 303-7.

Lee, J. W., Y. H. Soung, et al. (2005). "Mutational analysis of the ARAF gene in human cancers." APMIS 113(1): 54-7.

Li, S. and J. M. Sedivy (1993). "Raf-1 protein kinase activates the NF-kappa B transcription factor by dissociating the cytoplasmic NF-kappa B-I kappa B complex." Proc Natl Acad Sci U S A 90(20): 9247-51.

Li, Y., H. Du, et al. (2007). "Activation of the signal transducers and activators of the transcription 3 pathway in alveolar epithelial cells induces inflammation and adenocarcinomas in mouse lung." Cancer Res 67(18): 8494-503.

Maeda, Y., V. Dave, et al. (2007). "Transcriptional control of lung morphogenesis." Physiol Rev 87(1): 219-44.

Malumbres, M. and M. Barbacid (2003). "RAS oncogenes: the first 30 years." Nat Rev Cancer 3(6): 459-65.

Matallanas, D., M. Birtwistle, et al. (2011). "Raf family kinases: old dogs have learned new tricks." Genes Cancer 2(3): 232-60.

McCubrey, J. A., L. S. Steelman, et al. (2007). "Roles of the Raf/MEK/ERK pathway in cell growth, malignant transformation and drug resistance." Biochim Biophys Acta 1773(8): 1263-84.

McMahon, M. (2010). "RAF translocations expand cancer targets." Nat Med 16(7): 749-50.

Metzger, R. J., O. D. Klein, et al. (2008). "The branching programme of mouse lung development." Nature 453(7196): 745-50.

Meuwissen, R. and A. Berns (2005). "Mouse models for human lung cancer." Genes Dev 19(6): 643-64.

Michaloglou, C., L. C. Vredeveld, et al. (2005). "BRAFE600-associated senescence-like cell cycle arrest of human naevi." Nature 436(7051): 720-4.

Mikula, M., M. Schreiber, et al. (2001). "Embryonic lethality and fetal liver apoptosis in mice lacking the c-raf-1 gene." EMBO J 20(8): 1952-62.

Moelling, K., B. Heimann, et al. (1984). "Serine- and threonine-specific protein kinase activities of purified gag-mil and gag-raf proteins." Nature 312(5994): 558-61.

Mombaerts, P., J. Iacomini, et al. (1992). "RAG-1-deficient mice have no mature B and T lymphocytes." Cell 68(5): 869-77.

Morrisey, E. E., Z. Tang, et al. (1998). "GATA6 regulates HNF4 and is required for differentiation of visceral endoderm in the mouse embryo." Genes Dev 12(22): 3579-90.

Moyron-Quiroz, J. E., J. Rangel-Moreno, et al. (2004). "Role of inducible bronchus associated lymphoid tissue (iBALT) in respiratory immunity." Nat Med 10(9): 927-34.

Mucenski, M. L., S. E. Wert, et al. (2003). "beta-Catenin is required for specification of proximal/distal cell fate during lung morphogenesis." J Biol Chem 278(41): 40231-8.

Nekhoroshkova, E., S. Albert, et al. (2009). "A-RAF kinase functions in ARF6 regulated endocytic membrane traffic." PLoS One 4(2): e4647.

Nicod, L. P. (1999). "Pulmonary defence mechanisms." Respiration 66(1): 2-11.

O'Hagan, R. C., M. Wu, et al. (2005). Genetically Engineered Mouse Models of Human Cancer for Drug Discovery and Development. The Oncogenomics Handbook. W. J. LaRochelle and R. A. Shimkets, Humana Press: 247-261.

Pabst, R. and I. Gehrke (1990). "Is the bronchus-associated lymphoid tissue (BALT) an integral structure of the lung in normal mammals, including humans?" Am J Respir Cell Mol Biol 3(2): 131-5.

Palanisamy, N., B. Ateeq, et al. (2010). "Rearrangements of the RAF kinase pathway in prostate cancer, gastric cancer and melanoma." Nat Med 16(7): 793-8.

Panka, D. J., W. Wang, et al. (2006). "The Raf inhibitor BAY 43-9006 (Sorafenib) induces caspase-independent apoptosis in melanoma cells." Cancer Res 66(3): 1611-9.

Perl, A. K., S. E. Wert, et al. (2005). "Conditional recombination reveals distinct subsets of epithelial cells in trachea, bronchi, and alveoli." Am J Respir Cell Mol Biol 33(5): 455-62.

Polzien, L., A. Baljuls, et al. "Bad contributes to RAF-mediated proliferation and cooperates with B-RAF-V600E in cancer signaling." J Biol Chem.

Polzien, L., A. Baljuls, et al. (2009). "Identification of novel in vivo phosphorylation sites of the human proapoptotic protein BAD: pore-forming activity of BAD is regulated by phosphorylation." J Biol Chem 284(41): 28004-20.

Postma, D. S. and W. Timens (2006). "Remodeling in asthma and chronic obstructive pulmonary disease." Proc Am Thorac Soc 3(5): 434-9.

Poulikakos, P. I., C. Zhang, et al. (2010). "RAF inhibitors transactivate RAF dimers and ERK signalling in cells with wild-type BRAF." Nature 464(7287): 427-30.

Pritchard, C. A., L. Bolin, et al. (1996). "Post-natal lethality and neurological and gastrointestinal defects in mice with targeted disruption of the A-Raf protein kinase gene." Curr Biol 6(5): 614-7.

Puchelle, E. (1992). "Airway secretions: new concepts and functions." Eur Respir J 5(1): 3-4.

Qu, P., J. Roberts, et al. (2009). "Stat3 downstream genes serve as biomarkers in human lung carcinomas and chronic obstructive pulmonary disease." Lung Cancer 63(3): 341-7.

Raherison, C. and P. O. Girodet (2009). "Epidemiology of COPD." Eur Respir Rev 18(114): 213-21.

Rapp, U. R., J. Fensterle, et al. (2003). "Raf kinases in lung tumor development." Adv Enzyme Regul 43: 183-95.

Rapp, U. R., M. D. Goldsborough, et al. (1983). "Structure and biological activity of v-raf, a unique oncogene transduced by a retrovirus." Proc Natl Acad Sci U S A 80(14): 4218-22.

Rapp, U. R., C. Korn, et al. (2009). "MYC is a metastasis gene for non-small-cell lung cancer." PLoS One 4(6): e6029.

Rawlins, E. L. and B. L. Hogan (2006). "Epithelial stem cells of the lung: privileged few or opportunities for many?" Development 133(13): 2455-65.

Rawlins, E. L., T. Okubo, et al. (2009). "The role of Scgb1a1+ Clara cells in the long-term maintenance and repair of lung airway, but not alveolar, epithelium." Cell Stem Cell 4(6): 525-34.

Roberts, P. J. and C. J. Der (2007). "Targeting the Raf-MEK-ERK mitogen-activated protein kinase cascade for the treatment of cancer." Oncogene 26(22): 3291-310.

Robinson, M. J. and M. H. Cobb (1997). "Mitogen-activated protein kinase pathways." Curr Opin Cell Biol 9(2): 180-6.

Roskoski, R., Jr. (2010). "RAF protein-serine/threonine kinases: structure and regulation." Biochem Biophys Res Commun 399(3): 313-7.

Sato, M., D. S. Shames, et al. (2007). "A translational view of the molecular pathogenesis of lung cancer." J Thorac Oncol 2(4): 327-43.

Schreck, R. and U. R. Rapp (2006). "Raf kinases: oncogenesis and drug discovery." Int J Cancer 119(10): 2261-71.

Schubbert, S., G. Bollag, et al. (2007). "Deregulated Ras signaling in developmental disorders: new tricks for an old dog." Curr Opin Genet Dev 17(1): 15-22.

Schubbert, S., K. Shannon, et al. (2007). "Hyperactive Ras in developmental disorders and cancer." Nat Rev Cancer 7(4): 295-308.

Shapiro, S. D. (2005). "COPD unwound." N Engl J Med 352(19): 2016-9.

Shaw, A. T., A. Meissner, et al. (2007). "Sprouty-2 regulates oncogenic K-ras in lung development and tumorigenesis." Genes Dev 21(6): 694-707.

Skillrud, D. M., K. P. Offord, et al. (1986). "Higher risk of lung cancer in chronic obstructive pulmonary disease. A prospective, matched, controlled study." Ann Intern Med 105(4): 503-7.

Sminia, T., G. J. van der Brugge-Gamelkoorn, et al. (1989). "Structure and function of bronchus-associated lymphoid tissue (BALT)." Crit Rev Immunol 9(2): 119-50.

Sullivan, N. J., A. K. Sasser, et al. (2009). "Interleukin-6 induces an epithelial-mesenchymal transition phenotype in human breast cancer cells." Oncogene 28(33): 2940-7.

Takeda, K., K. Noguchi, et al. (1997). "Targeted disruption of the mouse Stat3 gene leads to early embryonic lethality." Proc Natl Acad Sci U S A 94(8): 3801-4.

Tidyman, W. E. and K. A. Rauen (2009). "The RASopathies: developmental syndromes of Ras/MAPK pathway dysregulation." Curr Opin Genet Dev 19(3): 230-6.

Tockman, M. S., N. R. Anthonisen, et al. (1987). "Airways obstruction and the risk for lung cancer." Ann Intern Med 106(4): 512-8.

Tschernig, T. and R. Pabst (2000). "Bronchus-associated lymphoid tissue (BALT) is not present in the normal adult lung but in different diseases." Pathobiology 68(1): 1-8.

Wan, P. T., M. J. Garnett, et al. (2004). "Mechanism of activation of the RAF-ERK signaling pathway by oncogenic mutations of B-RAF." Cell 116(6): 855-67.

Wang, H. G., U. R. Rapp, et al. (1996). "Bcl-2 targets the protein kinase Raf-1 to mitochondria." Cell 87(4): 629-38.

Weber, C. K., J. R. Slupsky, et al. (2001). "Active Ras induces heterodimerization of cRaf and BRaf." Cancer Res 61(9): 3595-8.

Wellbrock, C., M. Karasarides, et al. (2004). "The RAF proteins take centre stage." Nat Rev Mol Cell Biol 5(11): 875-85.

Wilhelm, S. M., C. Carter, et al. (2004). "BAY 43-9006 exhibits broad spectrum oral antitumor activity and targets the RAF/MEK/ERK pathway and receptor tyrosine kinases involved in tumor progression and angiogenesis." Cancer Res 64(19): 7099-109.

Willis, B. C. and Z. Borok (2007). "TGF-beta-induced EMT: mechanisms and implications for fibrotic lung disease." Am J Physiol Lung Cell Mol Physiol 293(3): L525-34.

Wilson, D. O., J. L. Weissfeld, et al. (2008). "Association of radiographic emphysema and airflow obstruction with lung cancer." Am J Respir Crit Care Med 178(7): 738-44.

Wojnowski, L., L. F. Stancato, et al. (1998). "Craf-1 protein kinase is essential for mouse development." Mech Dev 76(1-2): 141-9.

Wojnowski, L., A. M. Zimmer, et al. (1997). "Endothelial apoptosis in Braf-deficient mice." Nat Genet 16(3): 293-7.

Wright, J. L. and A. Churg (2006). "Advances in the pathology of COPD." Histopathology 49(1): 1-9.

Yildirim, A. O., V. Muyal, et al. (2010). "Palifermin induces alveolar maintenance programs in emphysematous mice." Am J Respir Crit Care Med 181(7): 705-17.

Zambrowicz, B. P. and A. T. Sands (2003). "Knockouts model the 100 best-selling drugs--will they model the next 100?" Nat Rev Drug Discov 2(1): 38-51.

7. Appendix

7.1 Abbreviations

Abbreviation	Full name
APS	Ammoniumpersulfate
ATP	Adenosine-5'-triphosphate
BCP	1-Bromo-3-Chloropropane (C_3H_6BrCl)
bp	Basepairs
BSA	Bovine Serum Albumin
°C	Degree Celsius
CCSP	Clara cell secretory protein
cDNA	Complementary DNA
CO_2	Carbon dioxide
DAPI	4',6-Diamidino-2-phenylindol
DMEM	Dulbecco's Modified Eagle Medium
DMSO	Dimethylsulphoxide
DNA	Deoxyribonucleic acid
dNTP	(Di)Desoxynucleotide triphosphate
DOX	Doxycycline
ECL	Enhanced Chemiluminescence
EDTA	Ethylenediaminetetraacetic acid
et al.	Et alii
FCS	Fetal calf serum
FITC	Fluorescein isothiocyanate
Floxed	Flanked by loxP site
g	Gram
GAPDH	Glyceraldehyde-3-phosphate dehydrogenase
HCl	Hydrochloric acid
H&E	Hematoxylin/eosin staining
hm	Hyper methylation
HPRT	Hypoxanthine guanine phosphoribosyl

	transferase
Kb	Kilo basepair
kDa	Kilo dalton
ko	Knock-out
L	Liter
LOH	Loss of heterozygosity
M	Month
mA	Milliampere
mg	Milligram
min	Minutes
mM	Millimolar
NaOH	Sodium hydroxide
NP40	Nonidet P-40 (octyl phenoxypolyethoxylethanol)
NSCLC	Non-Small-Cell Lung Cancer
OCT	Optimal cutting temperature
OD	Optical density
PAGE	Polyacrylamide Gel Electrophoresis
PCR	Polymerase Chain Reaction
PBS	Phosphate Buffered Saline
PFA	Paraformaldehyde
rpm	Rounds per minute
RT	Room temperature
RT-PCR	Reverse transcriptase polymerase chain reaction
rtTA	Reverse tetracycline transactivator
SCLC	Small-Cell Lung Cancer
SDS	Sodium dodecylsulfate
SP-C	Surfactant Protein C
TAE	Tris-Acetate-EDTA
TEMED	N,N,N’,N’-Tetramethylethylenediamine
tet	tetracycline-regulated

Tet-O	tetracycline operator
Tris	Tris(hydroxymethyl)aminomethane
TRITC	Tetramethylrhodamine isothiocyanate
TTF-1	Thyroid transcription factor 1
TUNEL	Terminal deoxynucleotidyltr.-mediated dUTP-biotin nick end labeling
V	Volt
wt	Wild type
µg	Microgram

8. Acknowledgments

It is a pleasure to thank those people who made this thesis possible.

First of all I would like to thank Prof. Ulf Rapp for giving me the opportunity to accomplish my PhD in his lab at the MSZ in Würzburg and at the MPI in Martinsried, respectively. I am especially grateful for the enthusiasm, the great ideas and the continuous support he gave me. I also wish to thank Mrs Rapp for her precious help during the last year.

I am thankful to Dr. Rudolf Götz for critical reviewing of this thesis and for his help during my time at the MSZ in Würzburg.

Special acknowledgments go to Prof. Axel Ullrich for welcoming our lab in his department and for his support.

I wish to thank Prof. Ricardo Benavente and Prof. Roland Benz for their agreement to review this thesis and for being part of my doctorate committee. I am also deeply grateful to BIGSS and to the GSLS of Würzburg for founding and support.

I would like to thank the current and former members of the Rapp´s lab, all co-workers at the MSZ and all members of the molecular biology department at the MPI for any help and advice. Special thanks go to Fatih, Semra, Vijay, Chitra, Andi, Katharina, Irene, Christiaan, Raj and Nefertiti.

I am grateful to all my “old” Italian friends for their wonderful friendship.

Finally, I wish to convey my gratefulness to Sandra. It is very difficult to express this in only few words; therefore all I can say is: thank you for everything!! Last but not least, I would like to express my deep gratitude to my parents and my brother. Thank you very much for your constant encouragement and for supporting me in every step of my life.

PUBLICATIONS

Expression of B-RAF V600E in Type II Pneumocytes Causes Abnormalities in Alveolar Formation, Airspace Enlargement and Tumor Formation in Mice. Zanucco E, Götz R, Potapenko T, Carraretto I, Ceteci S, Ceteci F, Savai R, Seeger W, Rapp UR. (Accepted for publication in *PLoS ONE)*.

Conditional expression of oncogenic C-RAF in mouse pulmonary epithelial cells reveals differential tumorigenesis and induction of autophagy leading to tumor regression. Ceteci F, Xu j, Ceteci S, Zanucco E, Thakur C, Rapp UR. *Neoplasia.* 2011 Nov; 13(11):1005(18).

MYC is a metastasis gene for non-small-cell lung cancer. Rapp UR, Korn C, Ceteci F, Karreman C, Luetkenhaus K, Serafin V, Zanucco E, Castro I, Potapenko T. *PLoS ONE*. 2009 Jun 24; 4(6):e6029.

PRESENTATIONS AND TALKS

Poster: “Lung-Targeted Expression of B-RAF V600E in Alveolar Type II Cells

Causes Emphysema and Delayed Adenoma in Mice". Zanucco E et al. AACR 2010. Washington DC, USA.

Poster and talk: "Lung-targeted expression of oncogenic B-RAF V600E in Alveolar Type II cells causes Emphysema in Mice". Emanuele Zanucco. Bayreuther Strukturtage 2009. Schloss Thurnau, Germany

Poster: "Myc is sufficient to induce Metastasis of NSCLC by a Reprogramming Mechanism". Ceteci et al. EMBO Workshop 2008. Can epigenetics influence reprogramming & metastatic progression? Bad Staffelstein, Germany

10. Affidavit

I hereby declare that my thesis entitled:

Role of oncogenic and wild type B-RAF in mouse lung tumor models

is the result of my own work. I did not receive any help or support from commercial consultants. All sources and / or materials applied are listed and specified in the thesis.

Furthermore, I verify that this thesis has not yet been submitted as part of another examination process neither in identical nor in similar form.

Würzburg: ……...……
Date, Signature